DOT/FAA/AR-99/8,III

Office of Aviation Research
Washington, D.C. 20591

Improved Barriers to Turbine Engine Fragments: Interim Report III

May 2001

Annual Report

U.S. Department of Transportation
Federal Aviation Administration

NOTICE

This document is disseminated under the sponsorship of the U.S. Department of Transportation in the interest of information exchange. The United States Government assumes no liability for the contents or use thereof. The United States Government does not endorse products or manufacturers. Trade or manufacturer's names appear herein solely because they are considered essential to the objective of this report. This document does not constitute FAA certification policy. Consult your local FAA aircraft certification office as to its use.

Technical Report Documentation Page

1. Report No.	2. Government Accession No.	3. Recipient's Catalog No.
DOT/FAA/AR-99/8,III		

4. Title and Subtitle	5. Report Date
IMPROVED BARRIERS TO TURBINE ENGINE FRAGMENTS: INTERIM REPORT III	May 2001
	6. Performing Organization Code

7. Author(s)	8. Performing Organization Report No.
D.A. Shockey, David C. Erlich, and Jeffrey W. Simons	

9. Performing Organization Name and Address	10. Work Unit No. (TRAIS)
SRI International 333 Ravenswood Avenue Menlo Park, CA 94025-3493	11. Contract or Grant No. 95-G-010

12. Sponsoring Agency Name and Address	13. Type of Report and Period Covered
U.S. Department of Transportation Federal Aviation Administration Office of Aviation Research Washington, DC 20591	Annual Report
	14. Sponsoring Agency Code ANE-100, ANM-100

15. Supplementary Notes

The FAA William J. Hughes Technical Center COTR are Robert H. Pursel and William Emmerling.

16. Abstract

In support of the Federal Aviation Administration's Catastrophic Failure Prevention Program, SRI International has identified advanced materials and is developing shielding concepts to protect critical aircraft components from uncontained engine debris.

Full-scale fragment impact tests on a commercial aircraft fuselage confirmed that barriers made from high-strength polymer fabrics in the fuselage wall could prevent penetration into the cabin. A computational capability is now being developed to enable efficient design of fabric fragment barriers.

A mathematical model of woven fabric made from Zylon polybenzazoles (PBO), Kevlar, or Spectra was constructed using the data and observations from laboratory tests to measure yarn tensile and friction properties, quasi-static penetration tests to measure the evolution and phenomenology of fabric deformation and failure, and projectile impact tests to measure effects of fabric material, mesh density, boundary conditions (how a fabric is gripped), and projectile sharpness.

The model was implemented in the LS-DYNA3D finite element code and used to simulate the failure behavior of yarns and fabrics under impact scenarios. The resulting insights are assisting barrier design. A simplified version of the computational model is being developed to enhance its usefulness to the commercial aircraft industry in designing engine fragment barriers.

17. Key Words	18. Distribution Statement
Aircraft engine fragments, Fragment barriers, PBO Armor, Zylon	This document is available to the public through the National Technical Information Service (NTIS), Springfield, Virginia 22161.

19. Security Classif. (of this report)	20. Security Classif. (of this page)	21. No. of Pages	22. Price
Unclassified	Unclassified	105	

TABLE OF CONTENTS

LIST OF FIGURES

LIST OF TABLES

EXECUTIVE SUMMARY

This annual progress report describes the procedures and results of year two of the SRI International Phase II effort to develop a computational capability for designing lightweight fragment barriers for commercial aircraft.

Fabric woven from high-strength polymers was modeled by treating the geometry, properties, and interactions of individual yarns of Zylon polybenzazoles (PBO), Kevlar, and Spectra. Input to the model was provided by laboratory tests to measure yarn tensile and friction properties, quasi-static penetration tests to measure the evolution and phenomenology of fabric deformation and failure, and projectile impact tests to measure effects of fabric material, mesh density, boundary conditions (how a fabric is gripped), and projectile sharpness.

The model was implemented in the LS-DYNA3D finite element code and used to simulate the failure behavior of yarns and fabrics under impact scenarios. The LS-DYNA-3D software code was developed by the Lawrence Livermore National Laboratory as a tool for simulating dynamic nonlinear events such as impact. The resulting insights assisted barrier design. Fuselage impact tests were performed to evaluate full-scale fragment barriers. A simplified version of the computational model is being developed to enhance its usefulness to the commercial aircraft industry in designing engine fragment barriers.

INTRODUCTION AND BACKGROUND

Over the years, several civil aircraft accidents with catastrophic consequences have occurred when fragments from in-flight engine failures damaged critical aircraft components. To reduce the probability of catastrophic consequences in future failures, the Federal Aviation Administration (FAA) established the Aircraft Catastrophic Failure Prevention Research (ACFPR) Program [1] to develop and apply advanced technologies and methods for assessing, preventing, and or mitigating the effect of such failures. In support of the ACFPR objective, SRI International is conducting research aimed at developing lightweight barrier systems for turbine engine fragments.

In Phase I of this program, SRI reviewed the extensive body of armor technology held by the Department of Defense to identify concepts, materials, and armor designs that could lead to practical barriers to engine fragments on commercial aircraft [2]. Because of their low density and high strength; highly ordered, highly crystalline high-molecular-weight polymers were identified as the advanced materials holding the greatest promise for engine fragment barriers on aircraft. Specifically, fibers of certain aramids, polyethylene, and polybenzazoles (PBO) appeared able to provide a useful measure of ballistic protection in the most weight-efficient manner.

Gas gun experiments, in which a fragment-simulating projectile was accelerated against barriers of these fabrics, confirmed that selected wovens, lay-ups, and felts made from strong polymer fibers can absorb significant fragment energy. Furthermore, these materials appear to have sufficient flame resistance, water absorption resistance, and thermal and acoustic insulation properties to serve as building blocks for barriers. The next step was to design practical barriers from these fibers. The barrier scheme must seek to minimize added weight and cost, if possible, by replacing existing materials in the fuselage wall with dual function ballistic materials.

A modeling effort was begun to facilitate design of barrier structures and assist in their evaluation. To ensure the model's reliability, the individual yarns of the fabric were treated explicitly, accounting for yarn geometry, properties, interactions with each other, and failure mechanisms. The model was implemented with brick elements in the LS-DYNA3D finite element code. The LS-DYNA-3D software code was developed by the Lawrence Livermore National Laboratory as a tool for simulating dynamic nonlinear events such as impact. Computational simulations of actual and virtual fragment impact experiments showed the role of yarn crimp, density, and gripping conditions and facilitated the design of barrier schemes.

To assist in model development, quasi-static penetration tests were performed with a tensile machine in conjunction with a video camera to elucidate the phenomenology and evolution of fabric failure. Tensile and friction properties of Zylon, by its composition poly(p-phenylene-2, 6-benzobisoxazole) PBO yarn were measured at several strain rates. The ballistic performance of various barrier structures of Zylon PBO fabric was measured in gas gun tests using fragment simulating projectiles. Failure mechanisms and the effects of multiple fabric plies and gripping mode were investigated.

During the current year, the model was extended and incorporated into the LS-DYNA3D finite element code. Computational simulations of ballistic experiments were performed to interpret

the failure behavior of yarns and fabrics under impact scenarios. Fragment barriers were designed using the insights gained from the simulations, the barriers were constructed, and their performance was evaluated in full-scale fragment impact experiments on a fuselage. An alternative shell-element form of the model is being developed that incorporates yarn behavior more implicitly and hence is more time efficient. The shell-element version is intended for use by aeronautical engineers in designing fragment barriers.

In the coming year, fragment impact experiments will be performed to examine various barrier gripping schemes, elucidate fragment dragging effects of insulation and interior wall panel characteristics, and provide data on the effects of fragment size, shape, orientation, and sharpness. The observed behavior will be modeled and the data incorporated into the model to produce a capability for simulating and investigating barrier implementation strategies. Experiments and computations will be performed to generate the data and understanding needed to modify the model for instances of multiple fragment impact. Finally, the conversion of the detailed fabric model into a time- and cost-efficient, user-friendly, shell-element format will be completed and the design capability transferred to the aircraft industry.

At the conclusion of this program, SRI expects to deliver to the FAA a computational model and information on advanced materials that will enable airframers to design and evaluate lightweight engine fragment barriers. An important direct result of this effort will be practical fragment barriers that could be implemented on commercial aircraft in a very short time.

This is a report of the progress made during calendar year 1999. The first section describes the full-scale barrier tests performed on a retired commercial aircraft fuselage using actual fan blade fragments. The results confirmed the effectiveness and efficiency of high-strength polymer fabrics and encouraged us to proceed with developing a computational design model. The next section describes smaller scale impact tests to examine the influence of fabric material, mesh density, boundary conditions, and projectile sharpness. These results guided model development and assisted in barrier design. The quasi-static penetration tests described in the next section showed how fabric deformation and failure evolves and hence how they must be modeled. The following section describes the tests and measurements for the tensile stress-strain curves and yarn-yarn friction behavior required to quantify the model. The next section describes how the model was developed, how it was evaluated by comparing results of experiments with computer simulations, and how it can be used to gain insight to ballistic penetration. Finally, plans for the next year are outlined.

FUSELAGE IMPACT TESTS AT NAWC-CHINA LAKE

During 1999, SRI International, in conjunction with the Naval Air Warfare Center (NAWC), performed two series of full-scale fragment impact tests on a Boeing 727 fuselage section at China Lake, CA. The objective was to evaluate the effectiveness of high-strength polymer fabrics used as ballistic barriers to mitigate the effects of uncontained turbine engine fragments on commercial aircraft.

MARCH 1999 TESTS—A BRIEF REVIEW.

The first series of tests (reported in detail) [3] was performed using the setup shown in figure 1. A matrix of the test parameters and ballistics results is given in table 1. The tests showed that high-strength fabric, positioned within the fuselage wall (as shown in figure 2), can be an extremely effective, practical, and low-weight ballistics barrier. For example, three plies of Zylon woven fabric, weighing only 0.05 g/cm^2 (0.1 lb/ft^2), glued to the outboard side of the insulation blanket, prevented a 166-g (0.37-lb) sharp-edged fan blade fragment impacting edge-on at 230 m/s (756 ft/s) from penetrating the cabin. The absorbed energy of 4400 joules (3250 ft-lb) is nearly an order of magnitude greater than that absorbed by the unfortified fuselage wall.

The following factors contributed to large amount of energy absorbed per unit areal density by the ballistic fabric barrier in the configuration shown in figure 2:

- The high strength-to-density property of the material, combined with a substantial strain-to-failure, enables each yarn to absorb a significant amount of energy before tensile failure.

- The ability of a woven fabric to deform during impact and spread the load over a much larger area than the impactor footprint.

- The ability of the fabric, if not completely perforated early in the impact, to cloak the fragment, which then results in acceleration of the entire barrier and some of the insulation blanket attached to it and dragging of the cloaked fragment through the hole punched in the interior wall panel (IWP). Figure 3 shows an example of this cloaking and dragging mechanism.

In summary, the tests showed that a Zylon barrier with an areal density of 0.05 g/cm^2 (0.1 lb/ft^2), or less than that of 0.2 mm (<0.008 in.) of aluminum would provide an increase in ballistic protection equivalent to adding a few mm (>0.1 in.) of aluminum, weighing more than 0.7 g/cm^2 (>1.4 lb/ft^2).

OCTOBER 1999 TESTS—A PRELIMINARY REPORT.

A second series of tests was performed in October. At the time this report was written only some of the test results have been received from NAWC–China Lake (the digital camera stills, but not the high-speed movies or the velocity and orientation results), so this will be only a preliminary report on these tests.

The principal goals for the second test series were (1) to test the effectiveness of the fabric barriers against larger, more energetic engine fragments, in accordance with engine failure analysis, and (2) to investigate the effect of various barrier attachment schemes on the ballistic capability.

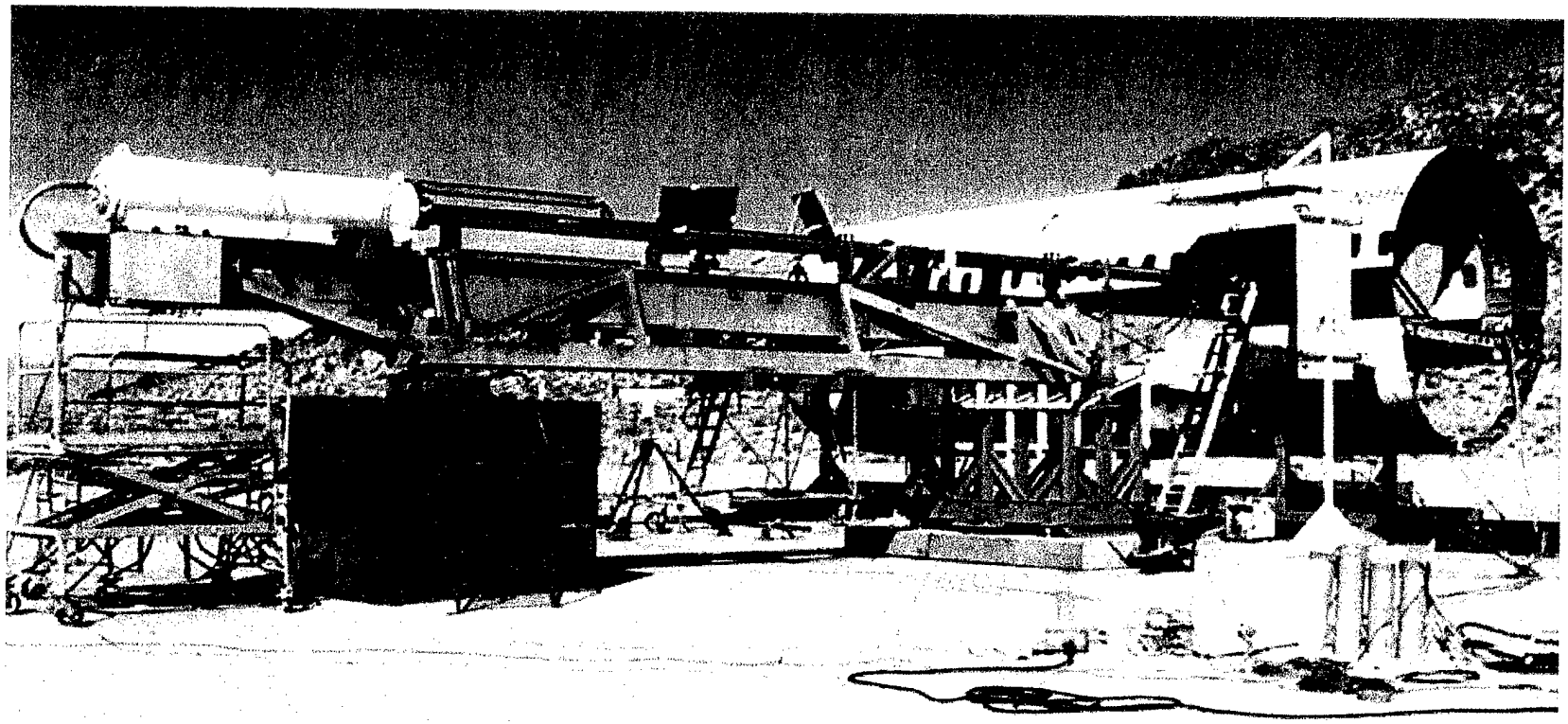

FIGURE 1. A SIX-IN.-BORE GAS GUN AND AIRCRAFT FUSELAGE SECTION SETUP AT NAWC-CHINA LAKE FOR IMPACT TESTING OF ENGINE FRAGMENT BARRIERS

TABLE 1. SRI FUSELAGE IMPACT TESTS AT NAWC-CHINA LAKE (1st Series—March, 1999)

Test No.	Skin Thick-ness[a]	Fabric Barrier					Impactor[d]			Impact			Residual			K.E. Absorbed			SEA[f]		Results
		Fabric Mat'l.	Mesh Density	# of Plies	A. D.[b]	Glued to[c]:		Mass (g)	Mass (lb)	Velocity (f/s)	Velocity (m/s)	K.E. (J)	Velocity (f/s)	Velocity (m/s)	K. E. (J)	Total (J)	Barrier[e] (J)	Barrier[e] (ft-lb)	(kJ / g/cm²)	(kft-lb / lb/ft²)	
38	1.68	—	— —	—	—	—	FS	25	0.05	615	188	438	400	122	185	253	—	—	—	—	Penetration
39	1.61	Zylon	35 x 35	1	0.016	Ins.	FS	25	0.05	631	192	461	0	0	0	461	182	134	≥ 11.5	≥ 4.1	No Pen. - Zylon-encased FS part way thru IWP
40	2.11	Zylon	35 x 35	1	0.016	IWP	FS	25	0.05	615	188	438	259	79	78	360	286	211	18.1	6.5	Penetration - perforated fabric
42	1.97	Zylon	35 x 35	1	0.016	Ins.	FS	25	0.05	797	243	735	616	188	439	296	164	121	10.4	3.7	Penetration - perforated fabric
43	1.61	Zylon	35 x 35	2	0.032	Ins.	FS	25	0.05	812	248	763	0	0	0	763	484	357	≥ 15.3	≥ 5.5	No Pen. - Zylon-encased FS part way thru IWP
44	1.55	Spectra	32 x 32	1	0.011	Ins.	FS	25	0.05	614	187	436	276	84	88	348	43	32	4.0	1.4	Penetration - perforated fabric
45	1.63	Kevlar	32 x 32	1	0.011	Ins.	FS	25	0.06	601	183	420	0	0	0	420	146	108	≥ 12.9	≥ 4.7	No Pen.- large yaw (≈30°) recorded at impact
46	1.71	—	— —	—	—	—	FB	152	0.34	647	197	2959	592	180	2477	482	—	—	—	—	Penetration
47	1.68	Zylon	35 x 35	2	0.032	Ins.	FB	166	0.37	634	193	3101	419	128	1354	1747	1235	911	39.1	14.1	Penetration - Perforated fabric
48	1.57	Zylon	35 x 35	3	0.047	Ins.	FB	158	0.35	634	193	2946	N.A.	N.A.	N.A.	N.A.	N.A.	N.A.	N.A.	N.A.	Penetration - FB escaped past fabric edge
49	1.79	Zylon	35 x 35	2	0.032	Ins.	FB	152	0.34	520	159	1914	214	65	324	1590	1168	862	37.0	13.3	Penetration - FB escaped past fabric edge
50	1.71	Zylon	35 x 35	3	0.047	Ins.	FB	166	0.37	622	190	2985	0	0	0	2985	2503	1846	≥ 52.8	≥ 19.0	No Pen. - FB encased in Zylon attached to IWP
51	2.41	Zylon Zylon	35 x 35 35 x 35	3 1	0.063 ↑	Ins. IWP	FB	158	0.35	619	189	2808	0	0	0	2808	2877	2122	≥ 45.5	≥ 16.4	No Pen. - FB encased in Zylon attached to IWP
52	2.34	Zylon	35 x 35	3	0.047	Ins.	FB	166	0.37	756	230	4409	0	0	0	4409	4418	3258	≥ 93.2	≥ 33.6	No Pen. – FB encased in Zylon attached to IWP
53	1.97	Zylon Zylon	35 x 35 35 x 35	3 1	0.063 ↑	Ins. IWP	FB	158	0.35	804	245	4738	0	0	0	4738	4456	3287	70.5	25.4	Penetration – FB (encased in Zylon) exits IWP with negligible velocity

[a] Thickness of fuselage skin in mm (targets include the fuselage skin, the thermal-acoustical insulation blanket, and the interior wall panel).

[b] Areal density in g/cm^2.

[c] Ins. is the thermal/acoustical insulation blanket; IWP is interior wall panel. For tests 50 and 52, fabric was glued to two adjacent insulation panels.

[d] FS (fragment simulator) has a blunt impact edge, with dimensions 0.25 x 1 x 1.38 in. FB (fan blade fragment) has a sharp impact edge, with dimensions 0.22 x 3.0 by ≈4 in.

[e] Difference in kinetic energy absorbed between this test (with the fabric barrier) and corresponding test (FS impactor—Test 38, or FB impactor—Test 46) without a barrier, with corrections included for difference in the fuselage wall thickness (based upon China Lake impact test data): 20 J (15 ft-lb)/0.001 in. increase in fuselage skin thickness for sharp-edged FB impactor (with negligible yaw and pitch); 10.5 J (7.7 ft-lb)/0.001 in. increase for blunt-edged FS impactor.

[f] Additional K.E. absorbed divided by areal density of the fabric barrier. For tests with no penetration, the SEA is a lower bound.

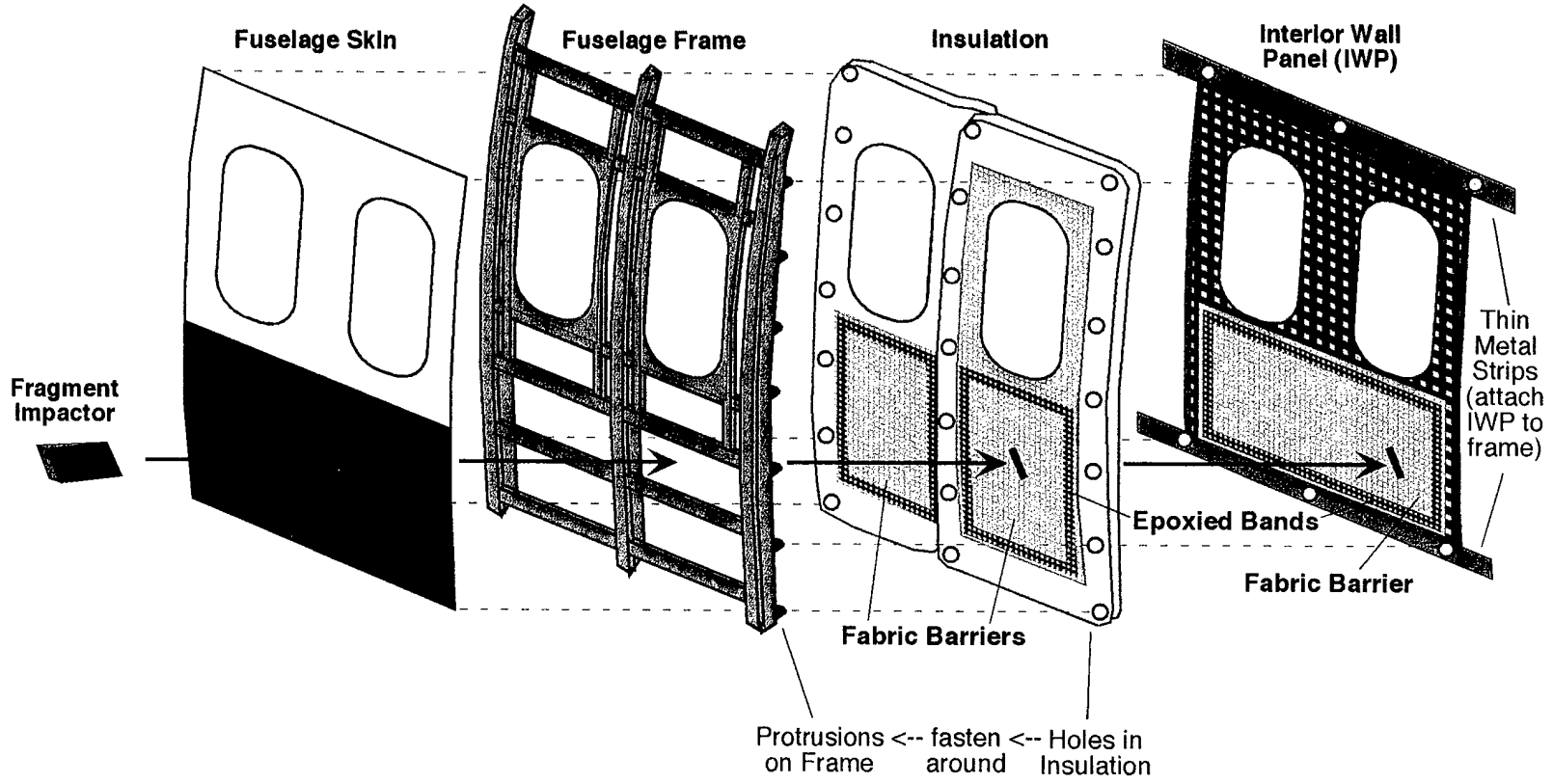

FIGURE 2. EXPLODED VIEW OF FUSELAGE WALL SHOWING LOCATIONS AT FABRIC FRAGMENT BARRIERS IN MARCH 1999 CHINA LAKE IMPACT TESTS

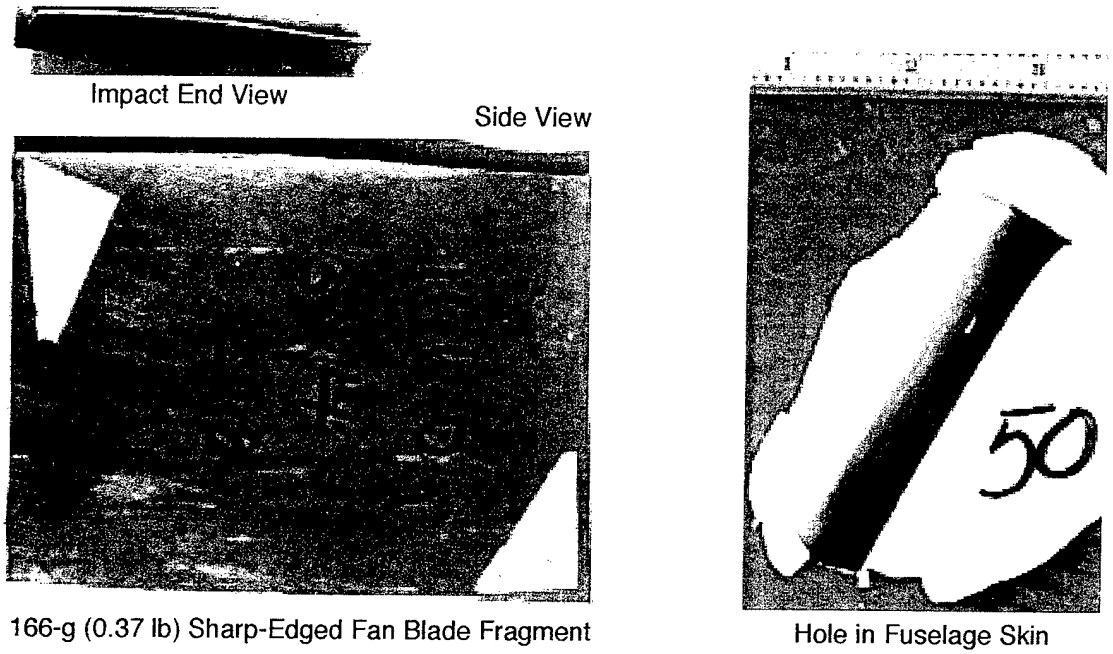

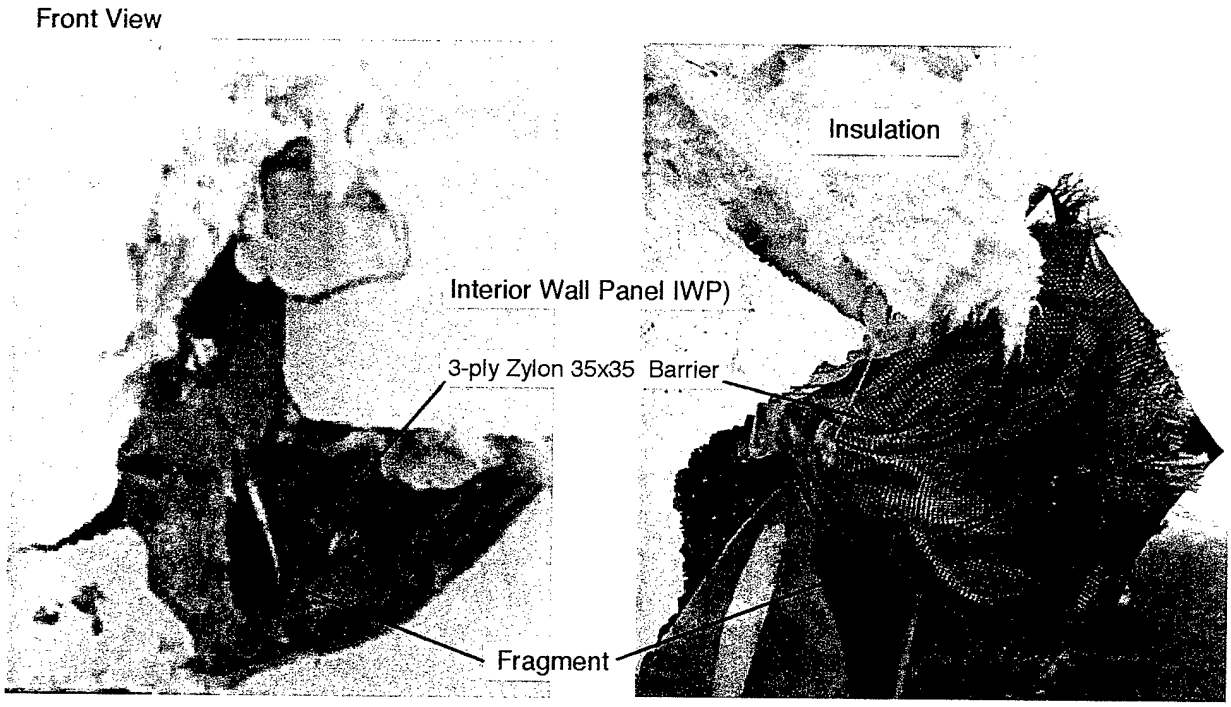

Post-Test Views Inside Fuselage after Impact at 190 m/s (622 f/s)

FIGURE 3. INCOMPLETE PENETRATION OF FABRIC-CLOAKED FRAGMENT THROUGH IWP

The fragments from fan disc event blade analysis [4]—a fan blade segment ≈5.5 in. wide by 7 in. long, weighing 1.0 lb (454 g)—had an estimated impact energy of 15.3 kJ (11,324 ft-lb), nearly four times that of the largest fragments whose penetration had been stopped in the first test

series, using a three-ply Zylon 35 x 35 fabric barrier glued to the insulation blanket. The primary concern in testing the larger fragments was not that additional plies would be unable to prevent fabric barrier perforation. Rather, the concern related to the structure on the inboard side of the barrier, specifically the IWP. Its purpose in a fuselage is not ballistic protection, and therefore, it is attached to the frame using hardware that simply holds it in place and allows for relatively easy removal. The top of the IWP slides under a thin aluminum strip which is attached to the frame ribs with screws, while the bottom has thin metal tabs that are screwed into another strip similarly attached to the frame ribs. During the earlier test series, the IWP remained attached to the frame, where even though it was punctured by the impactor, it provided a structure through which the cloaked fragment could drag the barrier and portions of the insulation blanket, thereby absorbing additional energy. In the highest energy tests, however, the IWP attachment strips became deformed and sections of the IWP had separated from the strips. It thus appeared that with significantly higher impact energies, the IWP might be torn completely or partially from the frame—this is exactly what happened in some of the higher-energy impacts—and the fragment would enter the fuselage, cloaked in the unperforated barrier, with relative large residual kinetic energy.

A method was needed to engage the frame itself in the retention of the barrier using existing frame hardware as much as possible. The fabric needed to be held onto the frame at the minimum number of points as far away from the impact region as possible to allow for as much stretching, distortion, and displacement as possible to maximize the amount of energy absorbed. Several methods were devised, as described in the next section.

EXPERIMENTAL SETUP AND TEST MATRIX.

The arrangement of the fabric barrier within the fuselage wall is shown in figure 4. The preliminary test matrix is shown in table 2. Note that the impact velocities and kinetic energies shown in the table are the intended values, not necessarily the actual values, because the measurements are not yet available.

The experimental setup was similar to that described in the report for the first series except for the following modifications:

- A 12-in.-bore section was added to the muzzle end of the NAWC-China Lake 6-in.-bore gas gun pictured in figure 1 to allow for acceleration of larger fragments. Fragments as large as 5 in. wide by 8 in. long and weighing as much as 597 g (1.32 lb) were used for some tests, and they were placed in the sabots at angles (yaws) as high as 45°. Other tests used the same 3-in.-wide by 4-in.-long fragments (at 0° yaw) used in the earlier test series for comparison of test results.

- The position of the gas gun was shifted with respect to the axis of the fuselage for some of the tests to attain impact obliquities of 15°.

- The opposite side of the fuselage section used in the previous test series was used in this series. As shown in figure 4, impact regions ranged from the first through the third vertical frame section below the window opening. The aluminum skin in the impact regions ranged from 0.065 to 0.108 in. (1.65 to 2.74 mm) in thickness. In tests with the

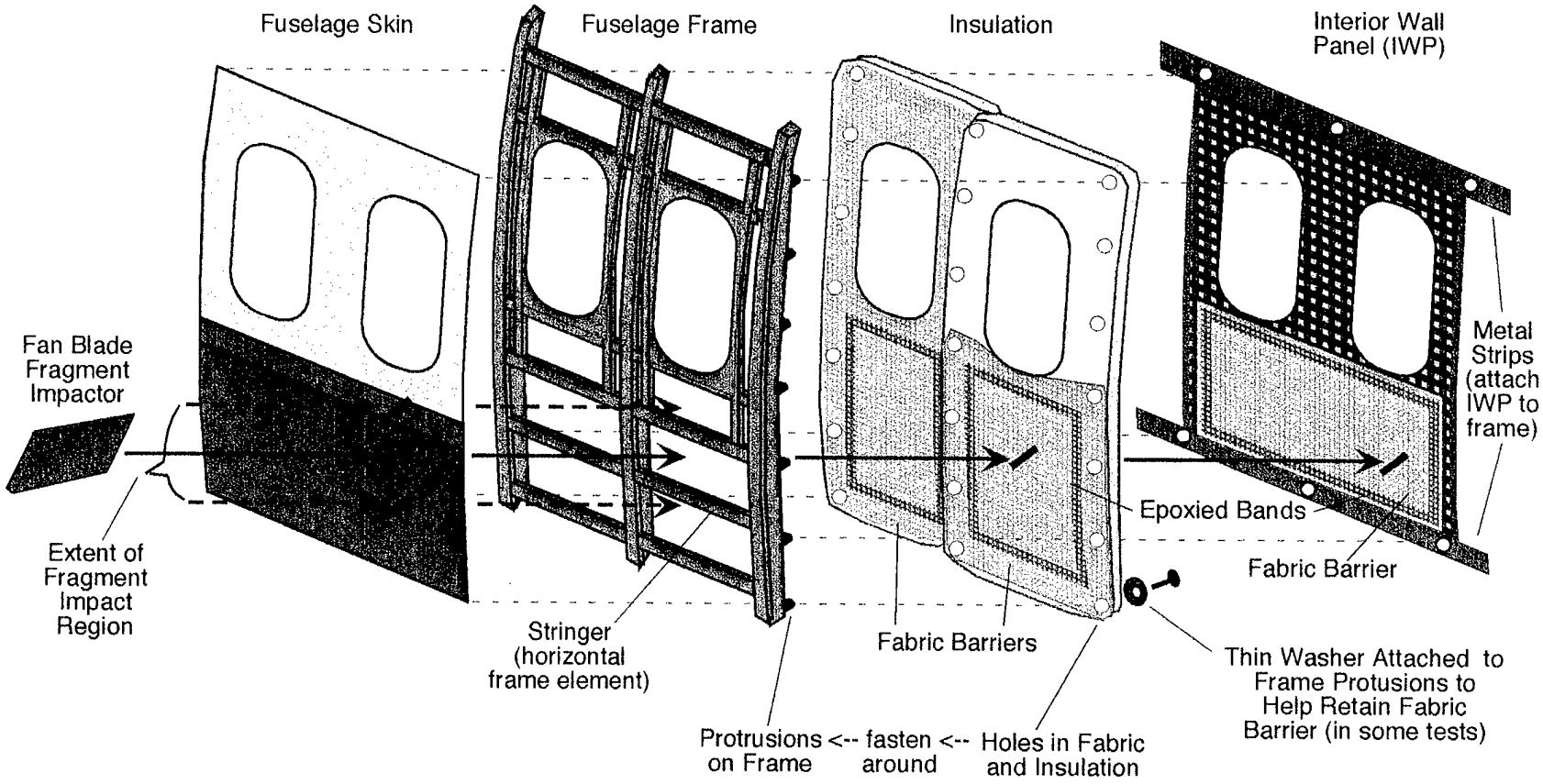

FIGURE 4. EXPLODED VIEW OF FUSELAGE WALL SHOWING REGIONS OF FRAGMENT IMPACT AND LOCATIONS OF FRAGMENT BARRIERS IN OCTOBER 1999 CHINA LAKE TESTS

TABLE 2. FUSELAGE IMPACT TESTS AT NAWC-CHINA LAKE (2nd Series—October, 1999): PRELIMINARY TEST MATRIX

Test No.	Fabric Barrier												Fuselage Location				Impactor						Intended Impact					
	Mat'l. &	No. of	Areal Density		Width		Height		Total Area	Total Mass	Attach-ment	Up-stream	Sections below	Thru Strin-	Al. Skin Thickness	Obli-quity	Mass		Size (in.)			Roll	Yaw	Velocity		Kin. Energy	
CL-	Mesh	Plies	g/cm²	lb/ft²	(In.)	(cm)	(in.)	(cm)	(m²)	(g)	Method*	of:	Window	ger	(.001 In.)	(°)	(g)	(lb)	Th.	W.	L.	(°)	(°)	(f/s)	(m/s)	(kJ)	(ft-lb)
18	Zy35	3	0.05	0.10	33	83	25	62	1.5	166	G/P	Insul.	2	No	65	0	166	0.37	0.22	3.0	4.0	+45	0	850	259	5.6	4,111
19	Zy35	3	0.05	0.10	33	83	25	62	1.5	166	G/P	Insul.	2	No	67	0	166	0.37	0.22	3.0	4.0	+45	0	750	229	4.3	3,201
20	Kev32	3	0.03	0.07	33	83	25	62	1.5	166	G/P	Insul.	2	No	63	0	181	0.40	0.25	3.0	4.0	+45	0	718	219	4.3	3,199
21	Spec32	3	0.03	0.07	33	83	25	62	1.5	166	G/P	Insul.	2	No	102	0	181	0.40	0.25	3.0	4.0	+45	0	718	219	4.3	3,199
22	Zy35	6	0.09	0.19	83	211	25	62	7.9	850	P	Insul.	2 & 3	No	95	0	597	1.32	0.33	5.5	7.0	0	+45	741	226	15.2	11,230
29	None	—	—	—	—	—	—	—	—	——	—	—	1 & 2	Yes	85	15	475	1.05	0.22†	5.0	8.0	+90	+45	830	253	15.2	11,222
30	Zy35	1	0.13	0.26	18	46	15	38	3.4	371	U	Insul.	1 & 2	Yes	85	15	475	1.05	0.22†	5.0	8.0	+90	+45	830	253	15.2	11,217
		6	↑	↑	33	83	25	62	↑	↑	G/P	Insul.															
		1	↑	↑	18	46	15	38	↑	↑	G	MP															
31	Zy35	3	0.05	0.10	33	83	25	62	1.5	166	G/P	Insul.	2	No	85	15	187	0.41	0.31	3.0	4.0	+45	0	755	230	5.0	3,654
32	Zy35	6	0.09	0.19	33	83	25	62	3.1	333	G/P	Insul.	2 & 3	No	108	15	482	1.06	0.22†	5.0	8.0	+45	0	668	204	10.0	7,367
33	Zy35	6	0.09	0.19	83	211	49	124	15.7	1700	G/P/W	Insul.	1 & 2	Yes	85-105	15	481	1.06	0.22†	5.0	8.0	+90	+45	825	252	15.2	11,223
34	Zy35	6	0.09	0.19	33	83	25	62	3.1	333	G/P/W	Insul.	1 & 2	Yes	85-108	15	413	0.91	0.22†	5.0	7.0	+90	+45	750	229	10.8	7,958
36	Zy35	4	0.16	0.32	33	83	25	62	17.8	1922	G/P	Insul.	2 & 3	Yes	92	15	419	0.92	0.27	4.0	7.0	+45	+45	800	244	12.5	9,197
		6	↑	↑	83	211	49	124	↑	↑	G/P/W	Insul.															

* G—glued (with epoxy around periphery), P—pegged (holes cut in fabric plies to fit around rubber protrusions on fuselage frame), U—unheld (lightly taped in place), W—washers (attached to frame protrusions to help retain fabric barrier).

† These impactors had small triangular fins extending outward on both faces, as did the fragments in the Pensacola incident.

smaller impactors, the impactor passed through the skin only without impacting any of the stringers; in tests with the larger impactors, particularly tests involving large yaw, either the impactor encountered the stringers or the stringer was removed before testing to eliminate such an encounter.

- Peak impact velocities were as high as 850 f/s (259 m/s), which is the upper limit of the expected velocity of fan blade tip fragments emerging from the impact containment.

- The fabric barriers were cut approximately the same width as the insulation blankets to which they were glued (see figure 5), and holes were cut near the vertical edges of the fabric at the same location as the holes in the insulation. For most tests, the fabric plies were glued to the insulation blanket (with a narrow-band of epoxy along the fabric periphery), and the holes in the fabric and insulation blanket were fastened around the protrusions in the fuselage frame ribs. Because the horizontal distance between the holes on the fabric is significantly greater than the distance between adjacent frame ribs (the fabric and insulation fold down into the recess between the ribs), there was substantial room for fabric stretching and deformation before the fabric tightened against the rib protrusions. For some tests, the barrier extended over three vertical fuselage frame segments, but was glued to the insulation blanket only in the middle segment, the segment in which impact occurred.

- After it had been determined that the flexible plastic clips that are used to hold the insulation blanket in place on the frame protrusions had failed to prevent the fabric barrier from slipping off the frame protrusions in some of the higher-energy tests, thin, wide metal washers were screwed onto the frame protrusions (see figure 6) to assist in retaining the fabric. These washers were used only on the frame protrusions that were not in the same horizontal band as the impact region; on tests that extended over three vertical fuselage frame segments, the washers were used only on the outermost frame protrusions.

PRELIMINARY TEST RESULTS.

Preliminary results of the fuselage impact tests are given in table 3, in terms of whether the impactor penetrated the interior of the fuselage, the number of fabric barrier plies that were completely perforated by the impactor, and some comments on the barrier structure and resultant impact failure. Because actual impact and residual velocities as well as impact orientations are currently unavailable, no energy absorption results can be presented.

Examination of the holes in the fuselage skin shows that there may be a poor correlation between the intended and actual impact yaws (due to tumbling of the impactor before impact). Figure 7 compares the two test series of impactor entrance holes in the fuselage skin for similar impactors within a similar impact velocity range and a 0° intended yaw. For the first test series, relatively small yaws (typically 3° or less) were measured from the high-speed cameras, and the resulting entrance hole was narrow and slit-like (figure 7(a)). For the second test series, the holes were much wider (figure 7(b)), likely indicative of a larger impact yaw. Conversely, a test in the second series with a large Pensacola-like impactor at an intended yaw of 45° yielded the relatively thin slit-like entrance hole shown in figure 8, indicating a small impact yaw.

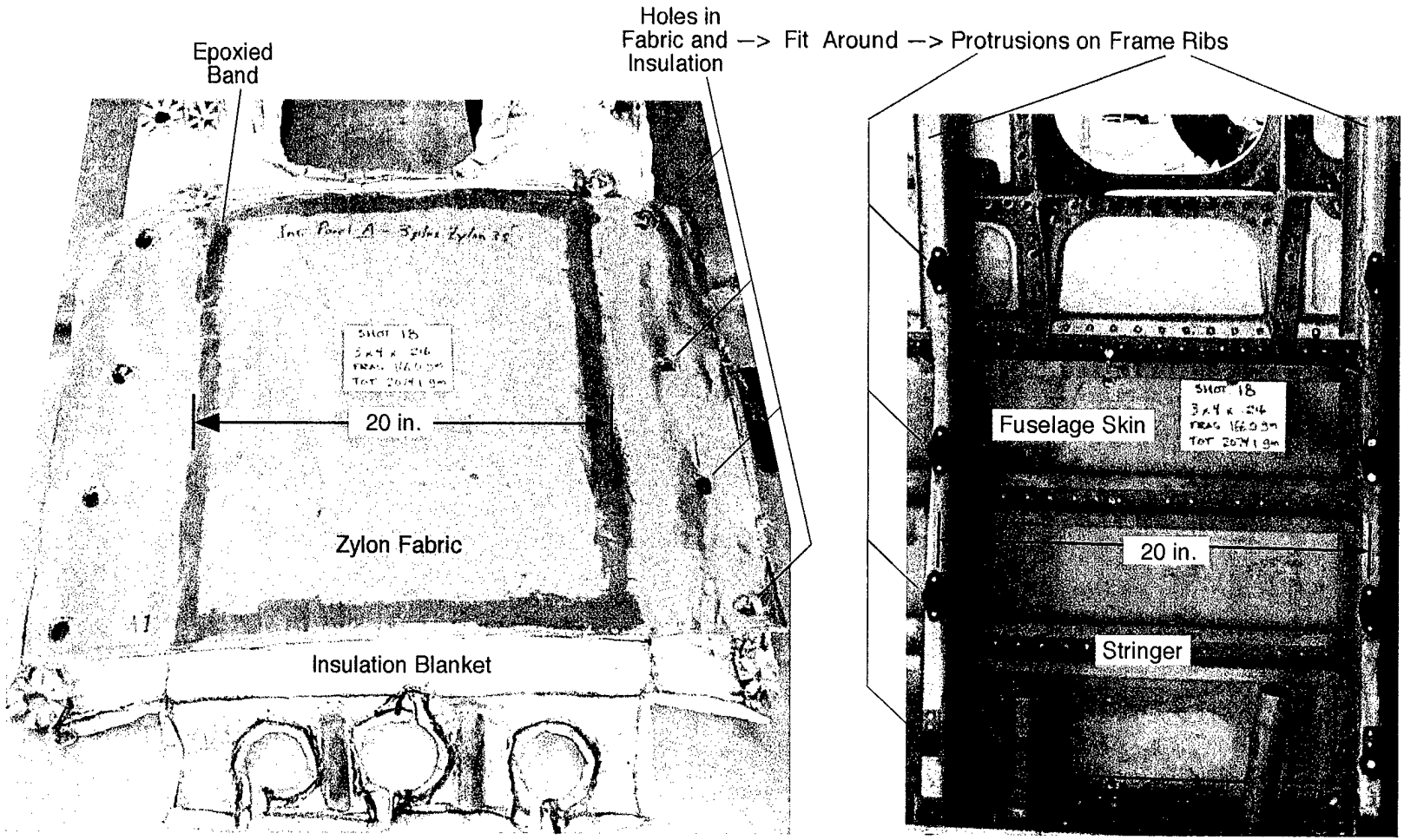

(**a**) Zylon fabric barrier glued to insulation blanket

(**b**) Boeing 727 fuselage vertical frame segment

FIGURE 5. PRETEST PHOTOS OF ZYLON BARRIER AND REGION IN FUSELAGE WHERE IT IS PLACED

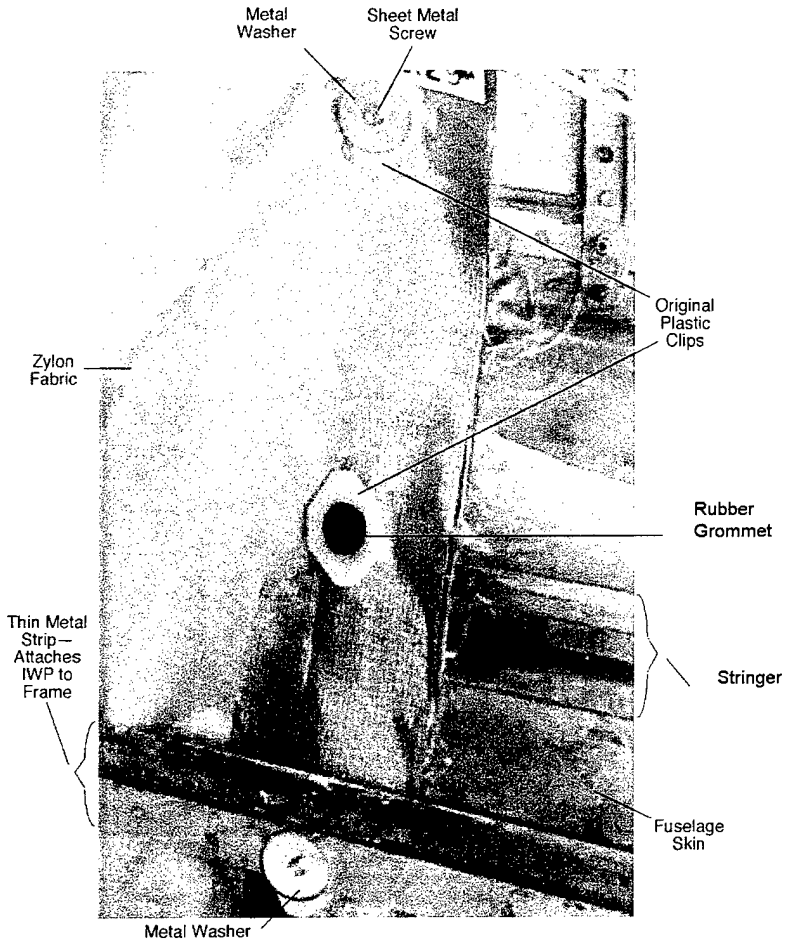

FIGURE 6. DETAIL OF FABRIC BARRIER INSTALLATION SHOWING ORIGINAL PLASTIC CLIPS AND ADDED METAL WASHERS

TABLE 3. FUSELAGE IMPACT TESTS (2nd Series—October, 1999): QUALITATIVE RESULTS

Test No. CL-	Penetrated Into Fuselage Interior	Number of Plies Perforated	Comments
18	Yes	**3 of 3**	—
19	No	**0 of 3**	Only a few yarns cut on each ply.
20	No	**0 of 3**	Nearly perforated all 3 plies.
21	No	**0 of 3**	Roughly half of the yarns necessary for perforation were cut on all 3 plies.
22	Yes	**6 of 6**	Barrier stretched over 3 vertical frame segments.
29	Yes	— — —	Baseline test without barrier, for Pensacola fragment test conditions.
30	Yes	**1 of 8**	Zylon barrier slipped off frame protrusions (& IWP broke away from frame), allowing fragment encased in fabric to enter fuselage.
31	Yes	**3 of 3**	—
32	Yes	**0 of 6**	Barrier slipped off (or broke) frame protrusions (& IWP broke away from frame), allowing fragment encased in fabric to enter fuselage.
33	Yes	**6 of 6**	Barrier stretched over 3 vertical frame segments, with washers on outermost frame rib protrusions only.
34	Yes	**0 of 6**	3 of 4 corners with washers failed to retain fabric, and part of IWP broke away from frame, allowing fragment to enter fuselage.
36	No	**1 of 10**	Barrier stretched over 3 vertical frame segments, with washers on outermost frame rib protrusions only.

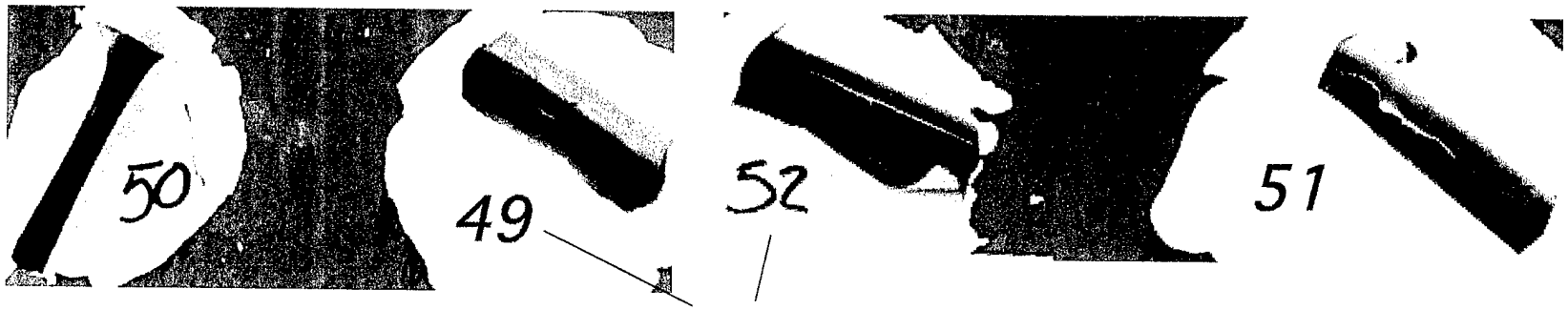

(**a**) Holes in fuselage skin observed in first NAWC-China Lake fuselage impact test series in March 1999

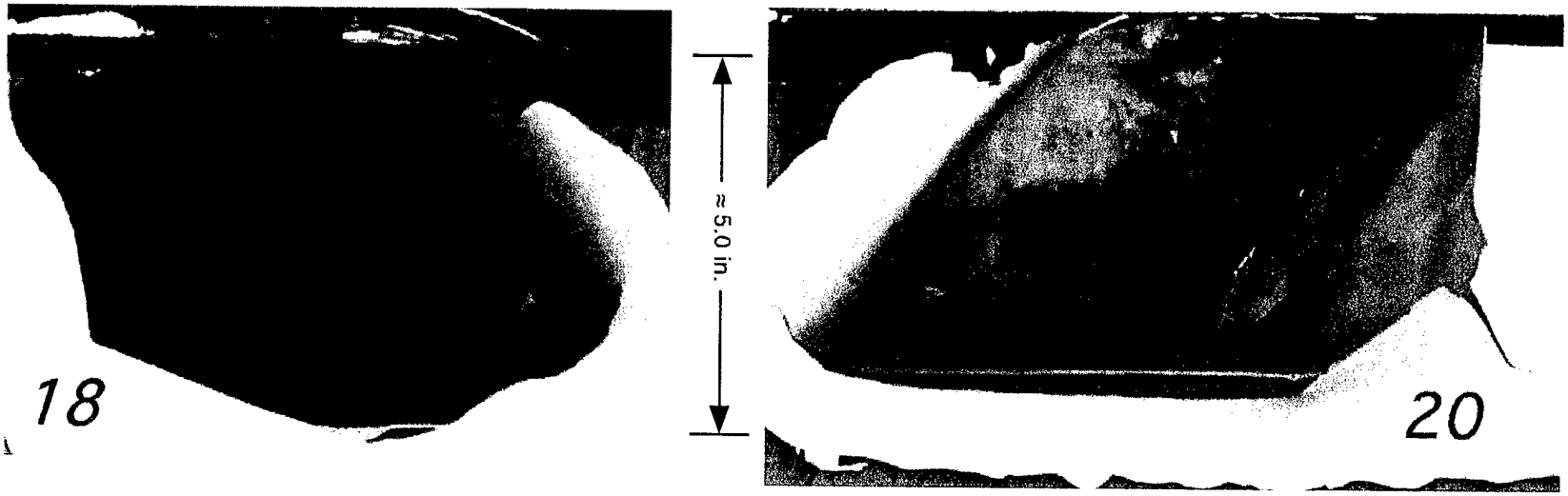

(**b**) Holes in fuselage skin observed in second NAWC-China Lake fuselage impact test series in October 1999

Note: All impactors had a sharp impact edge, dimensions of ≈ 3.0 x 4.0 x 0.23 in., and mass of 152 to 181 g (0.34 to 0.40 lb).

FIGURE 7. COMPARISON OF IMPACTOR ENTRANCE HOLES MADE BY SIMILAR IMPACTORS AT 0° INTENDED YAW AND OBLIQUITY AND SIMILAR IMPACT VELOCITIES FOR FIRST AND SECOND FUSELAGE IMPACT TESTS SERIES

Note: Impactor had a sharp impact edge, dimensions of ≈ 5.5 x 7.0 x 0.33 in., and mass of 597 g (1.34 lb).

FIGURE 8. ENTRANCE HOLES FOR LARGE IMPACTOR AT INTENDED YAW OF 45°

Preliminary results for the five tests involving the large (Pensacola-type) fragments impacting 6- to 10-ply Zylon fabric barriers showed the following:

- In one test (Test 33), the fragment penetrated the fuselage interior by perforating all the barrier plies.
- In three tests (Tests 30, 32, and 34), the fragment penetrated the fuselage interior because the barrier slipped off the frame (along with all or part of the IWP), even though the fragment perforated at most the first ply of the barrier.

- In the one test (Test 36) where penetration was prevented, the fabric, stretched over three vertical fuselage frame segments, remained attached to the outermost frame ribs (likely due to the presence of the added washers) and perforated only the first of its ten plies. It is likely that fewer than ten plies would have prevented the penetration in this case.

All the tests will be analyzed further when the high-speed movies are received and the impactor velocities and orientations are determined. An interim report will be issued when the analysis is complete.

IMPACT TESTS ON FABRIC TARGETS

Smaller-scale impact tests were performed using the SRI International 4-in.-bore gas gun and the NAWC 6-in.-bore gas gun to examine the influence of fabric material, mesh density, boundary conditions, and impactor sharpness on ballistic response. Presented below are descriptions of the high-strength fabrics tested, a brief review of the experimental technique (previously described in detail),[2], results from earlier tests in this series, a matrix of parameters and ballistic results for all the tests, an analysis of the most recent test results, and some overall conclusions.

HIGH-STRENGTH FABRIC MATERIALS.

Six high-strength woven fabric materials were used as ballistic targets in this program. These materials, along with a felt (used as an overlay) and an unwoven yarn (used in tensile tests) are described in table 4. Four Zylon fabrics with meshes varying from 30 x 30 to 45 x 45 yarns/in. were obtained from the manufacturer, Toyobo Company, along with commercially available Kevlar and Spectra 32 x 32 fabrics.

Woven fabrics consist of two perpendicular arrays of interwoven yarns, the fill yarns and the warp yarns. The size and shape of these yarns were used as input for the discrete modeling of yarns in the computational fabric model.

Examination of the Zylon fabrics revealed the following:

- The nominally 500 denier (g per 9 km) yarns vary from 450 to 570 denier.
- Yarns consist of 300 to 350 smooth cylindrical fibers (or filaments) 11-14 μm (0.00043-0.00055 in.) in diameter, or about 1.7 denier each.
- Fill yarns are relatively straight (only 0.6% increase in length when removed from fabric).
- Warp yarns weave over and under fill yarns and thus are crimped or kinked to a degree that depends on the mesh density (increase in length from 0.6% for 30 x 30 weave to 10.5% for 45 x 45 weave).

TABLE 4. HIGH-STRENGTH WOVEN FABRIC MATERIALS TESTED IN THIS PROGRAM[a]

Trade Name[b]		**Zylon-AS**								**Kevlar-29**		**Spectra-1000**	
Material[c]		PBO								P-Aramid		UMHW Polyethylene	
Volume Density	(g/cm^3)	1.54								1.44		0.97	
Nominal Yarn Denier[d]		500								400		375	
Mesh	(yarns/in.)	**30 x 30**		**35 x 35**		**40 x 40**		**45 x 45**		**32 x 32**		**32 x 32**	
Thickness	(in.)	0.006		0.007		0.009		0.011		0.007		0.008	
	(mm)	0.15		0.19		0.23		0.27		0.18		0.20	
Areal Density	(g/cm^2)	0.013		0.0158		0.0185		0.0219		0.0113		0.0108	
	(lb/ft^2)	0.0266		0.0324		0.0378		0.0449		0.0232		0.0221	
Unit Cell	(in.)	0.033 x 0.033		0.028 x 0.028		0.025 x 0.025		0.022 x 0.022		0.031 x 0.031		0.031 x 0.031	
Dimensions	(mm)	0.85 x 0.85		0.72 x 0.72		0.64 x 0.64		0.56 x 0.56		0.79 x 0.79		0.79 x 0.79	
Yarn Type		**Fill**	**Warp**	**Fill**	**Warp**	**Fill**	**Warp**	**Fill**	**Warp**	**Fill**	**Warp**	**Fill**	**Warp**
Width[e]	(in.)	0.029	0.032	0.024	0.031	0.021	0.028	0.018	0.0255	0.021	0.026	0.025	0.030
	(mm)	0.737	0.8128	0.61	0.7874	0.5334	0.7112	0.4572	0.6477	0.5334	0.66	0.635	0.762
Degree of Crimp[f]		0.6%	0.6%	0.6%	2.0%	0.6%	5.2%	0.6%	10.5%	—	—	—	—

[a] In addition to the woven fabrics, a Zylon felt—0.009 in. (0.23 mm) in thickness, 0.0080 g/cm^2 (0.0164 lb/ft^2) in areal density, with 1.5-denier fibers—and 500-denier unwoven Zylon-AS yarn were supplied by the manufacturer for testing in this program.

[b] Zylon was supplied by its manufacturer—Toyoba, Co., Ltd., Osaka, Japan; Kevlar was obtained from Fabric Development Inc., Quakertown, PA; and Spectra was obtained from Fiber Materials, Inc., Biddeford, ME.

[c] PBO is poly(p-phenylene-2,6-benzobisoxazole); UHMW means ultra-high molecular weight.

[d] Denier denotes linear density of yarns in terms of grams per 9 kilometers. Actual values varied by ±10% from nominal values.

[e] If the width is ≤ unit cell dimension, then width is average yarn width. If the width is > unit cell dimension (warp yarns only), then it is the maximum width at the bulge near the middle of the fill yarns.

[f] The fractional increase in length of a woven yarn when it is removed from the fabric and straightened.

The photographs of the woven fabrics in figure 9 show the variation in the width of the yarns as a function of their position in the weave. Yarn cross sections are shown in figure 10 as scanning electron microscope (SEM) views of one fabric (cast in a potting compound to allow sectioning and polishing in planes perpendicular to fiber direction). In all the fabrics, fill yarns are nearly uniform in cross section, and adjacent fill yarns do not touch (i.e., the yarn width is less than the unit cell dimension). The fill yarns are lenticular, they all lie nearly in the same plane (negligible offset between adjacent fill yarns in the direction perpendicular to the fabric plane), and they have a relatively low degree of crimping.

The warp yarns for fabrics with higher mesh densities (35 x 35 and up), however, are not uniform in cross section. Adjacent warp yarns do touch at the points where they cross over from below to above the fill yarns, they bulge out in width between these points, and they have a relatively high degree of crimping (as much as 10% increase in length for the 45 x 45 Zylon fabric). Warp yarns for all the fabrics are more flattened than the fill yarns, and adjacent yarns have a relatively large offset in the direction perpendicular to the fabric plane.

Higher magnification SEM photos (such as those in figure 11) show the individual fibers within the yarn. Although discrete modeling of individual fibers within a yarn is not planned, these views are useful in modeling the effective porosity of the yarns. For example, from the density of Kevlar, 1.44 g/cm^3, and the measured linear density of a Kevlar yarn, 0.448 mg/cm (or 403 denier), the solid cross-sectional area of the Kevlar yarn (the total of all the individual fiber areas) can be determined to be 0.031 mm^2. But measurement of the total cross-sectional area of the yarn envelope in figure 11(a) (including the fiber areas plus all the space between fibers) on the photo yields 0.071 mm^2, more than twice as much as the solid area. Therefore, the Kevlar 32 x 32 yarn has an effective porosity of 56%. A similar calculation for Zylon 40 x 40 yarn, shown in figure 10(a), yields an effective porosity of 45%. The closest packing for parallel right circular cylinders results in a porosity of only 9.3%, so the fibers in these yarns are far from being close-packed.

SMALL-SCALE IMPACT TESTS AT SRI INTERNATIONAL.

Small-scale impact tests were performed at SRI to examine the influence of fabric material, mesh density, boundary conditions (how the fabric is gripped), and impactor sharpness. A 4-in.-bore gas gun was used to launch impactors into fabric targets at velocities from 52 to 113 m/s (171 to 371 ft/s). A high-speed camera (≈20,000 frames/s) recorded the impactor motion before and after impact, allowing determination of the kinetic energy absorbed by the target.

The experimental setup is shown in figure 12, along with drawings of the various impactors. Impactors included a 25-g (0.055-lb) blunt-ended fragment simulator (FS); a 26-g (0.057-lb) sharp-ended fragment simulator (S-FS), whose impact edge more closely resembles that of an actual compressor blade; and a larger, 96-g (0.21-lb) blunt-ended fragment simulator (LFS). Impact velocities ranged from 52 to 95 m/s (171 to 312 f/s), and kinetic energies ranged from 34 to 420 J (25 to 310 ft-lb). The impactors hit approximately end-on, with a relatively small pitch and yaw ($\leq 5°$ in most cases).

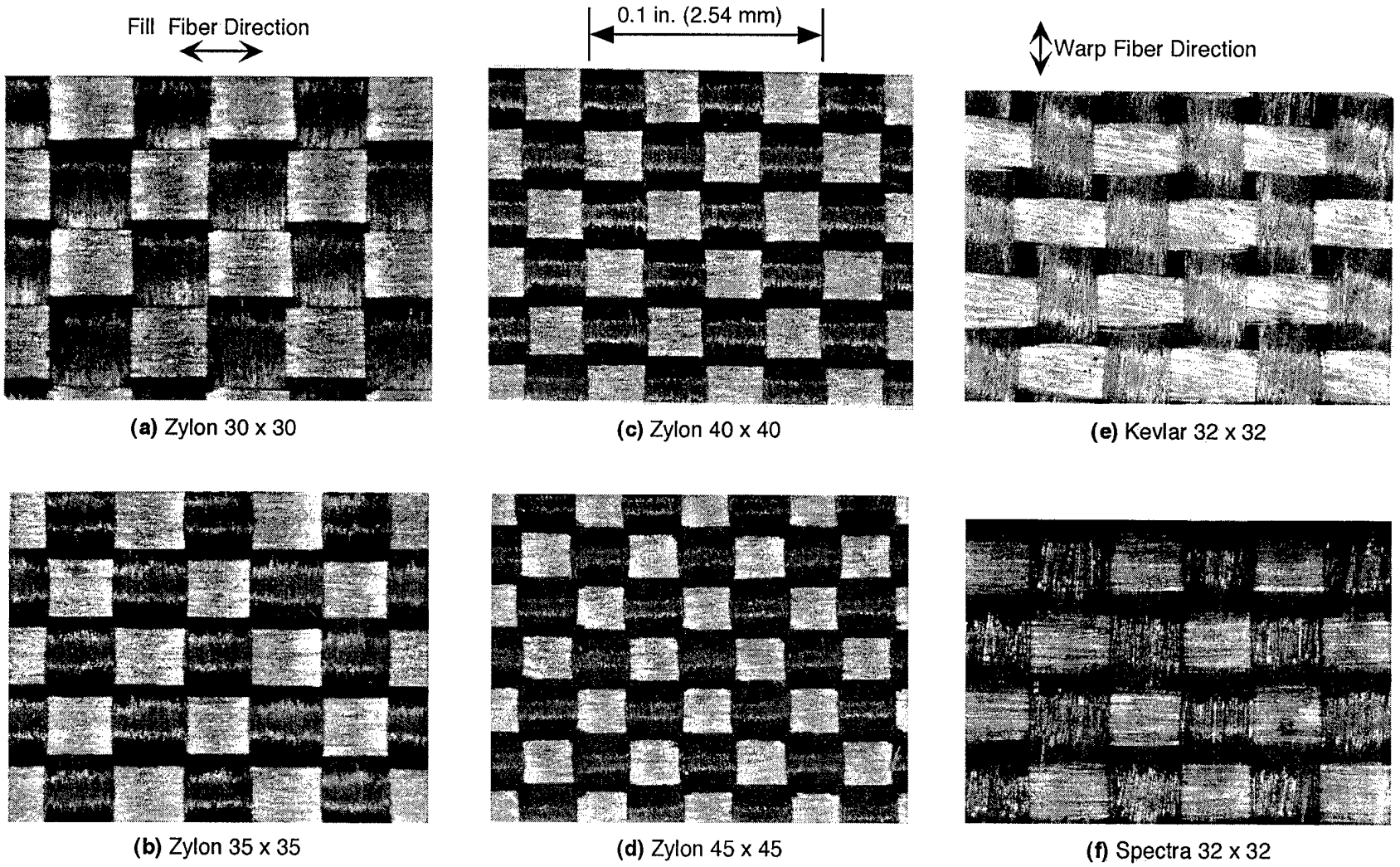

FIGURE 9. MACROPHOTOGRAPHS OF SIX HIGH-STRENGTH WOVEN FABRICS

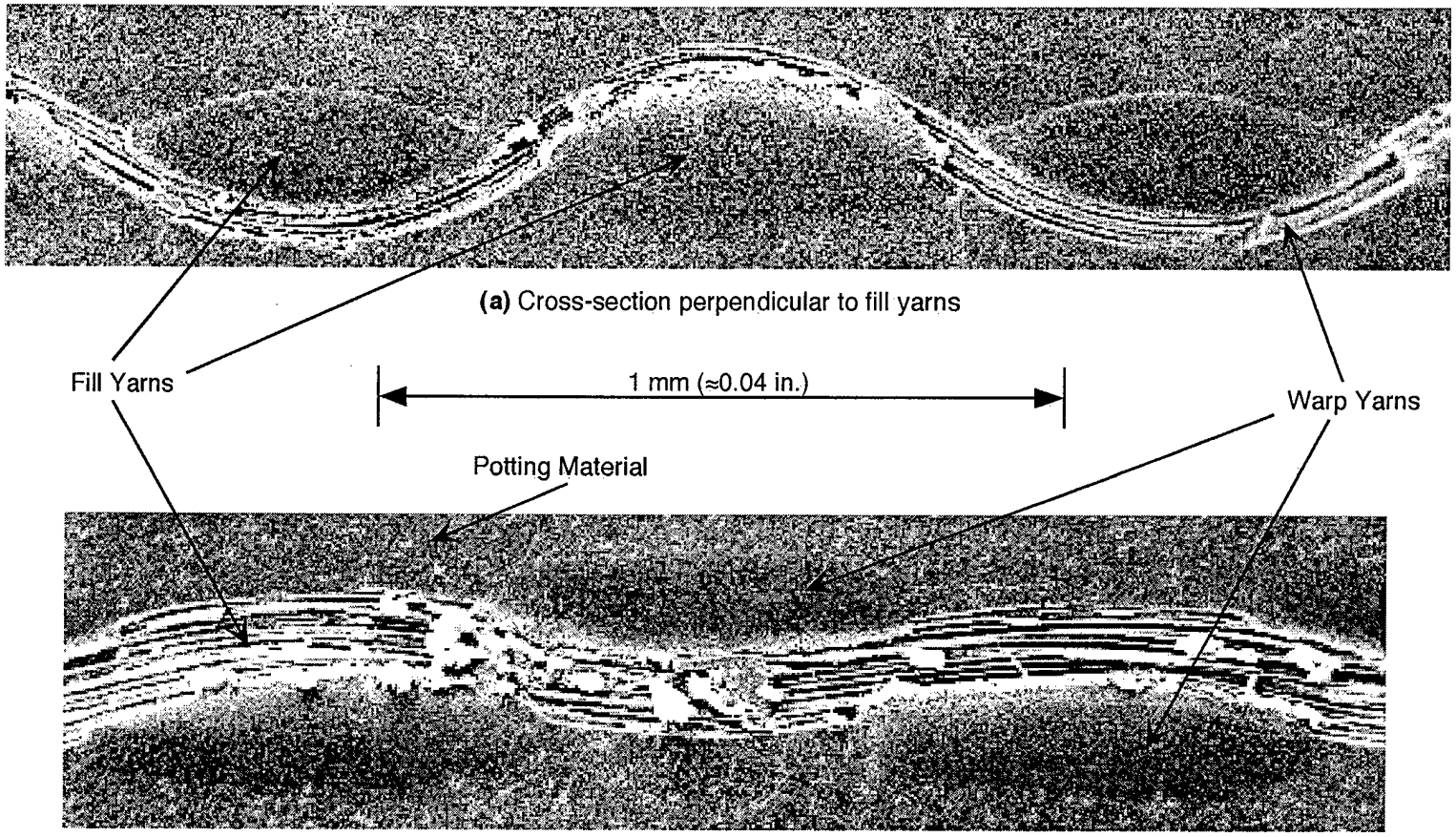

FIGURE 10. SCANNING ELECTRON MICROSCOPE (SEM) VIEWS OF ZYLON 40 x 40 YARNS

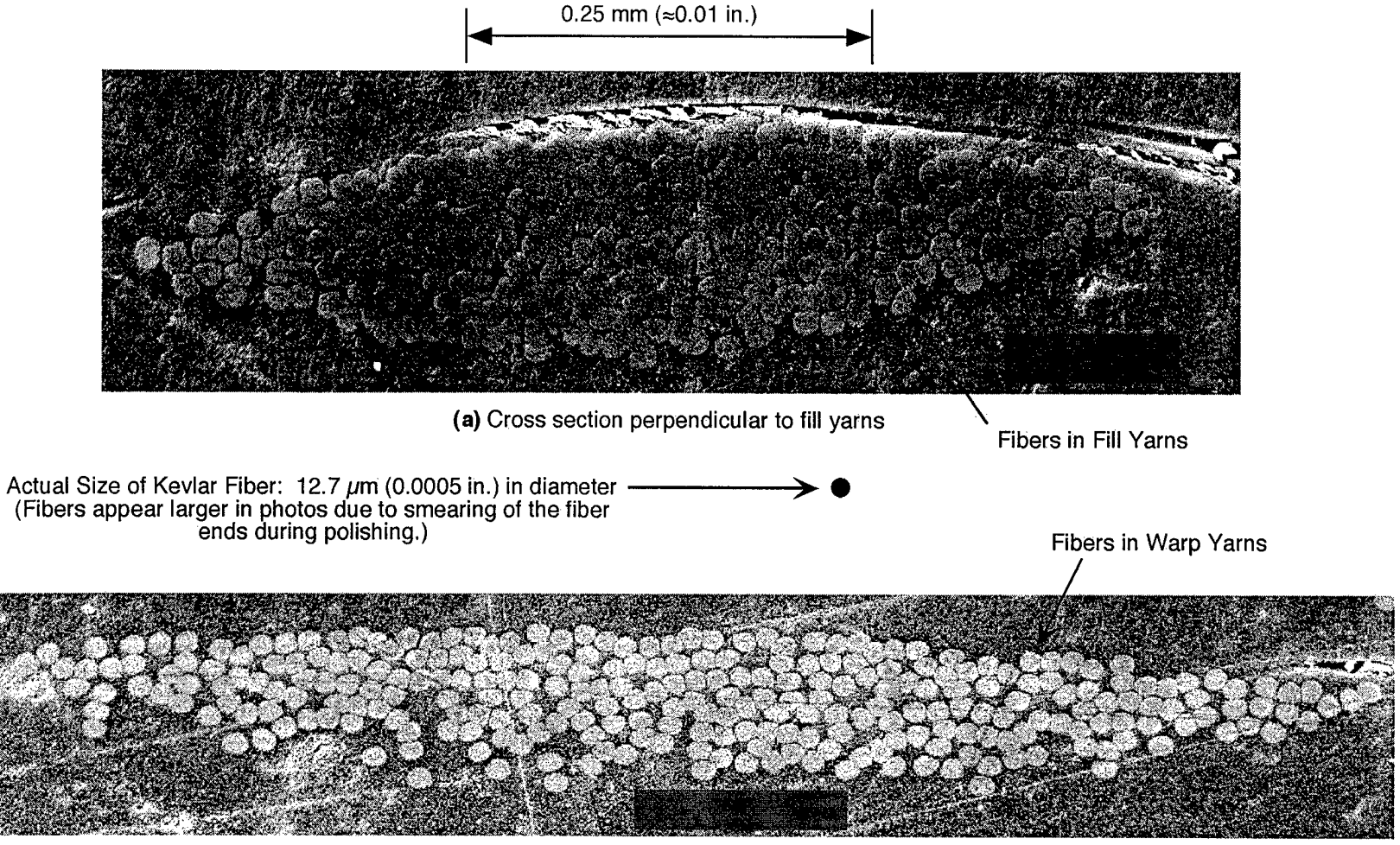

FIGURE 11. SCANNING ELECTRON MICROSCOPE VIEWS OF FIBERS IN KEVLAR 32 x 32 YARNS, SHOWING EFFECTIVE POROSITY OF YARNS

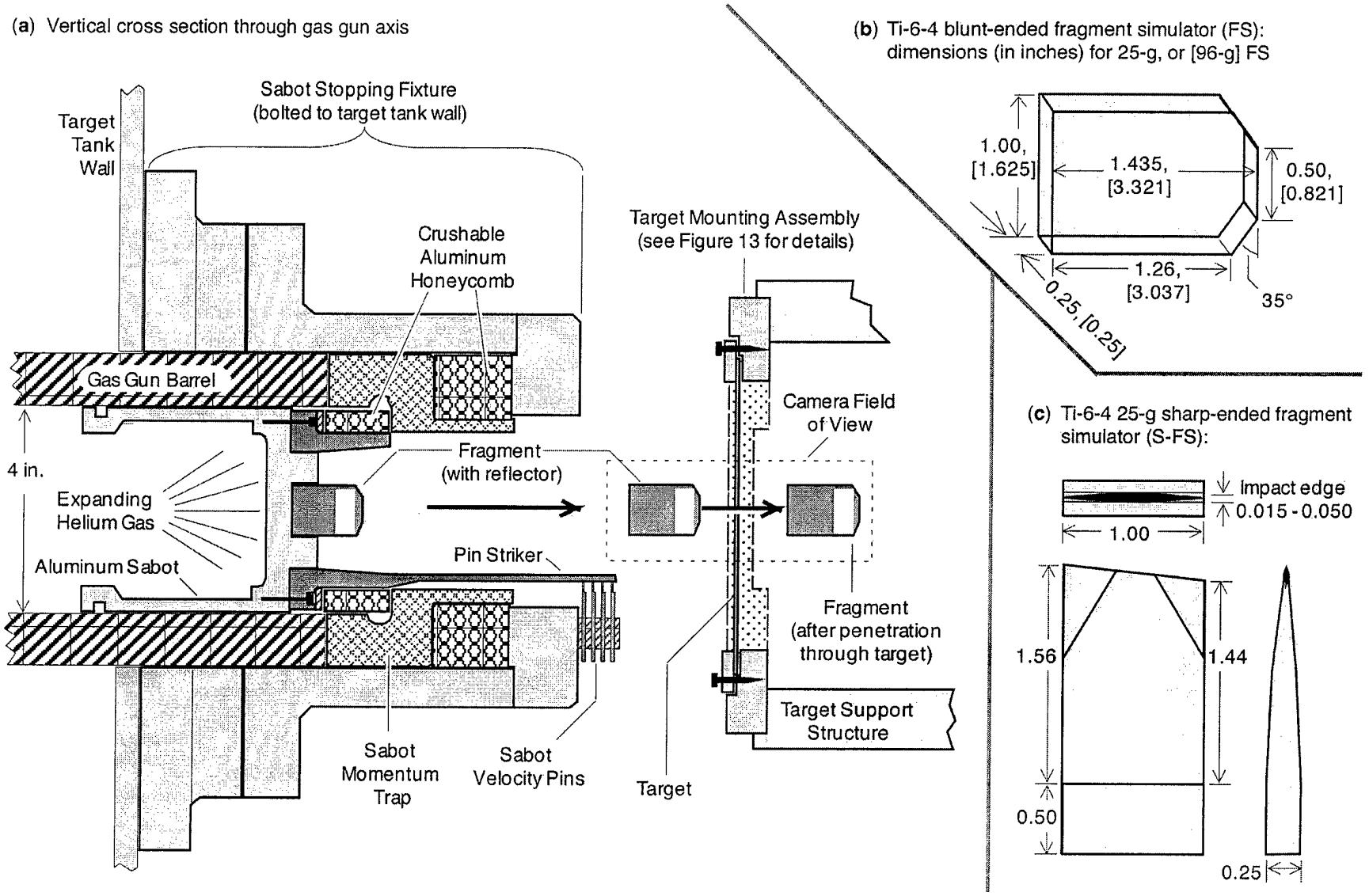

FIGURE 12. EXPERIMENTAL SETUP FOR GAS GUN IMPACT TESTS OF HIGH-STRENGTH FABRIC TARGETS

The shapes and boundary conditions for the fabric targets are shown in figure 13. Most tests involved fabric panels that were tightly gripped on either two or four edges. A few tests involved fabric panels that were glued to the impact side of IWPs or aluminum fuselage skin plates.

GRIPPED FABRIC TARGETS. Thirty-five impact tests were performed successfully with tightly gripped fabric targets. The parameters for these tests and ballistic results are shown in table 5. A figure-of-merit for ballistic effectiveness, the specific energy absorbed (SEA), (the SEA divided by the areal density) was defined for comparing ballistic results for fabrics of different areal densities. Tests included a wide range of target designs (including a variety of fabric materials, mesh densities, number of plies, and gripping geometries).

The following paragraphs summarize the key results attained from these tests (which are previously presented in detail) [5 and 6].

Fabric Material. Zylon woven fabric absorbs more energy per unit areal density (SEA) than any other material tested (see figure 14)—nearly twice that for Kevlar or Spectra fabrics, when tightly gripped on four edges, and over 12 times that of aluminum fuselage skin.

Target Areal Density. Ballistic effectiveness does not appear to be a strong function of mesh density (weave tightness). Zylon fabrics of different mesh densities have similar SEAs (although the 45 x 45 fabric has a slightly higher SEA than the 30 x 30 through 40 x 40 fabrics). This means that, for single-ply Zylon fabrics, the energy absorbed is roughly proportional to the fabric areal density. However, that is not always the case when the change in areal density is due to an increased number of plies, rather than a tighter mesh. The SEA can be significantly higher for multiple-ply targets than for single-ply targets (compare Tests 66 and 67, for example, or Tests 69 and 71, in table 5). This effect may be due partly to frictional forces between the plies following impact, which would make it more difficult for yarns in the first-hit ply to move sideways. Further computational studies with friction are needed to confirm this hypothesis.

Boundary Conditions. The target boundary conditions are a very significant factor in ballistic effectiveness. Gripping the fabric on two edges allows the fabrics to absorb significantly more energy than gripping on four edges (25%-60% more for Zylon, nearly double for Spectra). The reasons for this result are that (1) the load from the impacted yarns is transferred to adjacent nonimpacted yarns, allowing a larger area of the fabric to deform before penetration, and (2) a more energy-absorbing failure mode, remote yarn failure, can be triggered. More detailed explanations are provided below in the two sections on the quasi-static penetration test and on computational modeling.

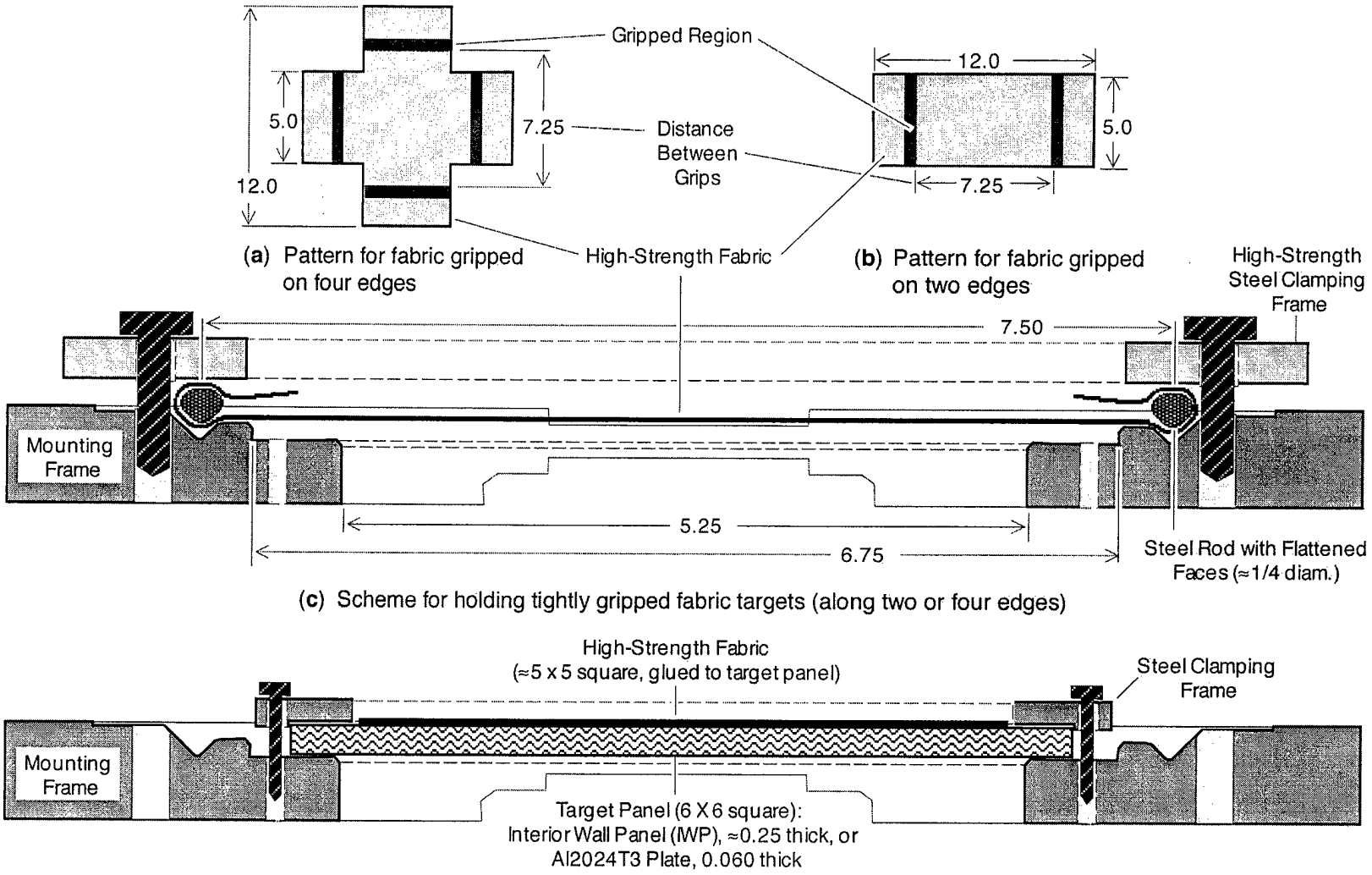

All dimensions in inches; fragment simulator impacts from top of drawing.

FIGURE 13. TARGET MOUNTING AND CLAMPING SCHEMES USED IN GAS GUN IMPACT TESTS OF HIGH-STRENGTH FABRIC TARGETS

TABLE 5. SRI GAS GUN IMPACT TESTS WITH GRIPPED FABRIC TARGETS

Test No.	Target					Impactor		Impact				Residual		K.E.		SEA[b]	
	Material	Mesh (Yarns/in.)	No. Plies	Edges Gripped	Areal Density (g/cm^2)	Type[a]	Mass (g)	Velocity (m/s)	Velocity (f/s)	K.E. (J)	K.E. (ft-lb)	Velocity (m/s)	Velocity (f/s)	Absorbed (J)	Absorbed (ft-lb)	J / g/cm^2	ft-lb / lb/ft^2
13	Zylon	45X45	1	4	0.0219	FS	25	78	256	76.1	56.1	29	95.1	65.5	48.3	2993	1077
20	Zylon	30X30	1	4	0.0130	FS	25	79	259	78	57.5	61.5	202	30.7	22.7	2364	851
26	Zylon	30X30	1	4	0.0130	FS	25	82.5	271	85.1	62.8	63	207	35.5	26.2	2728	982
25	Zylon	35X35	1	4	0.0158	FS	25	77.5	254	75.1	55.4	59	194	31.6	23.3	1998	719
24	Zylon	40X40	1	4	0.0185	FS	25	79	259	78	57.5	49.5	162	47.4	35	2561	922
29	Zylon	40X40	4	4	0.0740	LFS	96	79	259	300	221	27.5	90.2	263	194	3558	1281
32	Zylon	40X40	6	4	0.1110	LFS	96	79	259	300	221	No Pen.		300	221	≥ 2699	≥ 972
37	Kevlar	32X32	1	4	0.0113	FS	25	79.5	261	79	58.3	71.4	234	15.3	11.3	1352	487
38	Spectra	32X32	1	4	0.0108	FS	25	79	259	78	57.5	70.5	231	15.9	11.7	1471	529
39	Zylon	30X30	1	2	0.0130	FS	25	79.5	261	79	58.3	45.4	149	53.2	39.3	4095	1474
40	Kevlar	32X32	1	4	0.0113	FS	25	65	213	52.8	39	56.5	185	12.9	9.52	1142	411
41	Spectra	32X32	1	4	0.0108	FS	25	64.5	212	52	38.4	54.5	179	14.9	11	1377	496
42	Zylon	35X35	1	4	0.0158	S-FS	26	80	262	83	61.4	71.3	234	17.1	12.6	1083	390
43	Zylon	35X35	1	4	0.0158	S-FS	26	80	262	83.2	61.4	64	210	30	22.1	942	339
	Zylon Felt Overlay		2	ungripped	+ 0.0160	(0.0318 = Total areal density)											
44	Zylon	35X35	2	4	0.0316	S-FS	26	80	262	83.2	61.4	59.2	194	37.6	27.8	1191	429
45	Zylon	35X35	1	4	0.0158	S-FS	26	80	262	83.2	61.4	56	184	42.4	31.3	1343	483
	Zylon 35X35 Overlay		1	ungripped	+ 0.0158	(0.0316 = Total areal density)											
46	Zylon	35X35	1	2	0.0158	FS	25	80	262	80	59	46.7	153	52.7	38.9	3338	1202
47	Zylon	35X35	1	2	0.0158	FS	25	80	262	80	59	49.2	161	49.7	36.7	3148	1133
49	Zylon	35X35	1	2	0.0158	FS	25	52	171	34	24.9	No Pen.		33.8	24.9	≥ 2139	≥ 770
53	Zylon	35X35	1	2	0.0158	S-FS	26	80	262	83.2	61.4	61.9	203	33.4	24.6	2113	761
54	Zylon	35X35	1	2	0.0158	S-FS	26	80	262	83.2	61.4	53.9	177	45.4	33.5	1909	687
	Zylon Felt Overlay		1	ungripped	+ 0.0080	(0.0238 = Total areal density)											
55	Zylon	35X35	1	2	0.0158	S-FS	26	80	262	83.2	61.4	39.9	131	62.5	46.1	1978	712
	Zylon 35X35 Overlay		1	ungripped	+ 0.0158	(0.0316 = Total areal density)											
56	Zylon	35X35	1	2	0.0158	S-FS	26	80	262	83.2	61.4	45.7	150	56	41.3	1763	635
	Zylon Felt Overlay		2	ungripped	+ 0.0160	(0.0318 = Total areal density)											
57	Zylon	35X35	2	2	0.0316	S-FS	26	80	262	83.2	61.4	50.2	165	50.4	37.2	1596	575
58	Zylon	40X40	1	2	0.0185	FS	25	80	262	80	59	41.8	137	58.2	42.9	3144	1132
60	Spectra	32X32	1	2	0.0108	FS	25	65	213	52.8	39	36	118	36.6	27	3390	1220
61	Zylon	30X30	3	2	0.0390	LFS	96	79.5	261	303	224	No Pen.		303	224	≥ 7779	≥ 2800
62	Zylon	30X30	5	2	0.0650	LFS	96	93.5	307	420	310	No Pen.		420	310	≥ 6456	≥ 2324
63	Spectra	32X32	1	2	0.0108	FS	25	64.5	212	51.8	38.2	38.5	126	33.3	24.6	3087	1111
66	Zylon	30X30	1	2	0.0130	LFS	96	83	272	331	244	75	246	60.7	44.8	4667	1680
67	Zylon	30X30	2	2	0.0260	LFS	96	83	272	331	244	52.5	172	198	146	7630	2747
68	Spectra	32X32	2	2	0.0216	FS	25	80	262	79.7	58.8	0	0	79.7	58.8	3689	1328
69	Zylon	30X30	1	2	0.0130	FS	25	80	262	79.7	58.8	62.5	205	31	22.9	2388	860
70	Kevlar	32X32	2	2	0.0226	FS	25	80	262	79.7	58.8	30	98.4	68.5	50.5	3030	1091
71	Zylon	30X30	2	2	0.026	FS	25	95	312	112	82.9	20	65.6	107	79.2	4130	1487

[a] FS is blunt-ended fragment simulator; S-FS is sharp-ended fragment simulator.

[b] SEA = Specific energy absorbed = energy absorbed divided by areal density of the target. For tests with no penetration, the SEA value is a lower limit.

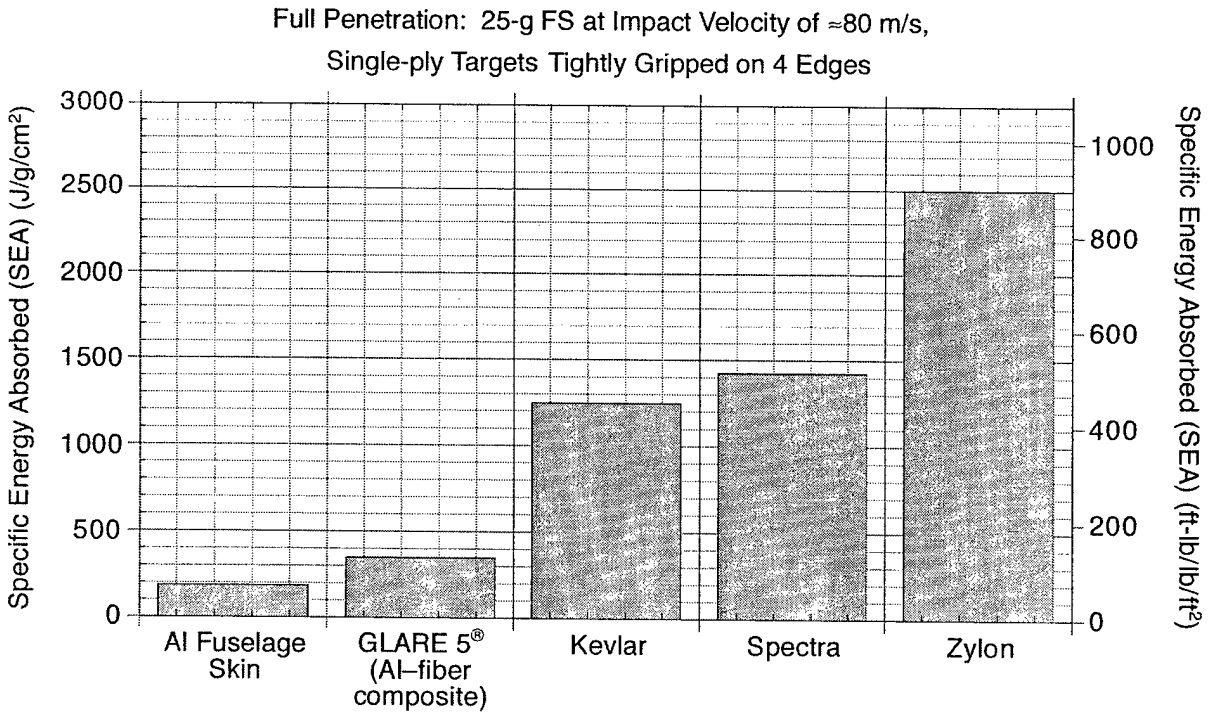

FIGURE 14. BALLISTIC RESULTS FOR A VARIETY OF MATERIALS

Impactor Sharpness. A sharp-edged impactor penetrates with much less energy absorption by a Zylon target than a blunt-edged impactor. Figure 15 compares the ballistic results (for single-ply Zylon 35 x 35 fabric targets) for impact tests with blunt-ended FS and sharp-ended S-FS impactors. For both 2-edge and 4-edge gripping, the SEA is significantly lower (46% less for 2-edge gripping, 35% less for 4-edge gripping) with the sharp impactor.

Attempts were made to improve the ballistic effectiveness of the Zylon fabric targets against a sharp impactor by using ungripped woven fabric or felt overlays. The impactor never perforated any of the overlays. The overlay wrapped itself around the impactor, and the impactor, cloaked within the overlay, penetrated the gripped target. Significant increases in the energy absorbed were obtained for tests with both 4-edge gripping (Tests 42 through 45, in table 5) and 2-edge gripping (Tests 53 through 56). Because of the additional weight of the overlays, a modest increase in the SEA was obtained for one test (Test 45) with 4-edge gripping.

GLUED FABRIC TARGETS. Although gripping the fabric tightly along two or four edges takes advantage of the high fiber strength in a fabric barrier, this method of holding the fabric is not likely to be practical. Weight considerations preclude the use of strong, rigid metal fixtures necessary for tight gripping. Small-scale impact tests were performed at SRI to explore alternative methods of fabric holding that are more practical, but still exploit the high fiber strength. Gluing the fabric directly to the impact side of an existing rigid fuselage material is a simple way to hold the fabric barriers and requires a very small amount of additional weight since there would be no gripping frame (the weight of the adhesive would be the only additional weight needed).

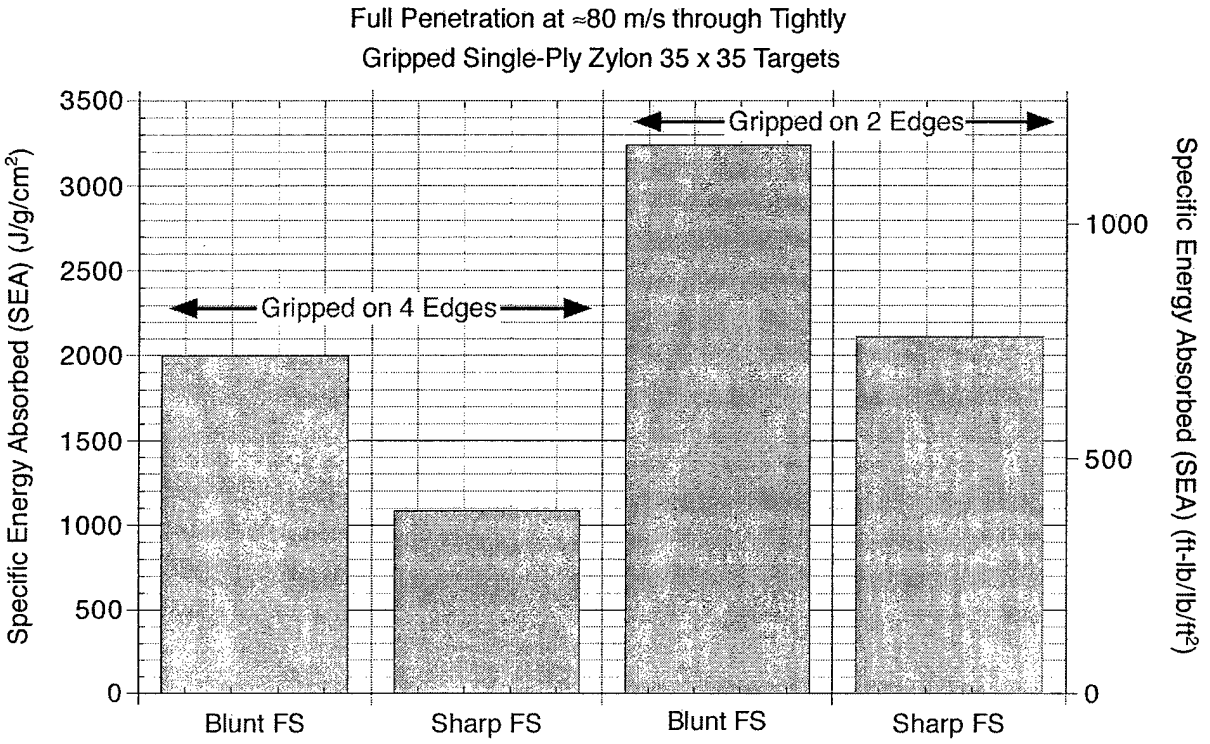

FIGURE 15. EFFECT OF IMPACTOR SHARPNESS AND TARGET BOUNDARY CONDITIONS

Two representative aircraft materials were selected to be the plates to which the fabric would be glued—IWPs and thin aluminum plates. Table 6 contains the experimental parameters and ballistics results for tests with the glued fabric targets, along with a few baseline impact tests that involve only an IWP or an aluminum panel. A full description of the experimental setup (including details of the gluing procedure), along with results of some early tests with the IWP and some photographs of the recovered targets, were presented previously [5]. These are briefly reviewed below along with the results of later tests on the IWP and aluminum panels.

Fabric Glued to an IWP. The IWP material, provided by United Air Lines,* is a lightweight, rigid sandwich structure 6.35 mm (0.25 in.) thick, consisting of a plastic honeycomb core bonded on both sides to thin two-dimensional fiber-reinforced resin sheets. Figure 13(d) shows how the 6-in.-square sections of the IWP were clamped; the roughly 5-in.-square Zylon fabric glued to the IWP did not extend into the clamped region. The 25-g FS impactor was used in these tests.

*Many different IWP materials and structures are used in airplanes. No attempt was made to characterize any particular IWP, but only to use a material that was readily available as an example of a representative IWP. The goal was to test the ballistic effectiveness of this fabric holding scheme. (For purpose of documentation, this IWP was labeled "Gillfab 4122A Faceside, 250 x 48 x 96 .020/.020, 3/16 - 3.0 lb core, SHE 2904C0250-202 REVNC, LOT 30144 mfg. 11/9/95.")

TABLE 6. GAS GUN IMPACT TESTS WITH ZYLON FABRICS GLUED TO AN IWP OR ALUMINUM PANEL[a]

Test No.	Target Components				Impactor[b]				Impact Results	Residual		K.E.		Total SEA[c]		Additional SEA[d]	
	Plies	Material	Mass	Areal Density	Velocity		K.E.			Velocity		Absorbed		(J / g/cm^2)	(ft-lb / lb/ft^2)	(J / g/cm^2)	(ft-lb / lb/ft^2)
			(g)	(g/cm^2)	(m/s)	(f/s)	(J)	(ft-lb)		(m/s)	(f/s)	(J)	(ft-lb)				
27	1	IWP[e]	55.3	0.238	76	249	72	53	Penetration	54.5	179	35	26	147	53	——	——
28	1	IWP	53.4	0.230					No Penetration: impactor rebounded after severing some Zylon yarns in impact region and damaging IWP near edges at 0°, 90° 180°, & 270°; negligible debonding of fabric from IWP								
	1	Zylon 45x45	3.73	0.022													
		Adhesive[f]	1.6	0.009													
		Total	58.7	0.2614	77	251	73	54		——	——	73	54	≥ 280	≥ 101	≥ 1211	≥ 436
30	1	IWP	55.1	0.237					No Penetration: impactor rebounded after severing some Zylon yarns in impact region and damaging IWP near edges at 90° 270°; negligible debonding of fabric from IWP								
	1	Zylon 40x40	2.9	0.018													
		Adhesive[f]	1.6	0.010													
		Total	59.6	0.2659	79	257	77	57		——	——	77	57	≥ 290	≥ 104	≥ 1462	≥ 526
31	1	IWP	54.9	0.236					Penetration: damage to IWP plate limited to region in and around impact zone; no debonding of fabric from IWP								
	1	Zylon 40x40	2.9	0.018													
		Adhesive[f]	1.6	0.010													
		Total	59.4	0.2651	96	315	115	85		66.0	216	61	45	229	83	895	322
64	1	IWP	53.9	0.232					No Penetration: impactor rebounded after severing some Zylon yarns in impact region, bending IWP (on 90-270° axis), and forcing it part way through mounting frame; negligible debonding of fabric from IWP.								
	1	Zylon 40x40	3.0	0.019													
		Adhesive[g]	1.2	0.008													
		Total	58.1	0.251	95	312	113	83		——	——	113	83	≥ 450	≥ 162	≥ 4113	≥ 1481
6	1	Al2024T3	64.2	0.274	95	312	112	83	Penetration	61.8	203	65	48	237	85	——	——
8	1	Al2024T3	64.2	0.274	81	266	82	60	Penetration	50.7	166	50	37	182	66	——	——
65	1	Al2024T3	64.2	0.276					Penetration: both Zylon and aluminum completely perforated; Zylon completely debonded from aluminum on one of four edges.								
	1	Zylon 40x40	3.0	0.019													
		Adhesive[g]	1.1	0.007													
		Total	68.3	0.295	95	310	112	82		27.7	91	102	75	346	124	2436	877

[a] Tests of the IWP alone and the aluminum panel alone (Tests 27, 6, and 8) are included for baseline information.

[b] Impactor is the blunt-ended 25-g fragment simulator (FS).

c The energy absorbed per unit areal density of the entire target (including the IWP or Al panel, the fabric, and the adhesive).

[d] Increase of the energy absorbed due to the addition of the fabric (as compared to the same impact conditions without the fabric), divided by the unit areal density of the added fabric and adhesive.

[e] Interior wall panel provided by United Air Lines.

[f] Shell Epon 815 adhesive was used over the entire face of the fabric panel.

[g] Adhesive was used only over a 1-in.-wide periphery around edge of fabric, leaving approximately a 3-in.-square unglued region.

Ballistic results for the series of tests with a single-ply of Zylon 40 x 40 fabric glued to an IWP (Tests 30, 31, and 64) are shown in figure 16, compared with a test with the IWP alone (Test 27). Although the addition of the Zylon (and the adhesive) increases the total target areal density by only about 8%, it increases the energy absorbed by more than a factor of 300%. When the Zylon is glued over the entire Zylon surface, it is less ballistically effective than when it is tightly gripped along four edges. The additional SEA shown is only about half of the ≈2500 J/g/cm^2 SEA determined from a similar 4-edge gripped test (Test 24) listed in table 5. However, when the Zylon is glued around the periphery of the target only, the additional SEA jumps to over 4000 J/g/cm^2, much higher than the SEA from either the 4-edge or the 2-edge-gripped test.

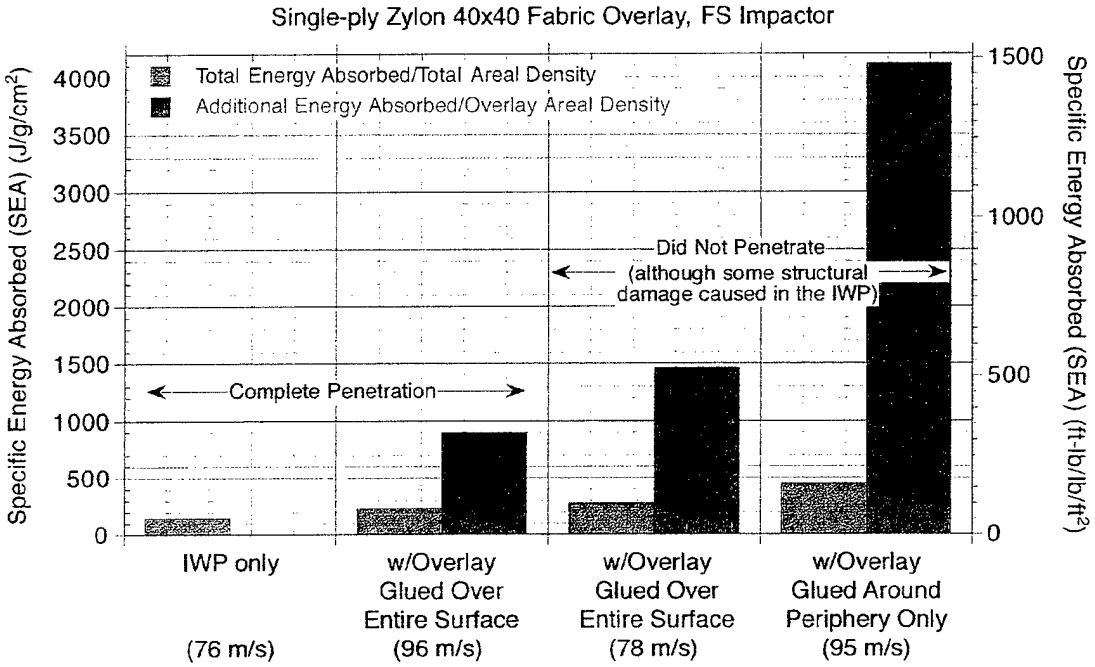

FIGURE 16. BALLISTICS RESULTS FOR ZYLON GLUED TO IWP

Since the amount of energy that a yarn can absorb by stretching before failure is proportional to the length of the yarn, it was expected that fabrics with longer distances between their held ends (either by gripping or gluing to a rigid panel) would absorb more energy before failure. This explains the large difference in absorbed energy between the fabric glued over its entire surface and the fabric glued along its periphery only. In the former, the ability of the yarn to stretch is limited to the region close to impact where the fabric debonds from the panel, while in the latter, the yarn can stretch along the distance between the peripheral glued regions. In the latter case, structural damage to the IWP, caused by the fabric's resistance to penetration, contributed to the large additional SEA.

Fabric Glued to an Aluminum Panel. A plate of aluminum fuselage skin, 1 mm (0.04 in.) thick Al 2024-T3, was selected for the glued fabric impact test, since baseline tests of these plates without any fabric, impacted by the 25-g blunt-ended FS, have been performed [2]. Results are given in table 6 (Tests 65) and shown in figure 17, along with results for similar impact tests of the aluminum plate alone and the Zylon fabric alone.

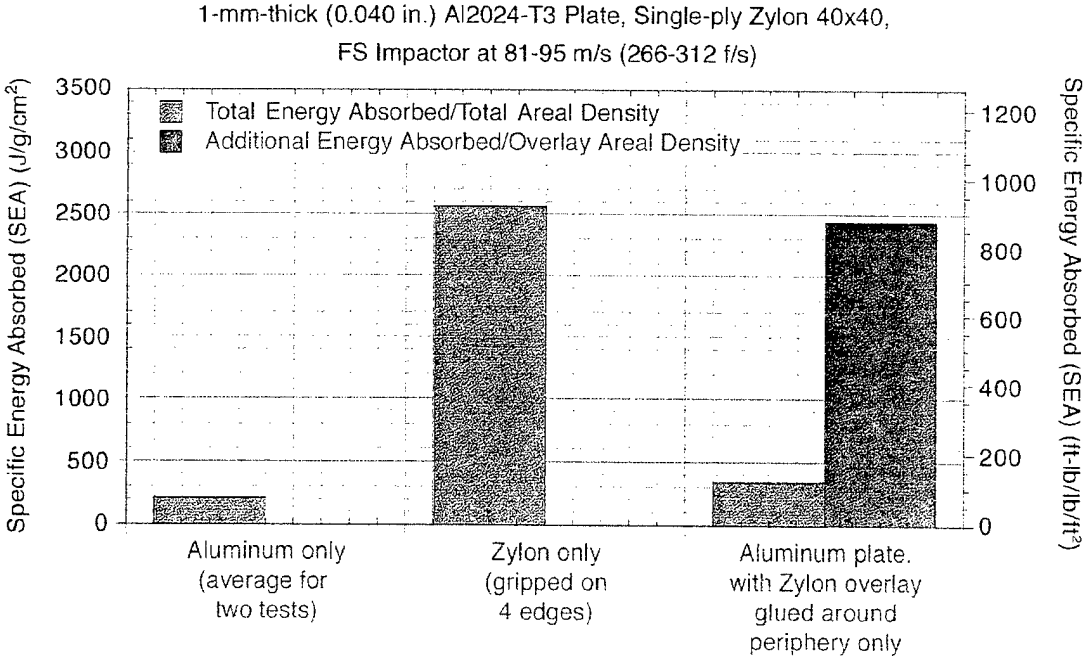

FIGURE 17. BALLISTICS RESULTS FOR ZYLON GLUED TO AN ALUMINUM PLATE

The aluminum plates recovered from tests with and without the Zylon overlay show the same failure mechanism, namely shear failure through the plate along the impact edges, followed by a petaling back of the perforated lobes. There is a larger region of deformation in the plate with an overlay, indicating that the fabric has spread the load over a wider region. The addition of the Zylon and the adhesive increases the total target areal density by only about 6%, but it increases the energy absorbed by an average of nearly 80%. The additional SEA was very nearly as large as the SEA of the Zylon alone, when gripped on four edges.

Conclusions About Glued Fabrics. Gluing high-strength fabric plies to existing aircraft structures is a simple method of installing fragment barriers. It adds relatively little excess weight, while significantly increasing fragment penetration resistance. The ballistics results for glued fabrics (provided the glue is applied around the periphery only, rather than over the entire fabric) are comparable to those of tightly gripped fabrics, indicating that gluing exploits the high fiber strength of the fabric about as much as tight gripping.

To design a fragment barrier of this type, one would also need to consider the failure of the structure to which the barrier is attached. One needs to examine the amount of energy needed to cause structural failure, the mode of failure, how that might change with the presence of the barrier, and the consequence of that failure.

For example, an unfortified IWP was easily perforated without structural damage by the FS impactor. But with a fabric barrier glued to it sufficient to prevent perforation, the IWP sustained significant structural damage extending far from the immediate impact region. In some of the fuselage impact tests at China Lake, IWPs were torn completely off the frame to which they were attached. Perhaps minor modifications in the frame attachment hardware can prevent this, or perhaps it is more beneficial to have a large panel of IWP moving inward into the

fuselage at a low velocity rather than a single hard fragment moving through at a much higher velocity.

So far only thin flat aluminum plates, which are relatively easy to deform, were tested with a glued fabric barrier. Further testing is needed with less deformable materials, such as titanium or thicker aluminum, to determine if the fabric barriers would remain as effective. Also, stand-offs which would hold the fabric overlay at a distance from the substrate need to be tested. Standoffs would allow the fabric to deform more before impacting the structure, and thereby possibly increase the absorbed energy.

LARGER-SCALE IMPACT TESTS AT CHINA LAKE.

Larger-scale impact experiments were performed in 1998 at the Navy Air Warfare Center's 6-in.-bore gas gun facility at China Lake, CA, to examine more realistic engine fragment impact scenarios. The experimental setup is shown in figure 18. A 12-in.-wide sheet of Zylon 40 x 40 fabric was continuously wrapped around two rigid rods to form targets with areal densities ranging from 0.0185 g/cm^2 (0.0378 lb/ft^2) for one ply to 0.166 g/cm^2 (0.34 lb/ft^2) for nine plies. The wrapped edges were clamped tightly by a second set of rods (see figure 19) to produce the equivalence of two-edge gripping.

Parameters for these tests and the ballistics results are shown in table 7. Impactors for these tests included relatively sharp-ended full-scale fan blade (FB) and turbine blade (TB) fragments from aircraft engines, with dimensions up to 13 x 8 x 1 cm (5 x 3 x 0.4 in.) and masses up to 194 g (0.43 lb), as well as a blunt-ended 25-g (0.005-lb) fragment simulator similar to SRI's FS. Impact velocities ranged from 106 to 210 m/s (349 to 687 ft/s) and kinetic energies ranged from 448 to 4250 J (330 to 3135 ft-lb).

Final velocities were often quite different from intended velocities, and the impactors tumbled as they left the barrel, so there was little control of the impact orientation. The impactor rarely impacted edge-on, as can be seen from the often large values of the pitch and yaw and the wide range in presented areas of impact for the same impactor. Because of the nonrepeatability of the impact velocity and orientation, it was impossible to perform a systematic study of the effect of various impactor or target parameters on the ballistic resistance. However, since an uncontained aircraft engine fragment scenario might involve a large range of fragment masses, velocities, and impact orientations, these tests nevertheless yielded a large set of realistic ballistic data.

In two of the tests (Tests CL-11 and CL-12), an overlay of four plies of Zylon felt was lightly taped to the impact side of the gripped fabric. The addition of the felt was successful, in that no penetration occurred in these two tests, whereas similar tests without the felt (Tests CL-9 and CL-1) had penetration. The additional weight of the four plies of felt decreased the total SEA somewhat, but a direct correlation cannot be made because the orientations and resultant areas of impact in the comparable tests were different.

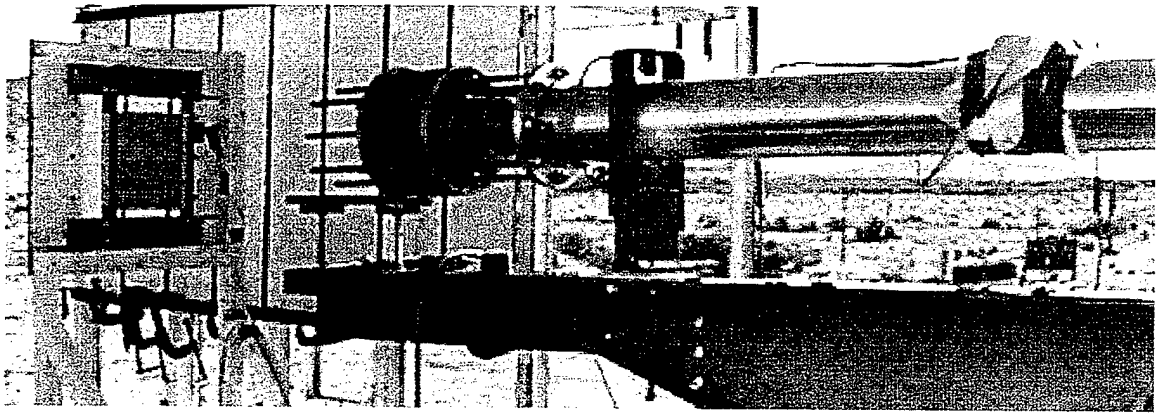

(a) 6-in.-bore gas gun muzzle and target mounting stand

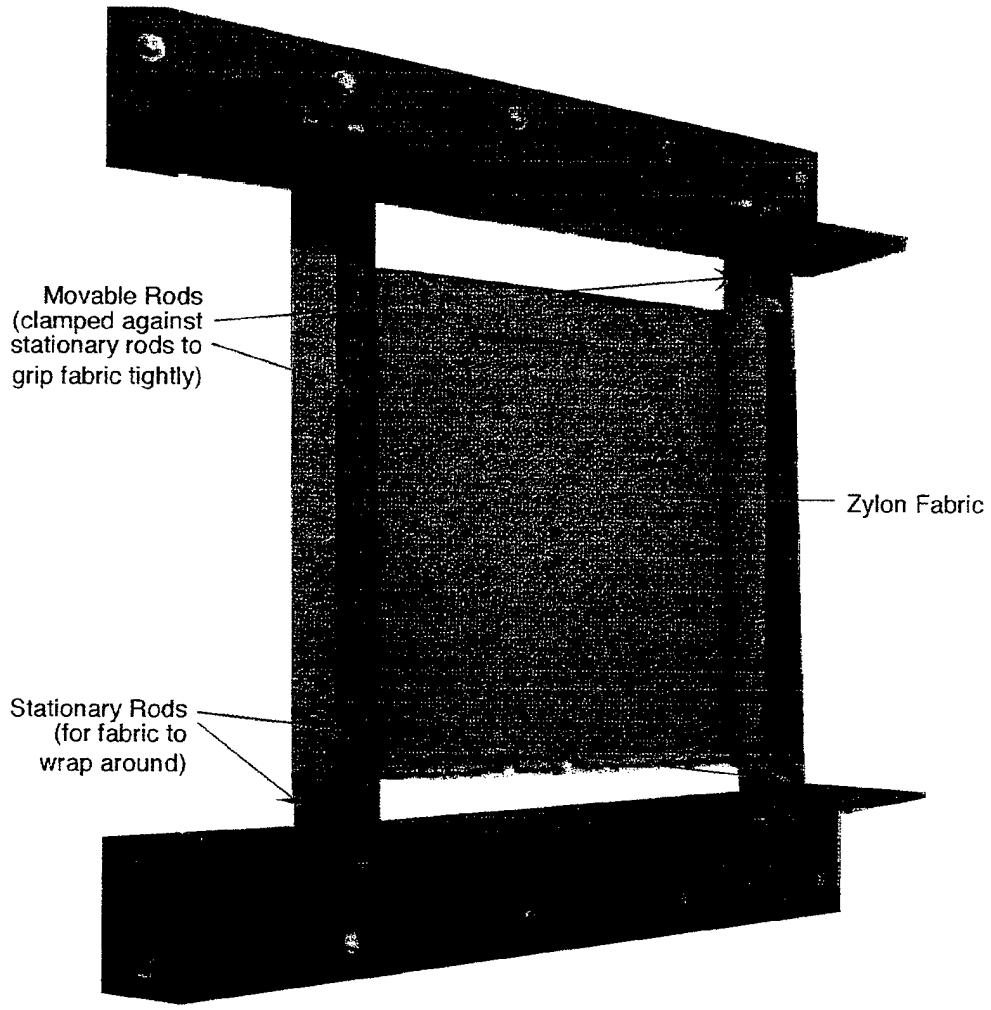

(b) Target gripping apparatus

FIGURE 18. EXPERIMENTAL SETUP FOR LARGER-SCALE IMPACT TESTS AT CHINA LAKE

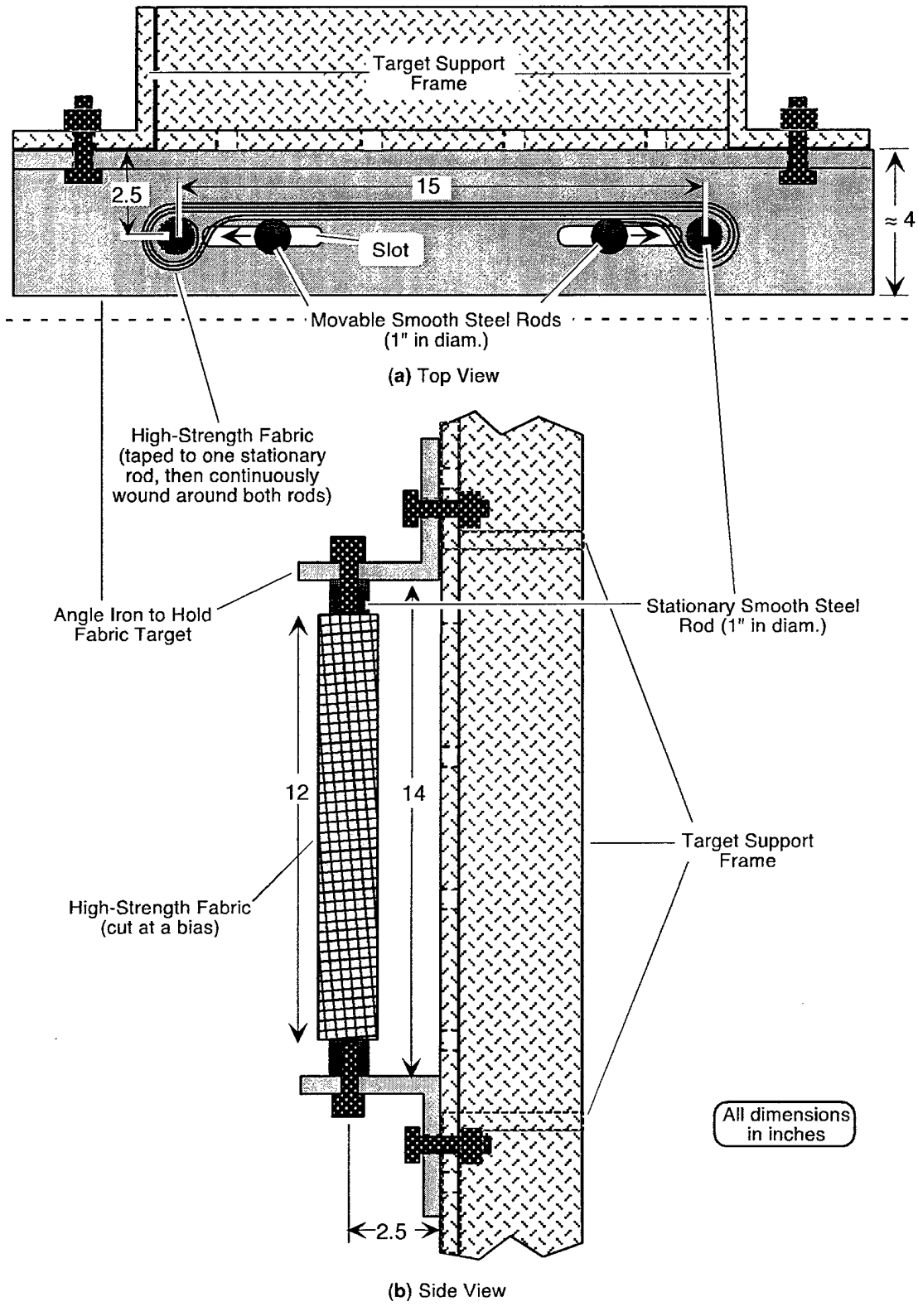

FIGURE 19. DETAILS OF TARGET CLAMPING APPARATUS FOR CHINA LAKE TEST

TABLE 7. TEST PARAMETERS AND BALLISTICS RESULTS FOR LARGER-SCALE IMPACT TESTS AT CHINA LAKE

SRI Test No. / China Lake Test No.		CL-1 71	CL-2 72	CL-3 73	CL-4 74	CL-5 75	CL-6 76	CL-8 79	CL-9 80	CL-12 83	CL-10 81	CL-11 82
Impactor[a]		CL-FS	TB	TB	CL-FS	FB	FB	FB	CL-FS	FB	CL-FS	CL-FS
Dimensions	(≈ in.)	1.4x1x.25	4x1.4x.15	4x1.4x.15	1x1.4x.25	5x3x.2	5x3x.14	5x3x.2	1.4x1x.25	4x3x.34	1.4x1x.25	1.4x1x.25
Mass	(lb)	0.055	0.174	0.174	0.055	0.336	0.320	0.321	0.055	0.427	0.055	0.055
Mass	(g)	25.1	79.1	79.1	25.1	152.4	145.1	145.5	24.8	193.8	24.9	24.9
Intended Velocity	(f/s)	450	350	450	450	450	375	350	250	550	250	450
Measured	(f/s)	632	349	432	679	486	350	357	382	687	367	640
Impact Velocity	(m/s)	192.7	106.4	131.7	207.0	148.2	106.7	108.8	116.5	209.5	111.9	195.1
Kinetic	(ft-lb)	344	330	506	397	1,234	609	636	124	3,136	115	350
Energy	(J)	465.9	447.8	686.1	537.8	1,673	826.1	861.8	168.2	4,251	155.9	474.0
Orientation[b]:	Pitch: ° down	-23	81	-18	-4	-20	-70	32	-7	-47	52	20
(last frame	Yaw: ° left	26	-21	26	-3	-15	-13	11	-32	19	50	-4
before impact)	Roll: ° c.w.	26	56	44	-43	-49	-82	73	52	31	-38	-5
Presented Area	(in.)	0.58	1.94	1.03	0.29	1.21	1.26	5.07	0.93	7.00	0.78	0.72
of Impact	(cm)	3.74	12.52	6.65	1.87	7.81	8.13	32.71	6.00	45.16	5.03	4.65
Target[c] Zylon	40x40: Plies	3	5	3	3	5	5	3	1	9	1	3
	Zylon Felt: Plies	0	0	0	0	0	0	0	0	0	4	4
Areal (incl.	(lb/ft^2)	0.1134	0.1890	0.1134	0.1134	0.1890	0.1890	0.1134	0.0378	0.3402	0.1034	0.1790
Density felt)	(g/cm^2)	0.0555	0.0925	0.0555	0.0555	0.0925	0.0925	0.0555	0.0185	0.1665	0.0505	0.0874
Ballistics Results[d]		Full Pen.	No Perf.	Full Pen.	Full Pen.	Full Pen.	Part. Perf.	Full Pen.	Full Pen.	Full Pen.	No Perf.	Part. Perf.
Residual	(f/s)	139	—	314	228	244	—	57	153	33	—	—
Velocity	(m/s)	42.4	—	95.7	69.5	74.4	—	17.4	46.6	10.1	—	—
Residual	(ft-lb)	16.6	0.0	267.3	44.7	311.0	0.0	16.2	19.9	7.2	0.0	0.0
Kinetic Energy	(J)	22.5	0.0	362	60.6	422	0.0	22.0	27.0	9.8	0.0	0.0
Energy	(ft-lb)	327	330	239	352	923	609	619	104	3128	115	350
Absorbed	(J)	443	448	324	477	1,251	826	840	141	4,241	156	474
SEA (Specific	($ft\text{-}lb/lb/ft^2$)	2,884	≥ 1747	2,105	3,104	4,883	≥ 3224	5,463	2,755	9,195	≥ 1112	≥ 1953
Energy Asorbed)	($J/g/cm^2$)	7,989	≥ 4841	5,831	8,598	13,527	≥ 8931	15,133	7,633	25,473	≥ 3087	≥ 5423

[a] CL-FS was a China Lake fragment simulator (similar to SRI's FS); TB and FB were fragments from turbine and fan blades, respectively, from aircraft engines.

[b] Orientations and presented areas were determined by Chuck Manchor of NAWC-China Lake from somewhat indistinct views of the impactors from two orthogonal cameras. Pitch angle is down from the gun axis, yaw is left of the gun axis, and roll is counter-clockwise from vertical.

[c] Zylon 40 x 40 woven fabric, tightly gripped on two sides, was used for all tests. Zylon felt was used as an ungripped overlay for Tests 10 and 11.

[d] No Perforation — negligible damage to the first fabric ply. Partial Perforataion — the impactor penetrated through some but not all of the plies.

Figure 20 graphs the ballistics results of all the gripped Zylon fabric tests performed in this program, including both the China Lake and SRI tests. The SEAs for the SRI tests with the 25-g impactors cluster around 2500 J/g/cm^2 (900 ft-lb/lb/ft^2), but those for the China Lake tests with the 25-g impactors cluster around 8000 J/g/cm^2 (2880 ft-lb/lb/ft^2). For the larger (145-194 g) FB impactors, the SEAs span the range from 13,500 to over 25,000 J/g/cm^2 (4860 to over 9000 ft-lb/lb/ft^2). Several factors may enter into this increase:

- Impactor size and presented impact area. A larger impactor has a larger presented area of impact, it needs to break more yarns to penetrate. So does an impactor that does not hit end-on, but instead hits at orientations with significant pitch or yaw.

- Fabric target dimensions. A longer yarn absorbs more deformational energy before failure than an identical shorter yarn. Therefore, the 12-in.-square targets used in the China Lake tests should absorb more energy than the roughly 6-in.-square targets used in the SRI tests.

- Number of fabric plies. As discussed in the section on the SRI gripped fabric tests, SEAs for multiple-ply targets have been found to be higher than those for single-ply targets.

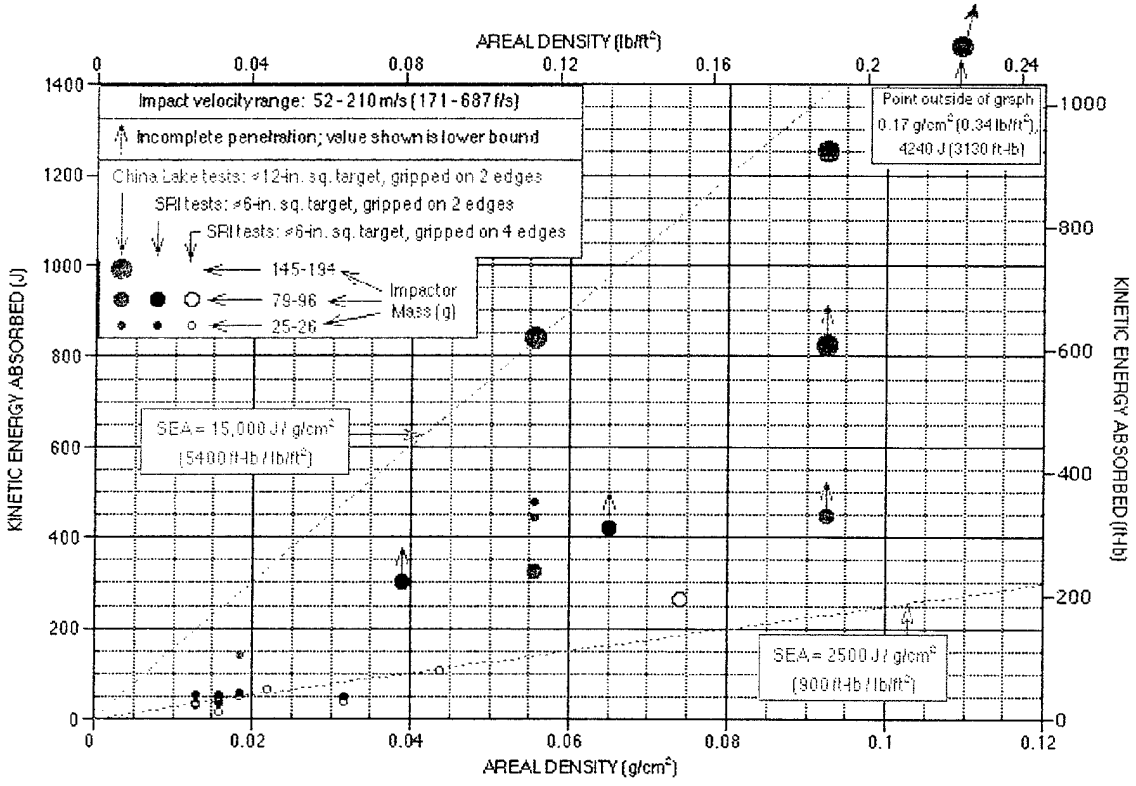

FIGURE 20. BALLISTICS RESULTS FOR ALL GRIPPED ZYLON FABRIC IMPACT TESTS AT SRI AND CHINA LAKE

Because there is currently insufficient data concerning the independent variation of these factors (impactor size and orientation, target size, and number of plies) over an adequate range, the influence of these factors cannot yet be delineated on the energy absorbed during fragment penetration. Further testing is needed to make such a determination. However, from the results of these larger-scale China Lake impact tests, it can be estimated that a relatively low areal density Zylon fabric (gripped on two edges)—roughly between 0.15 and 0.25 g/cm^2 (0.3 and 0.5 lb/ft^2)—can stop a relatively large engine fragment (roughly 200 g, or nearly 0.5 lb) traveling at a realistic engine fragment exit velocity (slightly more than 200 m/s, or nearly 700 ft/s).

QUASI-STATIC PENETRATION (PUSH) TESTS

A knowledge of the evolution and phenomenology of high-strength fabric target deformation and failure during fragment impact and penetration is important in designing an efficient fabric barrier and in developing and validating a computational fabric model. To assist in attaining this knowledge, a test was developed and implemented in the previous year of this program that allowed a rigidly held fragment to be pushed at a constant speed into and through a fabric target.

This section reviews the experimental technique (described in detail in reference 5), summarizes the key results (some of which are presented in reference 6), and discusses the phenomenology of fabric target failure.

EXPERIMENTAL TECHNIQUE.

The experimental setup is shown in figure 21. The test was performed on an MTS servo-hydraulic mechanical testing machine. Fabric panel targets were the same shape as those used in the gas gun impact tests, previously shown in figures 13(a) and 13(b), and they were mounted and clamped horizontally on the same mounting frame and support structure shown in figure 13(c). This structure was attached, through the load cell, to the crosshead of the MTS. A fragment simulator or actual compressor blade was rigidly attached to the top of the ram, and as the ram stroked upward (at constant rates from 0.0075 to 7.5 in./s), the fragment was forced into and through the target. The ram deflection and load were measured, and the energy absorbed by the fabric was determined by integrating the load-deflection curve.

A front-surface mirror, positioned inside the support structure at 45° to the target surface, illuminated the top surface of the fabric target. A video camera was positioned to look at the deforming target from two directions simultaneously (see the inset in figure 21): (1) at a very low angle to show the profile of the deforming fabric and (2) at an angle of 90° (through the mirror) to better observe yarn failure. The deformation and failure phenomena seen on the videotape, along with the acoustic emissions recorded with a microphone (a distinct popping sound accompanies a yarn break), were correlated in time with the features on the recorded load/deflection history for a clearer understanding of the evolution of damage and how the various damage phenomena affected the energy absorption capabilities of the fabric target.

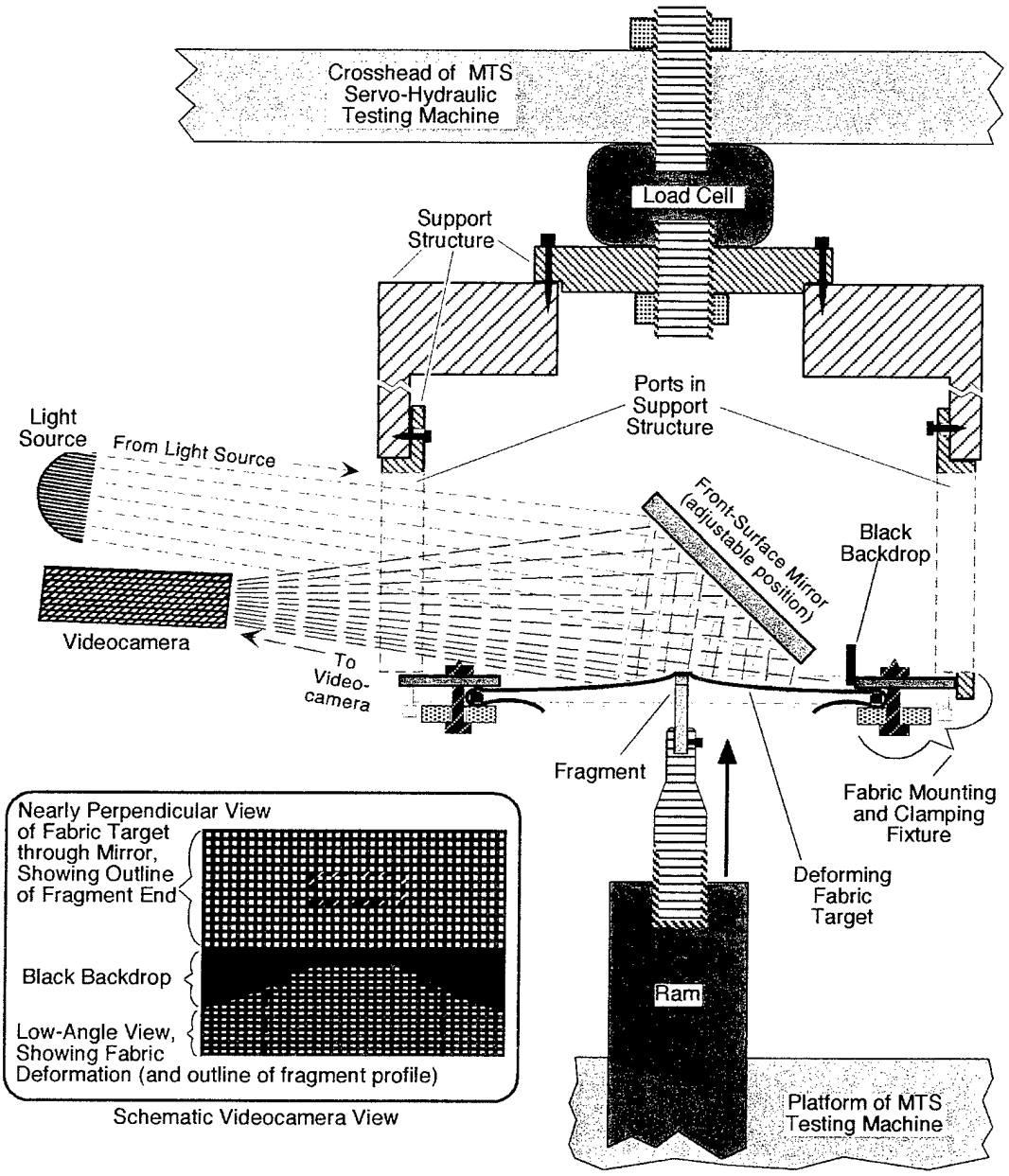

FIGURE 21. EXPERIMENTAL CONFIGURATION FOR FRAGMENT PUSH TESTS

An example of the time correlation capability is given in figures 22 and 23. Figure 22 shows selected video camera frames taken during a push test (Test P-6) in which a blunt-edged fragment simulator penetrated a single-ply target of Zylon 35 x 35 fabric gripped on four edges at a stroke rate of 0.0075 in./s. Individual yarns are clearly visible. The overall deformation profile can be seen, as can the individual yarns that break at late stages in the deformation, before complete fabric perforation. With the aid of acoustic emissions, these individual yarn failures can be precisely correlated to the load-deformation curve, shown in figure 23. The inset shows three sharp drops in the load, which occur as a result of one or more yarn failures. The first of these drops corresponds to the first yarn failure shown in the two consecutive video frames in figures 22(c) and 22(d).

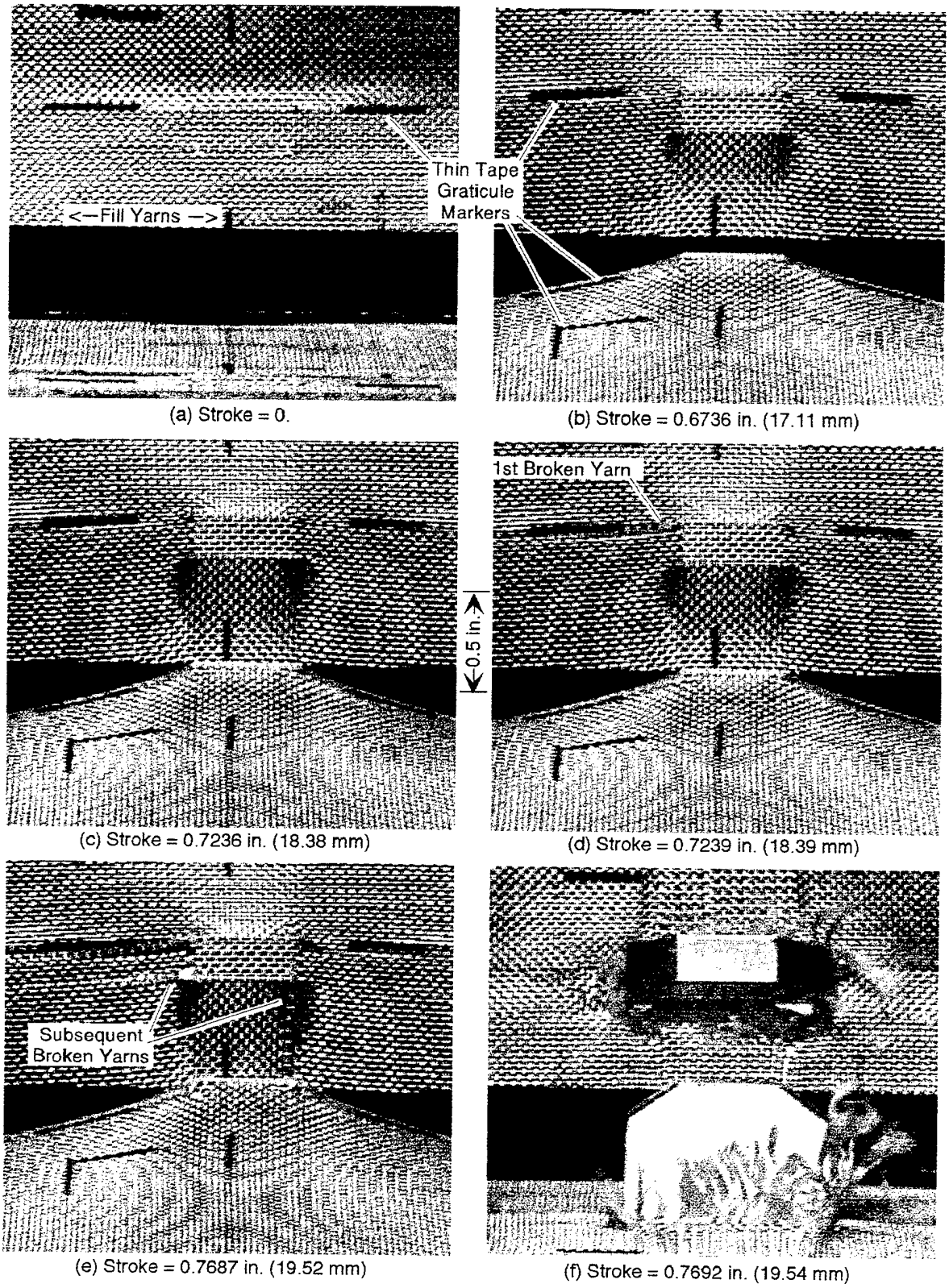

FIGURE 22. ZYLON FABRIC DEFORMATION AND FAILURE FROM FRAGMENT PUSH TEST

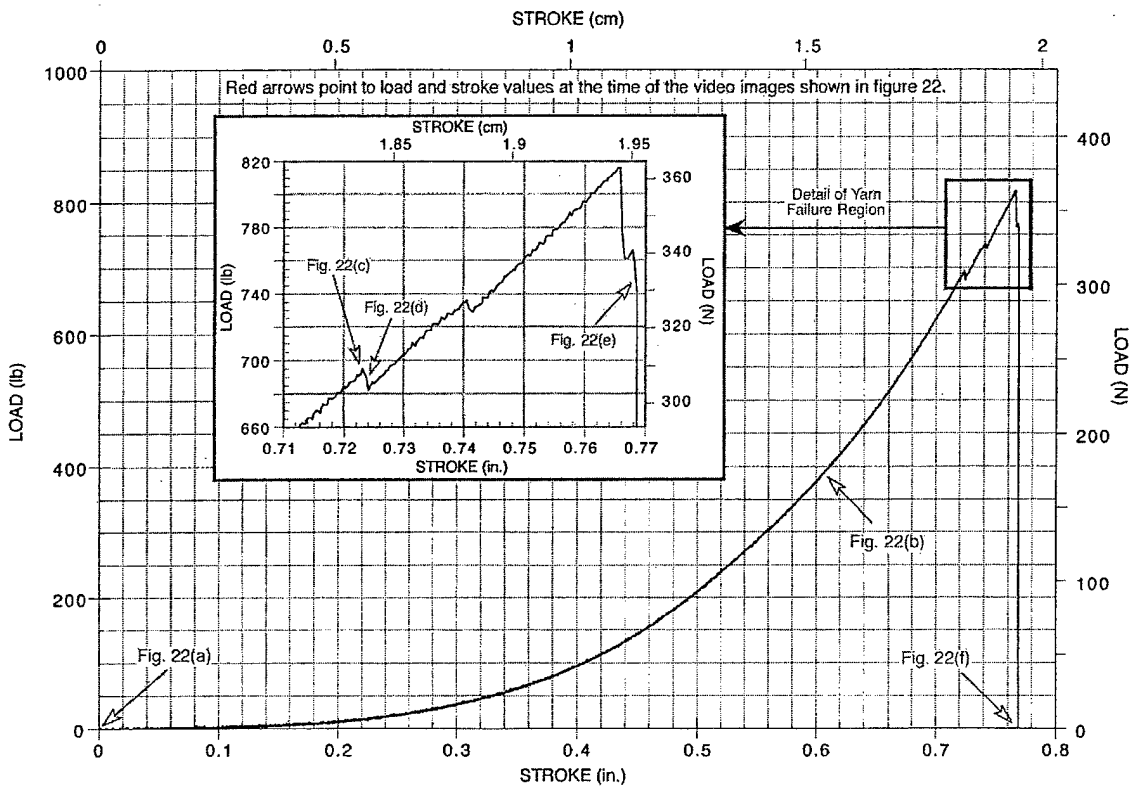

FIGURE 23. LOAD-DEFLECTION CURVE FROM FRAGMENT PUSH TEST: BLUNT-EDGED FS INTO ONE-PLY ZYLON 35 x 35 TARGET

TEST MATRIX AND RESULTS.

Table 8 is a matrix of the 37 push tests that were performed using the high-strength fabric materials of interest. Shown are the test parameters and some test results, maximum load and modulus (load divided by stroke), total energy absorbed by the fabric, and the SEA. Tests included a wide range of target designs (including a variety of fabric materials, mesh densities, number of plies, and gripping geometries), three types of fragment penetrator, and a range of penetration rates and orientation (roll) angles.

The three types of penetrators used are shown in figure 24. They were designated: (1) the FS which is the blunt-ended 25-g fragment simulator previously described for the gas gun tests (see figure 12(b)); (2) the FB, an actual compressor blade, whose slightly-slanted sharp impact edge is ≈1.3 in. wide, with a thickness that tapers from ≈0.050 in. at the center to <0.015 in. at both ends; and (3) the S-FS, a sharp-ended fragment simulator, whose impact edge width is the same as the FS, namely, 1.0 in., but whose thickness profile and impact edge taper are similar to the FB (see figure 12(c)).

Key results attained from a variation of the test parameters in table 8 are described below.

TABLE 8. PARAMETERS AND SOME RESULTS FOR QUASI-STATIC PENETRATION (PUSH) TESTS

Test No.	Target		No.	Areal Density	Gripped Edges[a]			Penetrator		Stroke	Maximum		Energy		SEA[f]	
	Material	Weave			No.	Yarns	Width	Type[b]	Roll[c]	Rate[d]	Load	Modulus	Absorbed[e]		$\left(\frac{J}{g/cm^2}\right)$	$\left(\frac{ft-lb}{lb/ft^2}\right)$
		(Yarn/in.)	Plies	(g/cm^2)		Held	(in.)		(°)	(in./s)	(lb)	(lb/in.)	(J)	(ft-lb)		
P-1	Zylon	35X35	1	0.016	4	W & F	5.0	FS	0	0.075	894	3640	19.1	14.1	1208	435
P-2	Zylon	35X35	1	0.016	4	W & F	5.0	FS	0	0.075	916	3389	22.1	16.3	1402	505
P-3	Zylon	35X35	1	0.016	4	W & F	5.0	FS	0	7.5	955	3386	22.2	16.4	1406	506
P-4	Zylon	35X35	1	0.016	4	W & F	5.0	FS	0	0.075c,i	897	4087	>13.7	>10.1	865	>311
P-5	Zylon	35X35	1	0.016	4	W & F	5.0	FS	0	0.0075	829	3040	20.1	14.8	1270	457
P-6	Zylon	35X35	1	0.016	4	W & F	5.0	FS	90	0.0075	816	2980	17.1	12.6	1080	389
P-7	Zylon	35X35	1	0.016	2	F	5.0	FS	0	0.075	895	2537	—	—	—	—
P-8	Zylon	35X35	1	0.016	4	W & F	1.5	FS	0	0.075	610	1209	—	—	—	—
P-9	Zylon	40X40	1	0.019	4	W & F	5.0	FS	0	0.075	1111	3137	32.1	23.7	1733	624
P-10	Zylon	30X30	1	0.0130	4	W & F	5.0	FS	0	0.075	592	2886	13.4	9.9	1032	372
P-14	Zylon	35X35	1	0.016	2	F	5.0	FS	0	0.0075	643	1600	92.0	67.8	5821	2095
P-15	Zylon	35X35	1	0.016	2	F	5.0	FS	0	0.0075i	647	1910	>105.2	>77.6	6657	>2397
P-16	Zylon	35X35	1	0.016	2	F	5.0	FS	0	0.0075	625	1816	72.8	53.7	4605	1658
P-17	Zylon	35X35	1	0.016	2	F	5.0	FS	0	0.0750	542	1744	39.8	29.3	2517	906
P-18	Zylon	35X35	1	0.016	2	F	5.0	FS	0	0.7500	662	1806	99.9	73.7	6321	2276
P-19	Zylon	35X35	1	0.016	2	F	5.0	FS	0	7.5000	677	1887	48.8	36.0	3089	1112
P-20	Zylon	35X35	1	0.016	4 Corners[g]		3.25	FS	0	0.0075	634	487	66.8	49.3	4226	1521
P-21	Zylon	35X35	1	0.016	4	W & F	5.0	FS	45	0.075	596	2214	30.3	22.3	1916	690
P-22	Zylon	35X35	1	0.016	4	W & F	5.0	FB	45	0.075	153	742	4.7	3.5	300	108
P-23	Zylon	35X35	1	0.016	4	W & F	5.0	FB	45	0.075	634	2545	24.9	18.3	1573	566
	Zylon	Felt	2	0.0160	Not gripped			Total Areal Density = 0.0318								
P-24	Zylon	35X35	2	0.032	4	W & F	5.0	FB	45	0.075	534	2299	20.0	14.8	633	228
P-25	Zylon	35X35	1	0.016	4	W & F	5.0	FB	45	0.075	546	2597	22.6	16.7	1430	515
	Zylon	35X35	1	0.016	Not gripped			Total Areal Density = 0.0316								
P-26	Zylon	35X35	1	0.016	4	W & F	5.0	FB	45	0.075	484	1778	23.5	17.3	1487	535
	Zylon	Felt	1	0.0080	Not gripped			Total Areal Density = 0.0238								
P-27	Zylon	35X35	1	0.016	2	F	5.0	FS	45	0.075	589	1688	72.6	53.6	4598	1655
P-28	Zylon	35X35	1	0.016	2	F	5.0	FB	45	0.075	277	954	19.7	14.5	1244	448
P-29	Zylon	35X35	1	0.016	2	F	5.0	FB	45	0.075	506	1585	77.6	57.3	4912	1768
	Zylon	Felt	2	0.0160	Not gripped			Total Areal Density = 0.0318								
P-30	Zylon	35X35	1	0.016	2	F	5.0	FB–r	45	0.075	214	829	13.6	10.0	858	309
P-31	Zylon	35X35	1	0.016	2	F	5.0	FB–r	45	0.075	478	1301	74.7	55.1	4727	1702
	Zylon	Felt	2	0.0160	Not gripped			Total Areal Density = 0.0318								
P-32	Kevlar	32X32	1	0.011	4	W & F	5.0	FS	90	0.075	336	1489	7.2	5.3	640	230
P-33	Spectra	32X32	1	0.011	4	W & F	5.0	FS	90	0.075	577	2631	12.0	8.8	1109	399
P-34	Kevlar	32X32	1	0.011	4	W & F	5.0	FS	90	7.5	342	1219	7.1	5.3	630	227
P-35	Zylon	35X35	1	0.016	2	F	5.0	FB	0	0.075	288	1127	12.0	8.8	758	273
P-36	Zylon	35X35	1	0.016	2	F	5.0	FB	0	0.075	587	1773	106.5	78.6	6743	2427
	Zylon	Felt	2	0.0160	Not gripped			Total Areal Density = 0.0318								
P-37	Zylon	35X35	1	0.016	2	F	5.0	S-FS	0	0.075	269	974	9.2	6.8	579	209
P-38	Zylon	35X35	1	0.016	2	F	5.0	S-FS	0	0.075	532	1475	48.9	36.1	3096	1115
	Zylon	Felt	2	0.0160	Not gripped			Total Areal Density = 0.0318								
P-39	Zylon	35X35	1	0.016	2	F	5.0	S-FS	0	0.075	453	1437	43.8	32.3	2774	999
	Zylon	35X35	1	0.016	Not gripped			Total Areal Density = 0.0316								
P-40	Zylon	35X35	2	0.032	2	F	5.0	S-FS	0	0.075	697	2306	36.3	26.8	1148	413

[a] W = warp yarns; F = fill yarns. Distance between grips is ≈7.2 in.

[b] FS = fragment simulator (blunt-edged, 1 in. wide, 0.25 in. thick); FB = actual fan blade (sharp-edged, 1.3 in. wide, 0.015-0.050 in. thick), FB–r = FB with rounded corners, S-FS = sharp-edged fragment simulator (1 in. wide, same thickness variation as FB).

[c] The angle between the direction of the warp yarns and the longest dimension of the penetrator's impact end (e.g. the blade direction).

[d] Tests involve constant stroke rate to complete penetration, except "c" = cyclical loading, "i" = interrupted before full penetration.

[e] Equals the area under the load-deflection curve.

[f] SEA = Specific Energy Absorbed = energy absorbed divided by areal density of the target.

[g] Specimen is 7.2 in. square, ungripped for 2.7 in. on each edge, gripped along diagonal (3.25 in. wide).

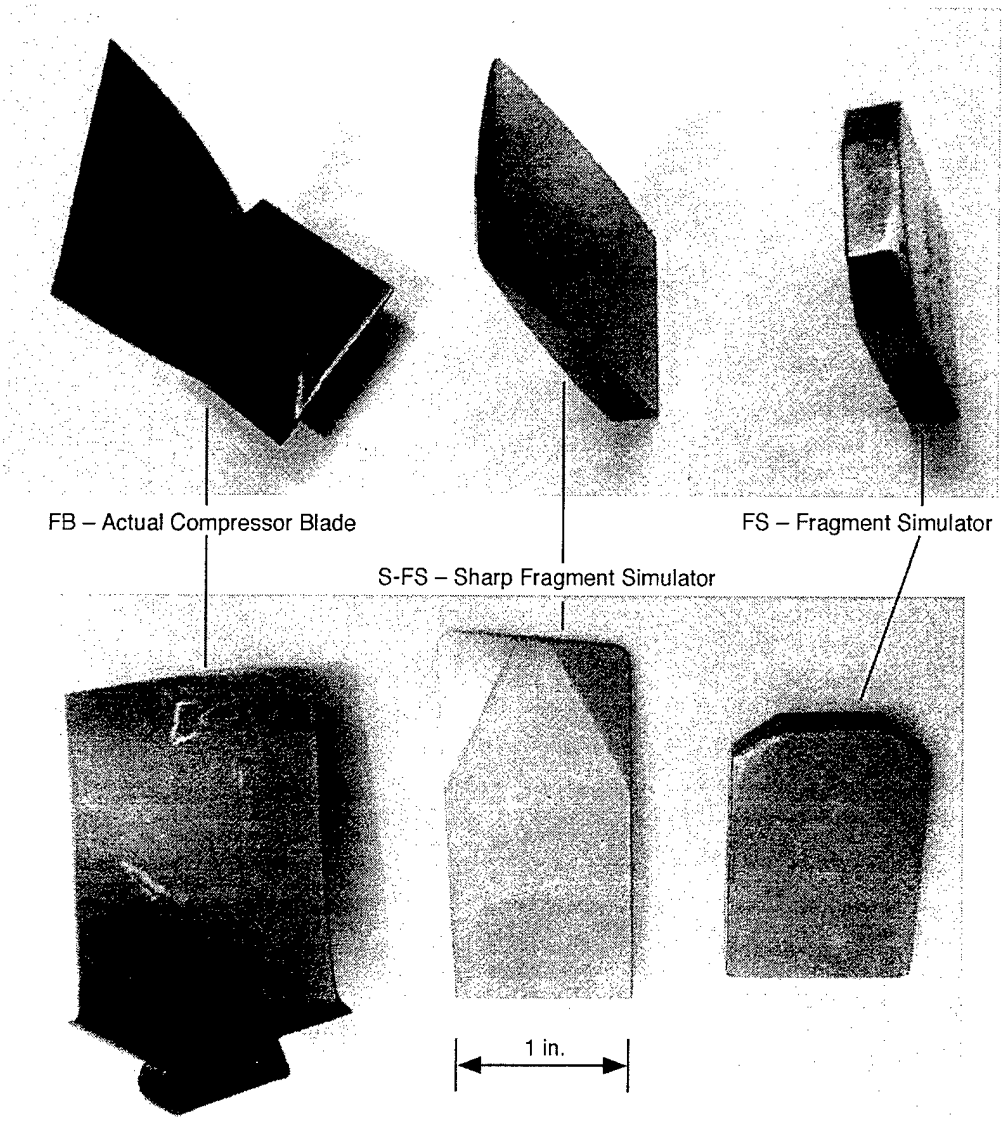

FIGURE 24. PENETRATORS USED IN THE PUSH TESTS

EFFECT OF MATERIAL. Five high-strength woven fabrics were examined as target materials in the push tests: Zylon 30 x 30, Zylon 35 x 35, Zylon 40 x 40, Spectra 32 x 32, and Kevlar 32 x 32. A single ply of Zylon 35 x 35 was selected as the baseline target; all Zylon targets described below are this baseline target unless otherwise designated. Thicknesses and areal densities for these materials were listed in table 1.

Figure 25 compares test results for all these materials under the same test conditions (namely, the FS into a single-ply target gripped on four edges). For Zylon, there is a significant variation in the measured values as a function of the mesh density. For a 42% increase in areal density (comparing Zylon 40 x 40 with Zylon 30 x 30), the peak load increases almost 90%, the energy absorbed by roughly 250%, and the SEA by nearly 70%. Spectra has an SEA only slightly less than that of the Zylon 30 x 30. Kevlar's SEA is significantly lower.

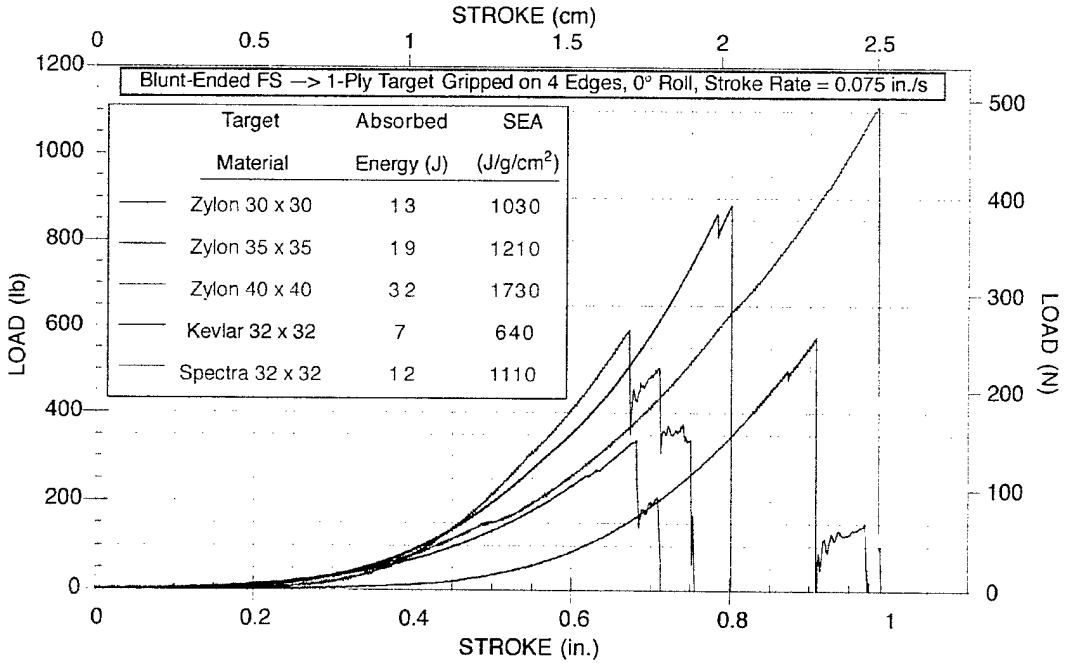

FIGURE 25. PUSH TESTS: EFFECT OF TARGET MATERIAL

EFFECT OF DEFLECTION RATE. The penetrator deflection (or stroke) rate for the push tests ranged over three orders of magnitude, from 0.0075 to 7.5 in./s (≈0.02 to ≈20 cm/s). The baseline stroke rate was 0.075 in./s; all tests are at this baseline rate unless otherwise designated. As shown in figure 26, there was a modest increase of ≈30% in the SEA for Zylon (gripped on four edges, penetrated by a FS) between those two extremes in stroke rate.

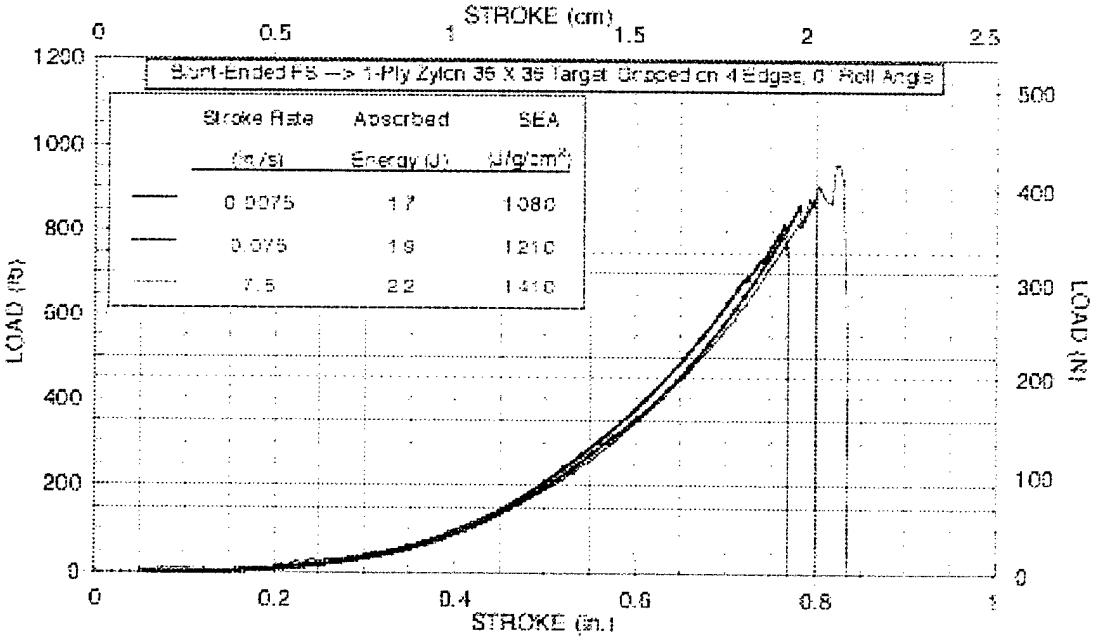

FIGURE 26. PUSH TESTS: EFFECT OF PENETRATION DEFLECTION (STROKE) RATE

EFFECT OF BOUNDARY CONDITIONS. Target boundary conditions—how the fabric target is held—were shown by impact testing to be of utmost significance in penetration resistance. A fabric target gripped on two edges absorbs significantly more energy during fragment impact than the same fabric gripped on four sides. Figure 27 compares 4- and 2-edged gripping of a Zylon target penetrated by the FS. Although the peak load is 65% higher for the Zylon targets gripped on four edges (and the peak modulus is more than twice as high), that target is perforated immediately following the peak load. The 2-edge-gripped target, however, continues deforming at a moderate load after the peak (which is at the same as the 4-edge gripped target); the load doesn't drop to zero until a deflection of roughly twice the peak load deflection is reached.

The SEA for the 2-edge-gripped target is more than twice that for the 4-edge-gripped target. Clearly a different mode of fabric failure is occurring in the 2-edge-gripped target than in the 4-edge-gripped target, a mode that absorbs significantly more energy. The different modes are discussed in detail below.

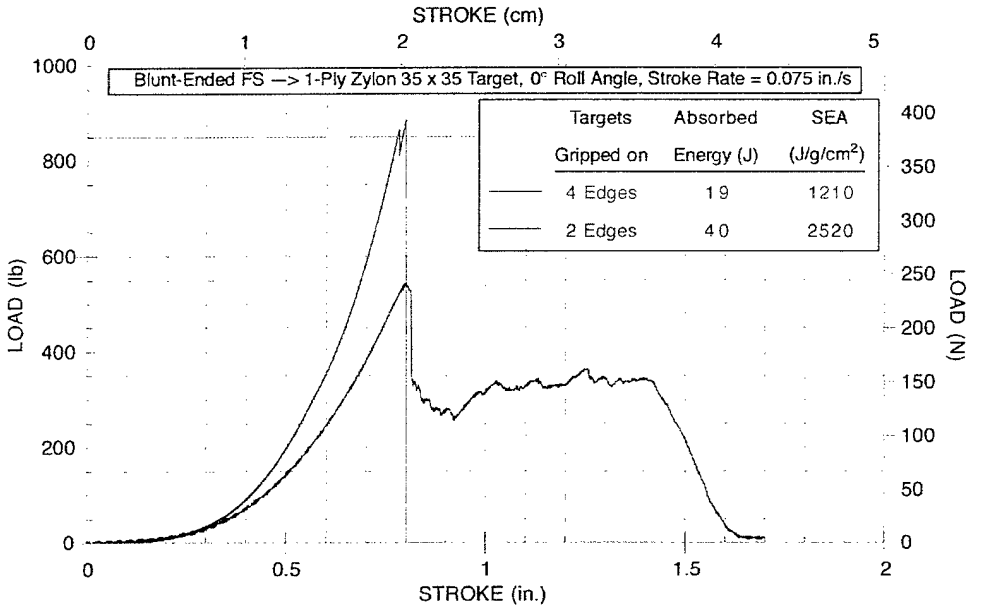

FIGURE 27. PUSH TESTS: EFFECT OF BOUNDARY CONDITIONS (GRIPPING GEOMETRY)

EFFECT OF PENETRATOR ORIENTATION. The cross-sectional area of the impact end of a blunt-nosed impactor is often used as a key ballistic parameter in describing impact resistance for standard armor materials (e.g., metals). A more relevant impact area parameter for fabrics is the number of yarns (both fill and warp yarns) that the impact edge of a fragment intersects; that is, the number of yarns that need to be severed (or pulled out) for the fragment to penetrate. This parameter can be referred to as the impact footprint. For a high-aspect-ratio fragment, such as a fan blade, this parameter will vary as a function of roll angle. The roll angle is defined as the angle between the warp yarn direction and longest dimension of the fragments impact end (i.e., the blade direction). For example, a knife-thin 1-in.-wide fragment impacting a 35 x 35 mesh fabric will intersect 35 fill yarns at a roll angle of 0°, but only 1 warp yarn. At a roll angle of 45°, the same fragment will intersect 50 yarns (25 fills and 25 warps).

Figure 28 shows the results of the FS penetrating a Zylon target gripped on two edges, for two roll angles. At 45°, the FS impacts 62 yarns (31 gripped fills and 31 ungripped warps). At 0°, the FS impacts 43 yarns (35 gripped fills and 9 ungripped warps). Roughly 80% more energy is absorbed for the 45° roll angle than for the 0° roll angle.

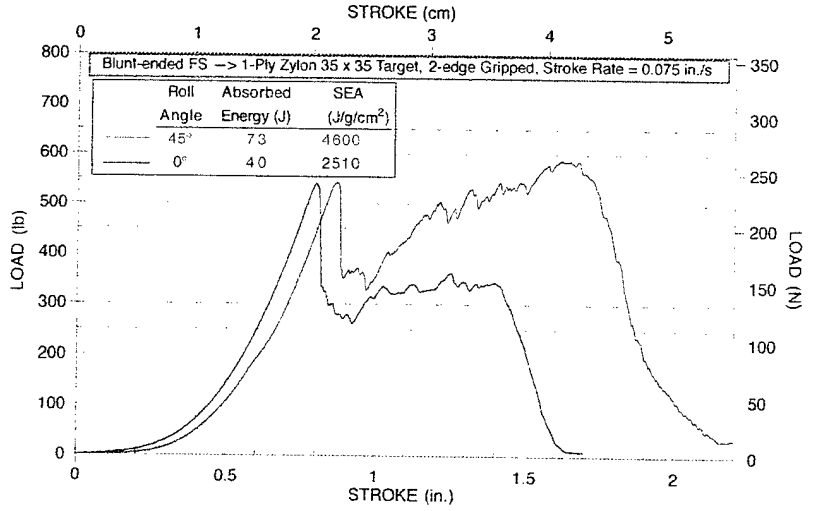

FIGURE 28. PUSH TESTS: EFFECT OF PENETRATOR ORIENTATION (ROLL ANGLE)

EFFECT OF PENETRATOR SHARPNESS. Impact edge sharpness has also proved to be a significant factor in fabric target penetration resistance. Fabric targets absorb significantly more energy when impacted by blunt-ended targets than by sharp-ended targets with a similar impact footprint. For the push tests, the effect of fragment sharpness was examined by comparing the results of FS and FB (or S-FS) penetrations. The blunt-ended FS and sharp-ended FB penetrators used in these tests have nearly the same impact footprint at a roll angle of 45°, namely, 62 to 64 yarns for the 35 x 35 mesh fabric.

Figure 29 shows the results for both 2-edge- and 4-edge-gripped Zylon targets. The absorbed energy is far higher for the blunt FS than for the sharp FB (more than a factor of six higher for the 4-edge-gripped targets, and nearly a factor of four higher for the 2-edge-gripped targets). Complete penetration occurs at much lower fragment deflections for the sharper fragment.

However, the fabric's relatively weak penetration resistance to sharp fragments was improved significantly by using multiple-ply targets or overlays. For Zylon targets gripped on four edges, the energy absorbed by a two-ply target is more than a factor of four higher than with a single-ply target (see figure 30), which means that despite the 100% increase in target areal density, the SEA more than doubles. Overlays, or ungripped layers of material positioned on the penetrator side of the gripped fabric target, improved penetration resistance even more. With an overlay consisting of a single ply of Zylon 35 x 35 fabric, or one or two layers of Zylon felt, the absorbed energy increases by nearly a factor of five over that of a test with no overlay (see figure 31). For the single-ply felt overlay, which has only about half the areal density of the woven fabric, and therefore the least increase in total target areal density, the SEA increase is more than a factor of three. Similar improvement in sharp fragment penetration resistance by use of an overlay is observed for 2-edge-gripped targets (see figure 32).

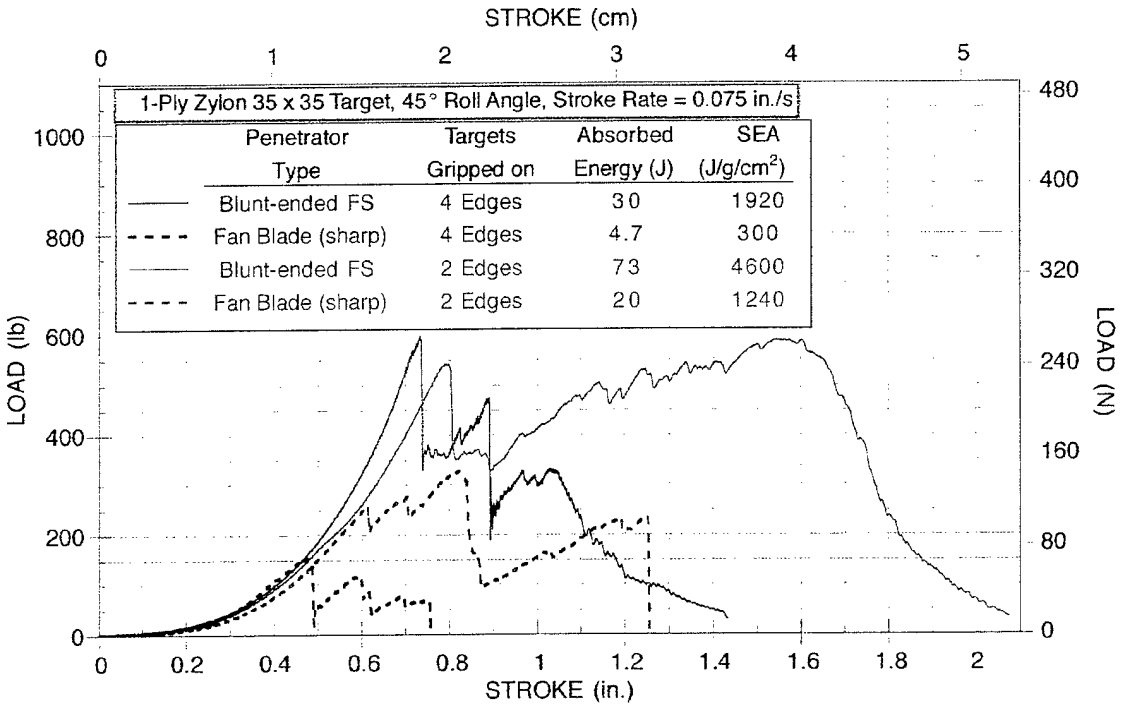

FIGURE 29. PUSH TESTS: EFFECT OF PENETRATOR SHARPNESS FOR DIFFERENT GRIPPING GEOMETRIES

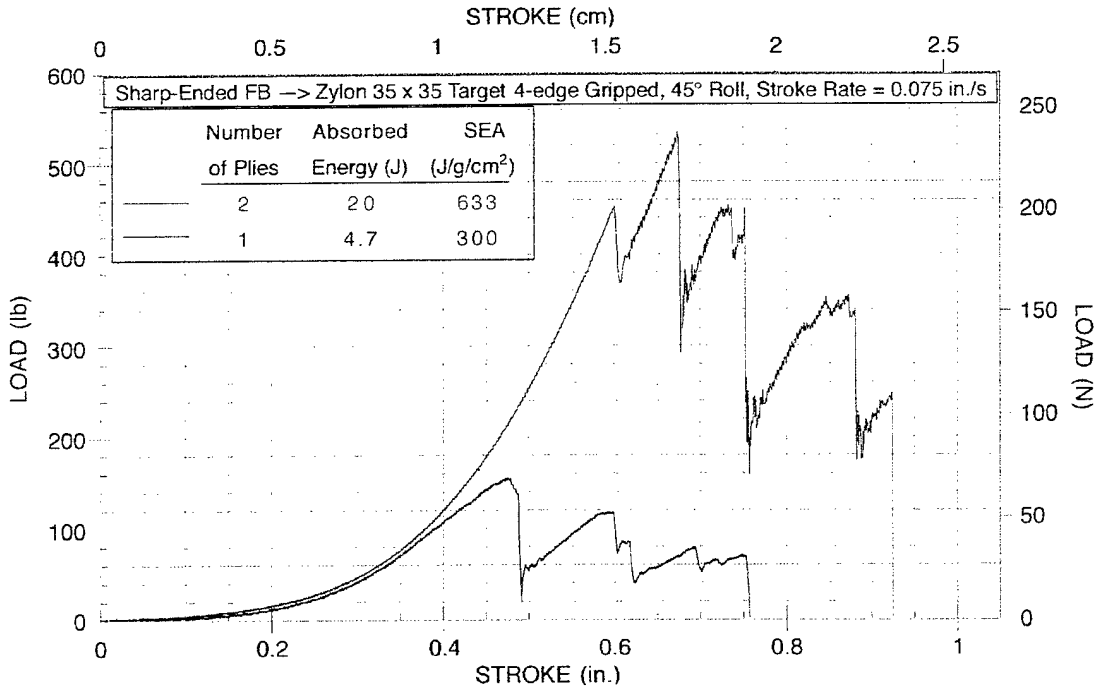

FIGURE 30. PUSH TESTS: EFFECT OF NUMBER OF PLIES FOR A SHARP PENETRATOR

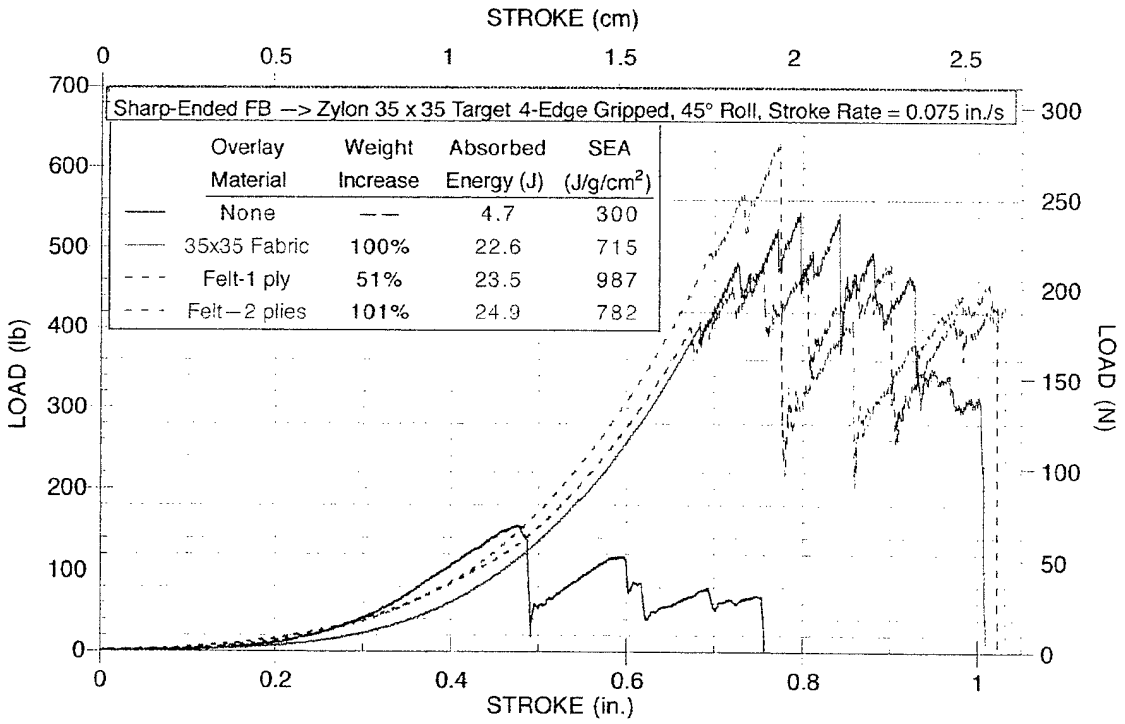

FIGURE 31. EFFECT OF UNGRIPPED OVERLAYS FOR SHARP PENETRATOR, 4-EDGE-GRIPPED TARGET

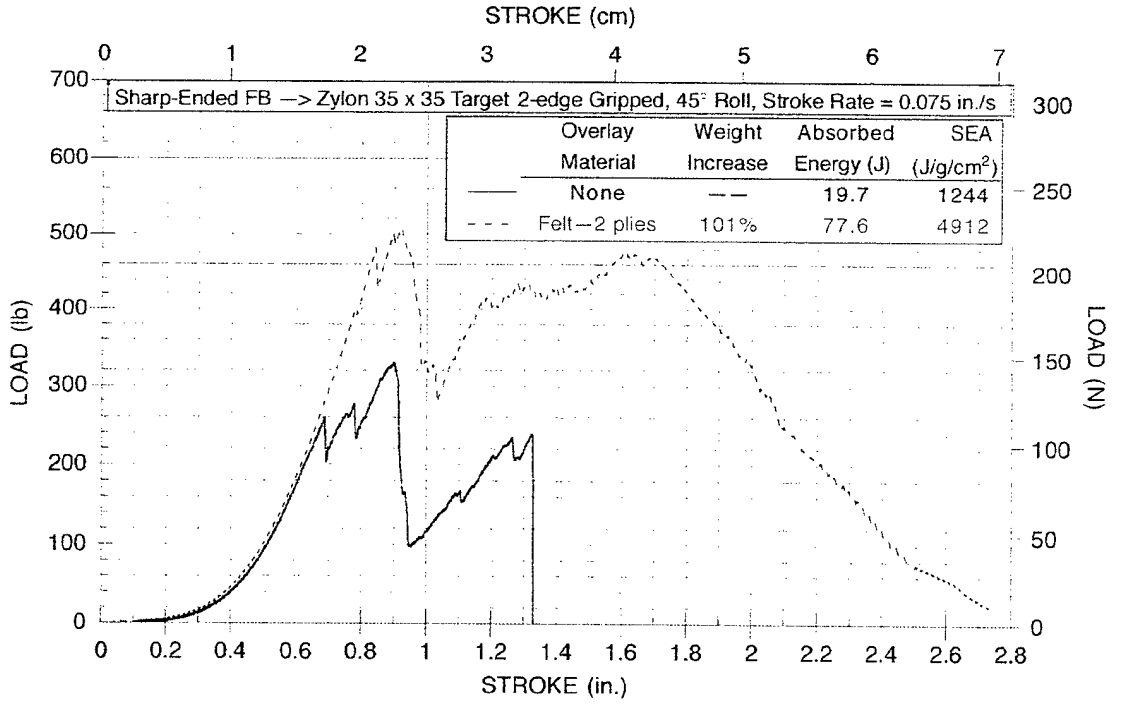

FIGURE 32. EFFECT OF UNGRIPPED OVERLAYS FOR SHARP PENETRATOR, 2-EDGE-GRIPPED TARGET

No matter what type of overlay is used, the FB penetrator does not perforate the overlay. Instead, the overlay wraps itself around the FB, and the FB, cloaked within the overlay, penetrates the gripped target (the same phenomenon observed in the impact tests). The higher absorbed energies for sharp fragment penetration when target overlays are used is due mostly to the decrease in the effective penetrator sharpness felt by the gripped layer, due to the cloaking of the penetrator by the overlay. Also contributing are the slight increase in the impact footprint and the increased drag.

PHENOMENOLOGY OF FABRIC TARGET FAILURE.

Three fabric failure modes were detected in the push tests. These modes have been designated local yarn rupture, remote yarn failure, and yarn pullout. The best way to observe the phenomena is by videotape, which provides both a visual and acoustic record of the failure progression. Unfortunately, only individual videotape stills and photographs of the recovered specimens can be shown in the report, along with the load-deflection curve.

The first of the failure modes, local yarn rupture, was shown in figure 22 along with its effect on the load-deflection curve (figure 23). The other modes, remote yarn failure and yarn pullout, are shown in figures 33 and 34, which show video stills and an annotated load-deflection curve, respectively, for push Test P-29; a test in which all three modes were experienced by different target yarns. More than one failure mode was observed in some individual yarns. For example, some, but not all, of the fibers in a yarn in push test targets ruptured locally by contact with a sharp fragment; the remainder failed remotely. Others yarns experienced both partial remote failure and pullout.

The following paragraphs describe the phenomenology of each failure mode, the effect on the load-deflection curve, and the test scenarios in which the mode was observed.

LOCAL YARN RUPTURE. If all of a yarn's fibers break apart at the same axial location—usually at the sharpest point of contact between the penetrator and the yarn—this type of failure is designated local yarn rupture. Individual yarn ruptures can be observed in figures 22(d) and 33(b). A popping sound accompanies this failure, along with a sudden drop in the measured load, as shown in figures 23 and 34.

Often more than one yarn fails within a short enough duration (a few tens of milliseconds) that their acoustic emission and load drop merge together. Then the loudness of the sound and the magnitude of the load drop are proportional to the number of nearly simultaneous yarn failures. Adjacent video frames, figures 22(e) and 22(f), show that 31 of the 34 total yarn ruptures occurred within 30 ms, causing the precipitous drop to zero load shown at the end of the curve in figure 23.

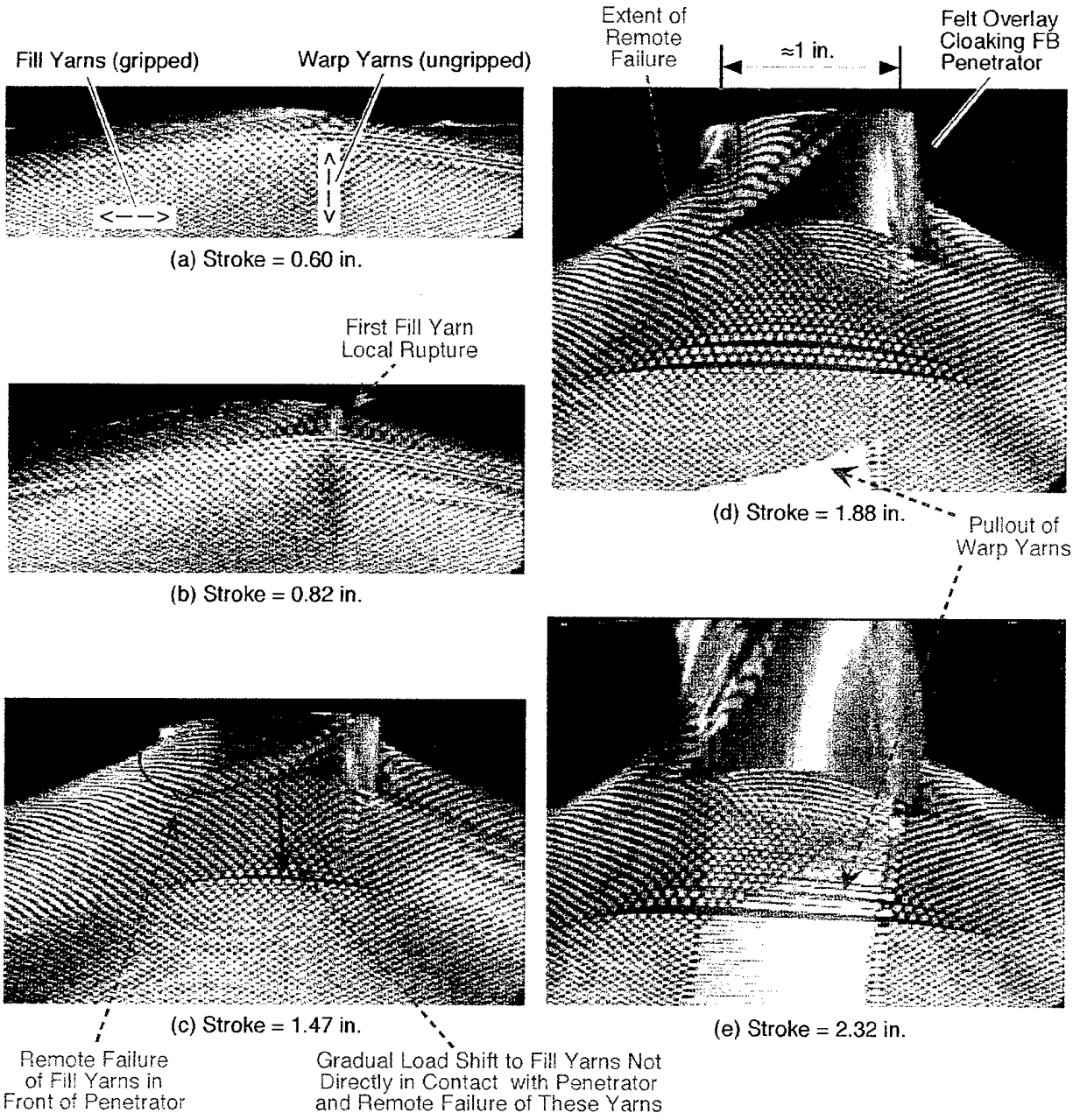

FIGURE 33. ZYLON PUSH TEST VIDEO STILLS, ILLUSTRATING THREE MODES OF YARN FAILURE

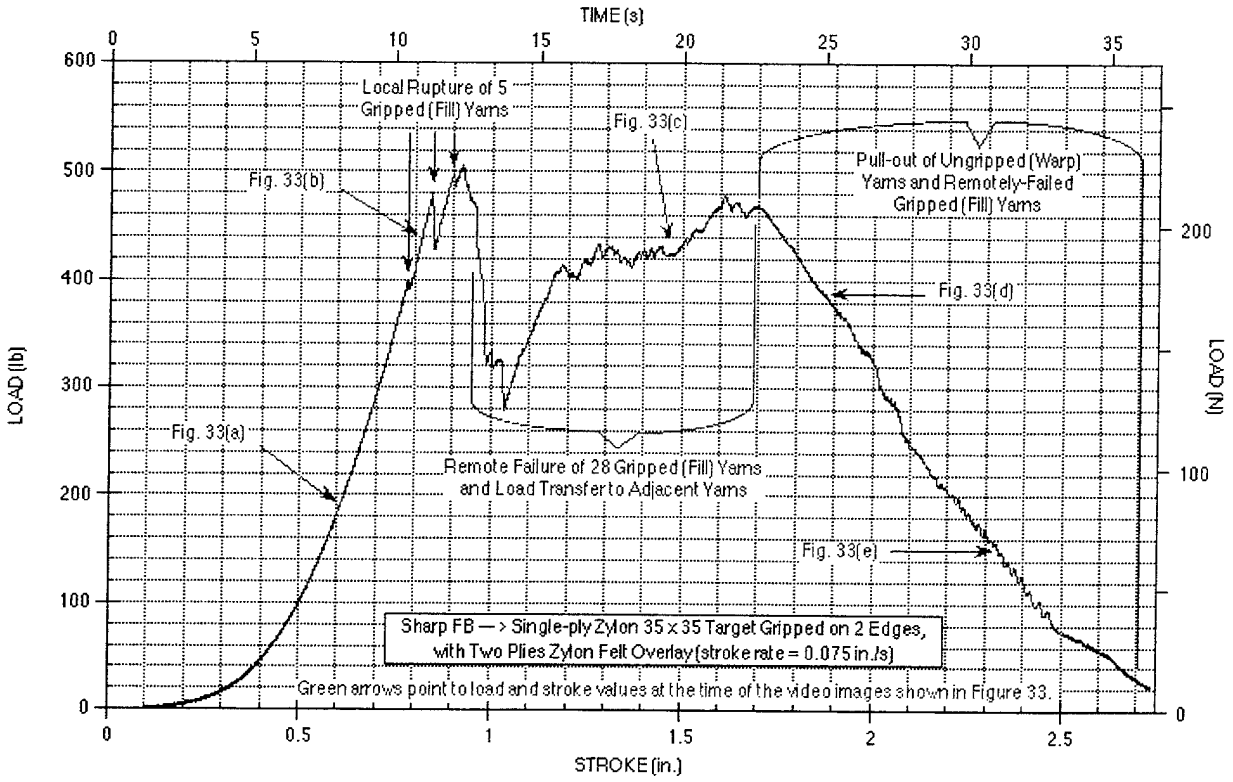

FIGURE 34. EFFECT OF OBSERVED FAILURE PHENOMENON ON THE PUSH TEST LOAD-DEFLECTION CURVE

Local yarn rupture was observed under the following test conditions:

- Impact tests at relatively high velocity (>500 f/s or 150 m/s)—most failed yarns, especially for sharp-ended impactors or wide fabric targets (where the impact point is far away from the fabric edge).
- Impact tests at relatively low velocity (<500 f/s or 150 m/s)—most failed yarns when target is gripped at four edges, mainly the gripped yarns when the target is gripped at two edges.
- Push tests with 4-edge target gripping—all failed yarns.
- Push tests with 2-edge target gripping—for sharp-ended penetrators (without overlays), most failed yarns (gripped and ungripped); for blunt-ended penetrators (or sharp penetrators with overlays), some failed gripped yarns (particularly at higher stroke rates).

It is also the dominant failure mode observed in the yarn transverse load tests with a knife-edge fragment (see the section on the tensile tests below).

REMOTE YARN FAILURE. If the various fibers within a yarn break at different points along the yarn's length (not necessarily at the point of impact), this type of failure is designated remote

yarn failure. The distance over which the fiber breaks can be many inches. Breaks can occur anywhere between the impact point and the grip or can span that entire distance.

Remote yarn failure is more difficult to perceive while it is happening. The failed yarn does not appear any different on the video. There is no apparent break in the yarn, and the severed ends of the very thin ($\approx$12 μm) individual fibers are extremely difficult to see, especially when they remain within the woven fabric mesh. Also the acoustic emission is less distinct. There is not a sudden popping sound when a single yarn undergoes remote failure, only a softer hissing or rustling sound. If many yarns undergo remote failure simultaneously, the acoustic emission is louder, but still less abrupt than that of local rupture.

The effect of remote failure on the load-deflection curve is more complex than that for local rupture. For the case of simultaneous multiple yarn failure (which often occurs on the gripped yarns directly in contact with the penetrator), there is a significant drop in load (see figure 34), but never down to zero. For local rupture, once all the yarns in front of the penetrator have failed, the penetrator pops through the fabric, and the load falls to zero. But for remote failure, even if all of the yarns in front of the penetrator have failed, they still remain in place, exerting a significant load on the penetrator. This load results from the friction between the fibers on the failed yarns (which are not all severed at the same axial location) and the force between those yarns and the intersecting perpendicular yarns.

Further deflection by the penetrator following remote failure increases the load along the yarns adjacent to those that have failed, even if these yarns are not in direct contact with the penetrator. This can continue for a significant duration (see figure 34), during which the load on the penetrator can stay constant or even increase slightly. This load transfer and resultant remote yarn failure continue until the frictional forces on the yarns remaining in front of the penetrator (the ungripped warp yarns, as well as the remotely failed gripped fill yarns) decrease to less than what is required to sustain additional remote yarn failure.

Figure 35 shows a Zylon fabric specimen recovered from a push test (P-16) representative of tests for which remote yarn failure was the dominant failure mode. Inspection of the specimen revealed 83 remotely failed fill yarns (no local rupture) and no failed warp yarns. The distinct bulge in figure 35(a) delineates the extent of the remote yarn failure. Since the 1-in.-wide FS penetrator directly contacted only 35 fill yarns, the remaining 48 remote yarn failures occurred by load transfer through the fabric. Clearly, this failure mode is an effective way of involving a larger region of the fabric target in the deformation and yarn failure, which significantly increases the energy absorbed.

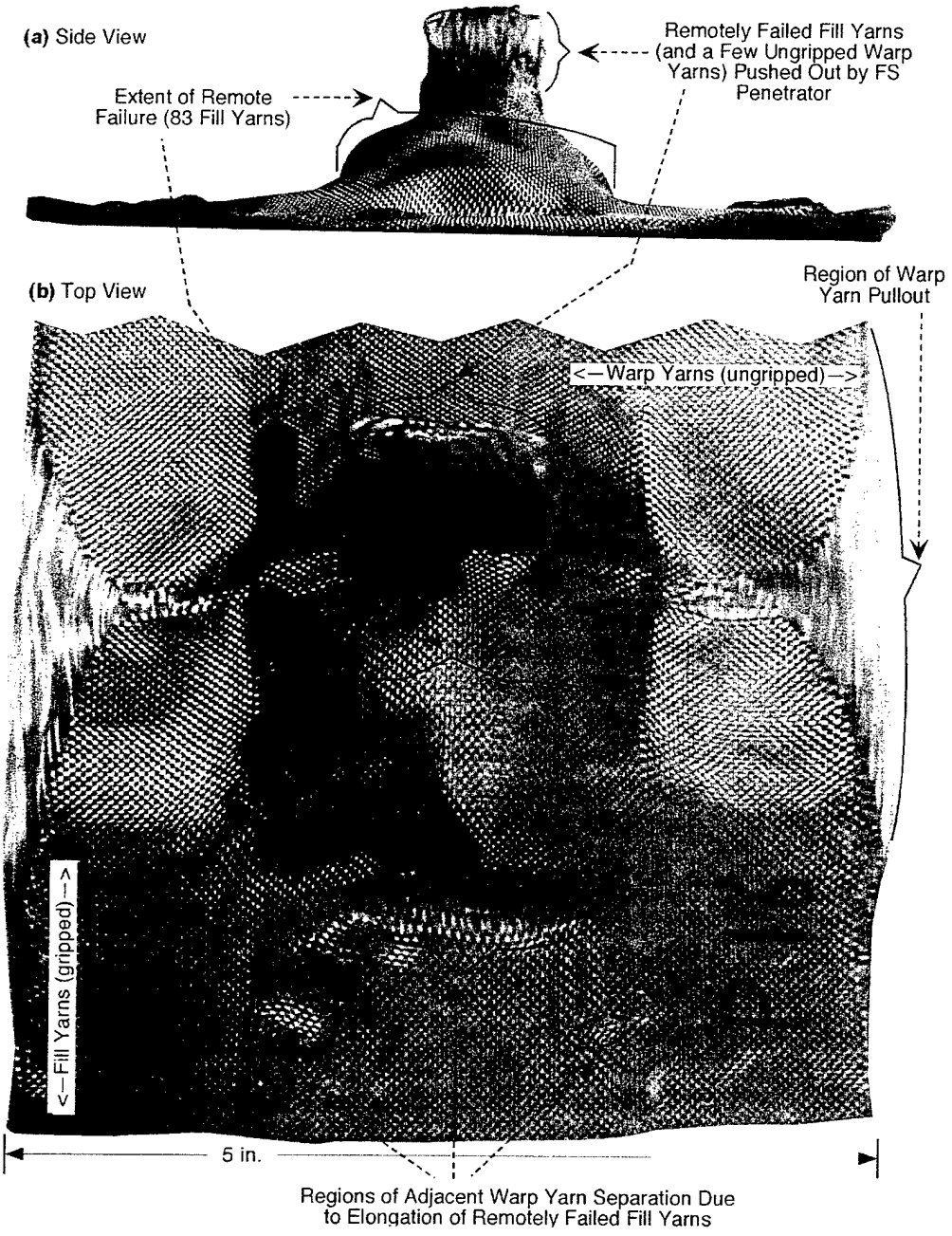

FIGURE 35. ZYLON 35 x 35 FABRIC SPECIMEN RECOVERED FROM FRAGMENT PUSH TEST

Remote yarn failure was observed under the following test conditions:

- Impact tests with 2-edged-gripped targets—some failed gripped yarns (primarily with blunt-ended impactors and at lower velocities).
- Push tests with 4-edged-gripped targets—some failed yarns, but only for blunt-ended penetrators (or sharp penetrators with overlays).

- Push tests with 2-edged-gripped targets—almost all failed gripped yarns, especially for blunt-ended penetrators (or sharp penetrators with overlays).

Remote yarn failure is also the dominant failure mode observed in the yarn tensile tests and in the yarn transverse load tests with a blunt fragment (see the section on the tensile tests below).

YARN PULLOUT. If none of the fibers in a yarn break, but one end of the yarn is pulled out of the fabric mesh, this type of failure is designated yarn pullout. This type of failure can of course occur only with an ungripped (or loosely gripped) yarn. Yarn pullout can be readily observed visually (see the progression from figures 33(d) to 33(e), and also the recovered specimen in figure 35), but only a faint whisper of an acoustic emission can be heard, and only with many simultaneous yarn pullouts.

The force required to pull out an ungripped yarn from its fabric mesh is due to the frictional forces on the areas of contact between the yarn and all of its intersecting perpendicular yarns (refer to the section on the pullout tests below for a description of tests performed to measure this frictional force and determine the coefficient of friction). Unfortunately, the coefficient of friction cannot be measured directly in a push test by noting the decrease of the number of yarn intersections as the yarn pullout progresses (readily observable on the video), because, in addition to the frictional forces on the ungripped pullout yarns, there are invariably some remotely failed gripped yarns adding an additional force (from the severed fibers dragging against one another as well as from their contact with intersecting perpendicular yarns). As the yarn is pulled out in a push test, the length of yarn within the mesh (and hence the total contact area) decreases, resulting in a steady gradual drop in the measured load (as shown in figure 34).

Yarn pullout was observed under the following test conditions:

- Impact tests with 2-edge gripping—ungripped yarns, particularly when a relatively small target is hit by a relatively large fragment, or when the fragment hits close to the ungripped edge of the target.

- Push tests with 2-edge gripping—ungripped yarns, especially for blunt-ended penetrators (or sharp penetrators with overlays).

SUMMARY AND CONCLUSIONS.

Push tests were performed and analyzed for a wide range of fabric parameters, fragment sharpnesses, and penetration rates and geometries. Thus a substantial database is now available for verifying computational models.

The push test has contributed greatly to understanding the evolution and phenomenology of fabric failure by fragment penetration. Even though the deformation rates involved are lower than those of ballistic impacts, the three modes of yarn failure observed are all modes that were also observed in impact tests. An understanding of all three modes is essential to developing a reliable predictive computational model.

MECHANICAL PROPERTIES TESTS

Laboratory tests were performed to measure the mechanical properties of yarns necessary for modeling the deformation and failure phenomenology observed in fragment penetration of high-strength fabrics.

YARN DEFORMATION AND FAILURE TESTS.

Yarn tensile deformation and failure play a major role in the ballistic response of high-strength woven fabrics subjected to fragment impact. Yarns within the impact region are deflected perpendicular to their length and subjected to axial tensile strain (as well as some transverse compressive strain). Yarns adjacent to but not directly within the impact region also are stretched, and possibly severed, by the forces transmitted from the impact regions by the deflection of the intersecting transverse yarns.

As described previously in the section on the quasi-static penetration (push) tests, yarn failure in a fabric penetration scenario can occur in two modes; local rupture of the yarn's fibers at the point of contact, or remote failure of the yarn's fibers at various points along the yarn length away from the point of contact. Yarn pullout (the third mode described in the previous section) is considered a mode of fabric failure but not yarn failure. Characterization of the yarn's tensile deformation and both modes of yarn failure is essential in developing a realistic computational fabric model.

Previous tensile tests that SRI performed on yarns from the various high-strength fabrics [6] provided a preliminary database for the fabric model. However, only one of the two yarn failure modes was observed in standard tensile testing, namely, remote yarn failure (as seen in figure 36). These tests, in which the strain was computed from the ram deflection divided by the initial gauge length (the distance between the grip edges at the start of the test), have indicated an apparent variation of modulus and strain-to-failure as a function of gauge length. Analysis of this variation showed that it could not be the result of any reasonable material property, but could be consistent with slippage in the grip region.

The issue of the apparent gauge length variation observed in tensile testing was successfully resolved by measuring the strains directly on the yarns. Also, a new test, called the transverse load test, was designed and implemented to characterize local yarn rupture and to delineate the effect of impactor sharpness on yarn failure. Highlights of these efforts are described below.

TENSILE TESTS WITH EXTENSOMETRY. The experimental technique for yarn tensile testing was modified (see figure 37) to directly measure the strain on the yarn. A method of clipping a standard extensometer onto the yarn was devised which supports the weight of the extensometer and firmly attaches the extensometer to the yarn without damaging any of the fibers. Tensile tests on a variety of high-strength yarns were performed using this new technique, and results were greatly improved over that of the previous tests without the extensometer.

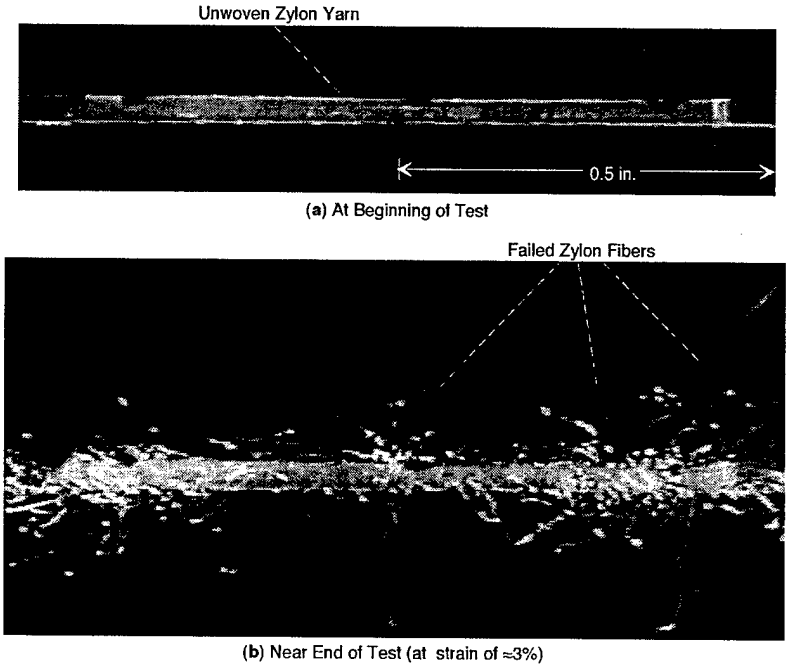

FIGURE 36. REMOTE YARN FAILURE OBSERVED DURING ZYLON TENSILE TEST

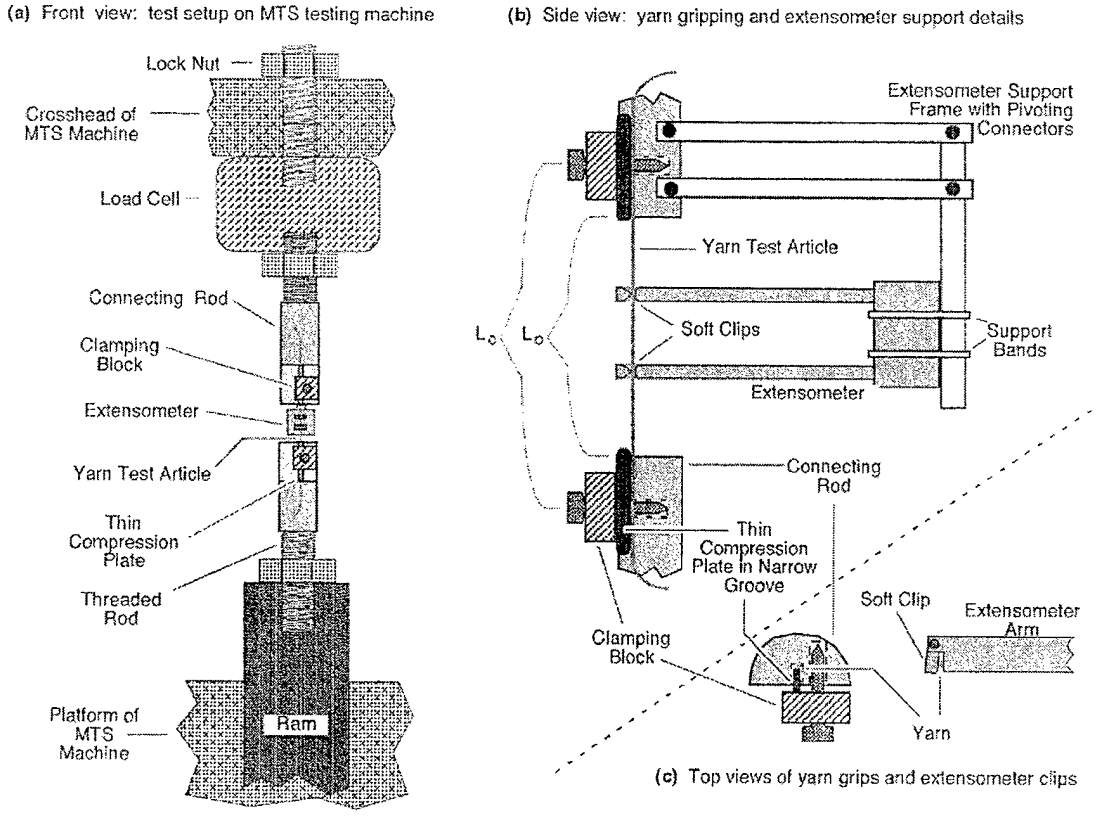

FIGURE 37. SETUP FOR YARN TENSILE TESTS WITH DIRECT STRAIN MEASUREMENT BY EXTENSOMETRY (L_o and L_c are the original and corrected gauge lengths used for previous tests without extensometry.)

Tests with the extensometer revealed no variation of material properties as a function of gauge length. The tests confirmed that the yarns were indeed slipping within the proximal halves of their two grips, and a consistent correction for the gauge length was determined that would account for this slippage and allow a proper analysis of the previous tests (performed without the extensometer).

For example, figure 38 shows various stress-strain curves for a tensile test on a fill yarn from a Kevlar 32 x 32 fabric. The strain (ε) determined from the ram deflection (d), using the formula $\varepsilon = d/L_0$, where L_0 (the gauge length) is taken to be the distance between the grips (as shown in figure 37), differs significantly from the strain measured directly by the extensometer. However, when the gauge length is increased to L_C, a correction approximately equal to half of the width of the grips, the strain determined from $\varepsilon = d/L_C$ is nearly identical to that from the extensometer.

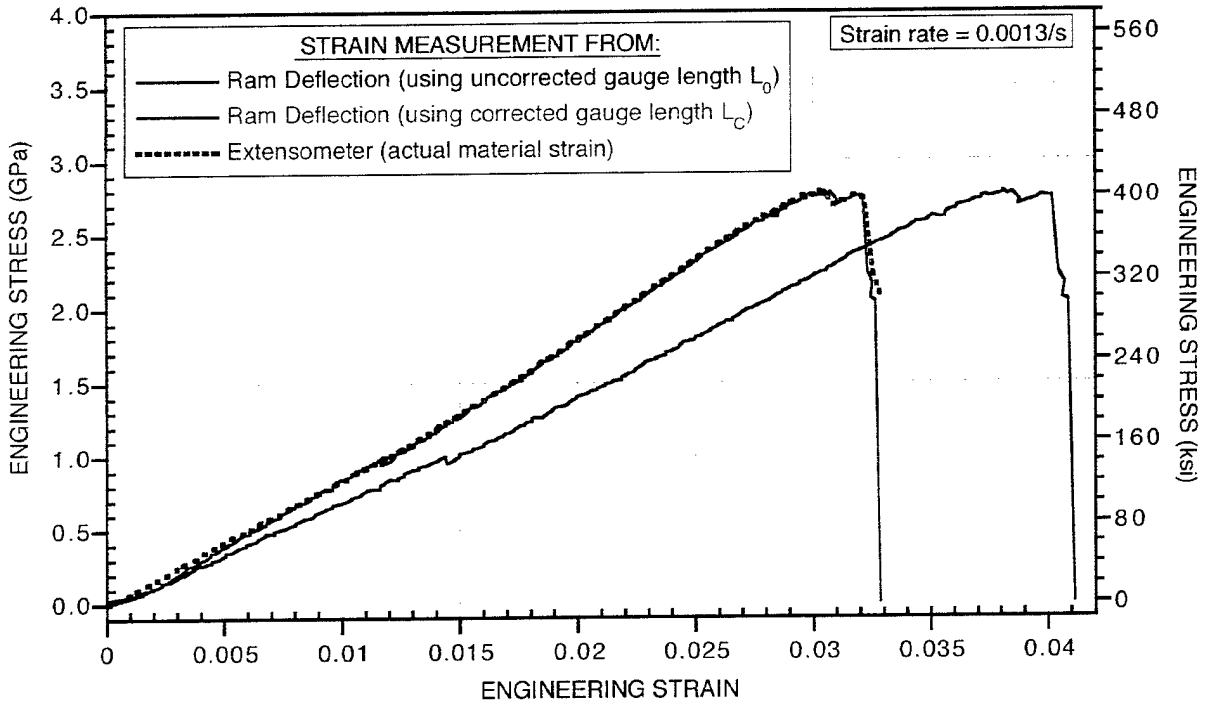

FIGURE 38. TENSILE TEST RESULTS FOR FILL YARN FROM KEVLAR 32 x 32 FABRIC, SHOWING STRAIN DETERMINED BY DIFFERENT METHODS

Numerous tests with Zylon and Kevlar yarns over a wide range in gauge lengths showed the validity of this correction, which indicates that results from previous tests with the same grip, but without an extensometer, can be corrected and used along with data from tests using extensometers. Tests on Spectra yarns will be completed in the next year.

Table 9 presents the results from various yarn tensile tests as well as from the transverse load tests to be discussed below, along with manufacturer's data on the fibers. In addition to the standard material properties usually obtained from tensile testing (i.e., tensile modulus, tensile

TABLE 9. TENSILE PROPERTIES OF HIGH-STRENGTH YARNS

Material (and Origin)	Test Type[a]	Linear Density			Area of C.S.[c]		Tensile Modulus[d]		Ultimate Tensile Strength (UTS)		Strain at UTS	Strain at Failure[e]	Energy per Unit Length[f]		Specific Yarn Energy (SYE)[g]	
		(denier[b])	(mg/cm)	(lb/in. x10^{-6})	(cm^2 x10^{-4})	(in^2 x10^{-5})	(GPa)	(Msi)	(GPa)	(ksi)	(%)	(%)	(J/m)	(ft-lb/ft)	(J/g)	(kft-lb/lb)
Zylon-AS (PBO) *(Manufacturer's data—fiber)*							*180*	*26*	*5.8*	*840*	—	*3.5*				
Unwoven	Tensile	508	0.564	3.16	3.66	5.68	180	26.1	4.5	650	3.0	3.4	3.20	0.720	56.7	19.0
30x30 Fill	"	506	0.562	3.15	3.65	5.66	171	24.8	4.1	595	2.9	3.4	3.02	0.679	53.7	18.0
30x30 Warp	"	476	0.529	2.96	3.44	5.32	168	24.4	3.9	565	2.8	3.4	2.61	0.586	49.2	16.5
40x40 Fill	"	515	0.572	3.20	3.71	5.76	165	23.9	3.7	535	2.7	3.4	2.72	0.611	47.5	15.9
40x40 Warp	"	489	0.543	3.04	3.53	5.47	169	24.5	2.5	360	1.7	2.5	1.32	0.297	24.3	8.1
	Transverse Load:															
Unwoven	Cylindrical edge	509	0.565	3.16	3.67	5.69	180	26.1	4.5	650	3.0	3.3	3.25	0.732	57.6	19.3
Unwoven	Knife edge	509	0.565	3.16	3.67	5.69	180	26.1	3.2	465	2.4	3.0	2.30	0.517	40.7	13.6
Kevlar 29 (p-aramid) *(Manufacturer's data—fiber)*							*109*	*16*	*2.92*	*423*	—	*3.6*				
32x32 Fill	Tensile	403	0.448	2.51	3.11	4.82	104	15.1	2.7	390	3.0	3.3	1.47	0.331	32.9	11.0
32x32 Warp	"	408	0.453	2.54	3.15	4.88	103	14.9	2.5	360	2.65	2.7	1.05	0.237	23.3	7.8
	Transverse Load:															
32x32 Fill	Knife edge	403	0.448	2.51	3.11	4.82	99	14.4	2.0	285	2.2	2.5	0.80	0.180	17.9	6.0

[a] Strain rate for tensile tests is ≈0.0013/s. For transverse load tests, stroke rate = 0.05 in./s; strain rate varies from 0 to ≈0.14/s.

[b] Denier equals grams per 9 kilometers.

[c] Total cross-sectional area of all of the yarn's fibers, not including any of the void space within the yarn's envelope.

[d] Slope of the steepest (substantial) upward portion of the stress-strain curve.

[e] Point past UTS at which a straight line extending along the steepest (substantial) downward portion of the stress-strain curve intersects zero stress.

[f] Energy per unit length needed to cause yarn failure (equals the area under the stress-strain curve multiplied by the cross-sectional area).

[g] Specific Yarn Energy — defined as energy per unit length divided by the linear density.

strength, and strain at failure), the following properties relating to the energy needed to stretch the yarn to failure are reported in the table:

- The energy per unit length, which equals the area under the load-deflection curve, divided by the gauge length (equivalent to the area under the stress-strain curve, multiplied by the yarn's cross-sectional area), is a measure of a yarn's ability to absorb energy before failure. Because the energy needed to fail a yarn is directly proportional to the yarn length, dividing this energy by the length results in this length-invariant parameter.

- The specific yarn energy (SYE), which is defined as the energy per unit length divided by the yarn's linear density (equivalent to the energy absorbed divided by the mass of a gauge-length of the yarn), is a parameter for comparing yarns of different materials and thicknesses, since it reflects the energy absorbed in yarn failure on a per-weight basis. The SYE for yarns is analogous to the SEA defined previously for fabrics.

Figure 39 shows stress-strain curves from tensile tests with extensometry on a variety of 500-denier Zylon yarns. The unwoven yarn has the highest tensile modulus (180 GPa, or 26 Msi) million number per sq in. $26E^6$ or 26×10^6 Msi and tensile strength (4.5 GPa, or 650 ksi). The modulus is the same reported by the manufacturer for the Zylon fiber, but the ultimate tensile strength (UTS) is less than the 5.8 GPa (840 ksi) reported. It is reasonable for the measured UTS for the yarn to be less than that for the fiber. It is impossible to grip all the fibers in a yarn with precisely equal prestrain, so some of the fibers in the yarn break at an earlier applied axial deflection, which increases the load on the remaining fibers, causing a reduced UTS. Because this would also happen in an actual penetration scenario, the UTS measured for the yarns is used in the model, rather than the idealized data for the fiber. All the woven Zylon yarns are clustered in a range from 165 to 171 GPa (24 to 25 Msi) in modulus and have strengths that vary from 4.1 GPa (595 ksi) for the 30 x 30 fill yarn down to 2.5 GPa (360 ksi) for the 40 x 40 warp yarn.

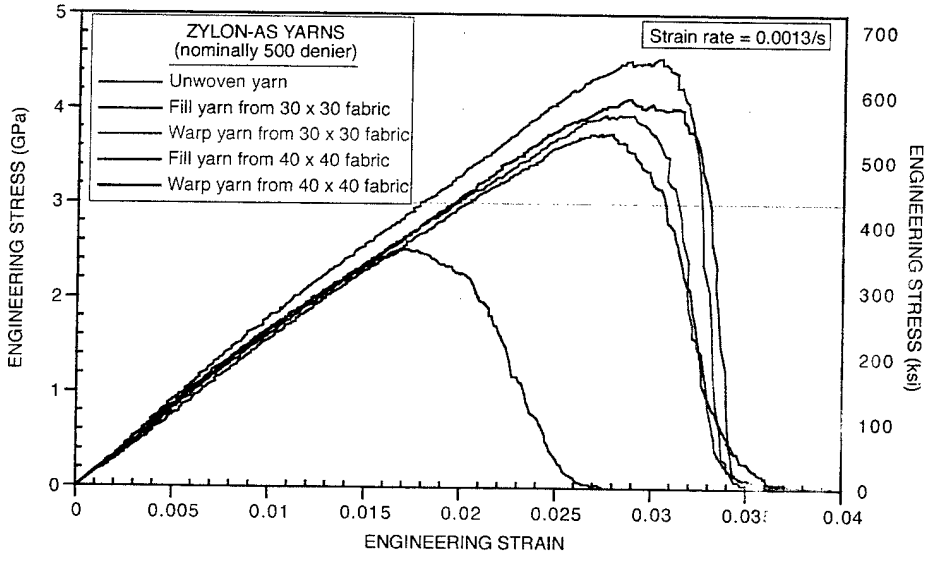

FIGURE 39. TENSILE TEST RESULTS FOR VARIOUS ZYLON YARNS

The weaving process, thus, appears to cause a modest decrease in both the yarn modulus and failure strength, and the degree of crimp of the yarn correlates with a decrease in the yarn strength. What is particularly relevant to the fragment penetration scenarios is the effect of weaving and crimping on the energy absorbed in yarn deformation and failure. Although the tensile modulus decreases by only ≈6% (comparing the 40 x 40 warp yarns to the unwoven yarns) and the UTS by 44%, the energy absorbed decreases by 59%. A comparison of similar yarns from the 30 x 30 Zylon and 32 x 32 Kevlar fabrics shows that Zylon has a strength roughly 50% higher than Kevlar and has an SYE from 60% to 110% higher.

TRANSVERSE LOAD TESTS. As previously discussed, gas gun impact tests with high-strength fabric targets showed that the sharpness of a fragment's impact edge has a major effect on the energy absorbed by the fabric in an impact scenario. During penetration of tightly gripped Zylon targets, blunt-ended fragments lost 50%-80% more kinetic energy than sharp-ended fragments of similar size, mass, and impact velocity. Even greater differences were observed in quasi-static push tests, where different failure modes were often observed for sharp-ended and blunt-ended fragment penetration (local rupture and remote failure, respectively).

The tensile tests described above are certainly valid tests for determining mechanical properties of an individual yarn that is gripped on one end and pulled on the other in the axial direction, but this is not exactly the type of loading that a yarn in a fabric target experiences during fragment impact, particularly for yarns directly in the path of the impactor. These yarns are held at both ends (either tightly by a clamping mechanism for gripped yarns, or more loosely by the fabric's intersecting transverse yarns for ungripped yarns) and are deflected at some point in the middle, in a transverse direction (perpendicular to the axis for normal impacts). Furthermore, tensile tests cannot distinguish between loading by sharp- or blunt-ended impactors.

Experimental and Analytical Techniques. A new mechanical test was therefore devised that would subject an individual yarn to a loading closer to that experienced in a fragment impact scenario and make it possible for the effects of impactor sharpness to be determined. The test (shown in figure 40) is called the transverse load test. In this test, a rigidly held fragment (the loader) was pushed perpendicularly to the yarn axis at a constant rate into a yarn whose ends were tightly gripped within grooves machined in two arms of a clevis.

The contacting edge of the loader could have any desired shape and sharpness. The two steel loaders that were used had edge shapes spanning a wide range in sharpness. The first (called the knife-edge loader) had a 45° included angle, machined as sharp as the steel would allow. Its radius of curvature was not measured, but was certainly far smaller than the cross-sectional dimensions of a yarn (roughly 0.1 to 0.4 mm, or 0.004 to 0.016 in.) and was likely on the order of the diameter of an individual fiber (≈12 μm, or 0.0005 in.). The second loader (called the cylindrical loader) had a right circular cylinder edge with a 3.2-mm ($^1/_8$-in.) radius of curvature, much greater than the yarn thickness.

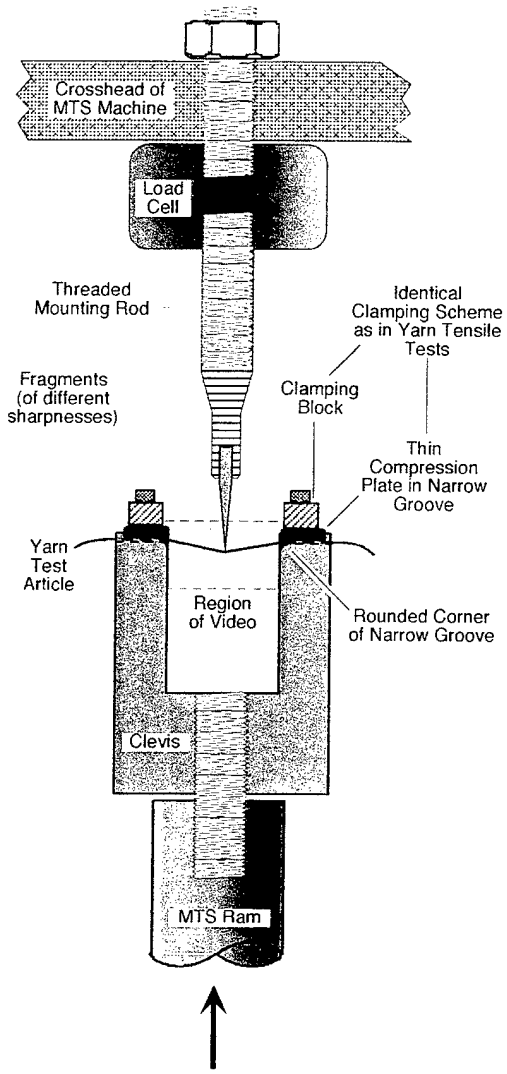

FIGURE 40. EXPERIMENTAL SETUP FOR YARN TRANSVERSE LOAD TEST

Histories of the ram displacement (d) and the vertical force on the fragment (F_f) were recorded during the test. From these histories, the axial force along the yarn (F_y) and yarn elongation (ΔL) were determined as follows (refer to figure 41):

$$F_y = {}^1/_2 F_f / \sin(\theta) \tag{1}$$

$$\Delta L = 2\left[d^2 + (L_0/2)^2\right]^{1/2} - L_0 = 2d/\sin(\theta) - L_0 \tag{2}$$

where θ = Arctan ($2d/L_0$), d = ram deflection, and L_0 = distance between grips. Because of the curvature of the inside edge of the clevis grooves (and, for the blunt fragment, the curvature of the cylindrical end), the precise ΔL can be slightly larger than given in equation 2. However, the difference is negligible for small angles (a change of only 3×10^{-4} in strain for $\theta = 15°$, which is approximately where the yarns fail). By dividing the force along the yarn by the yarn's cross-

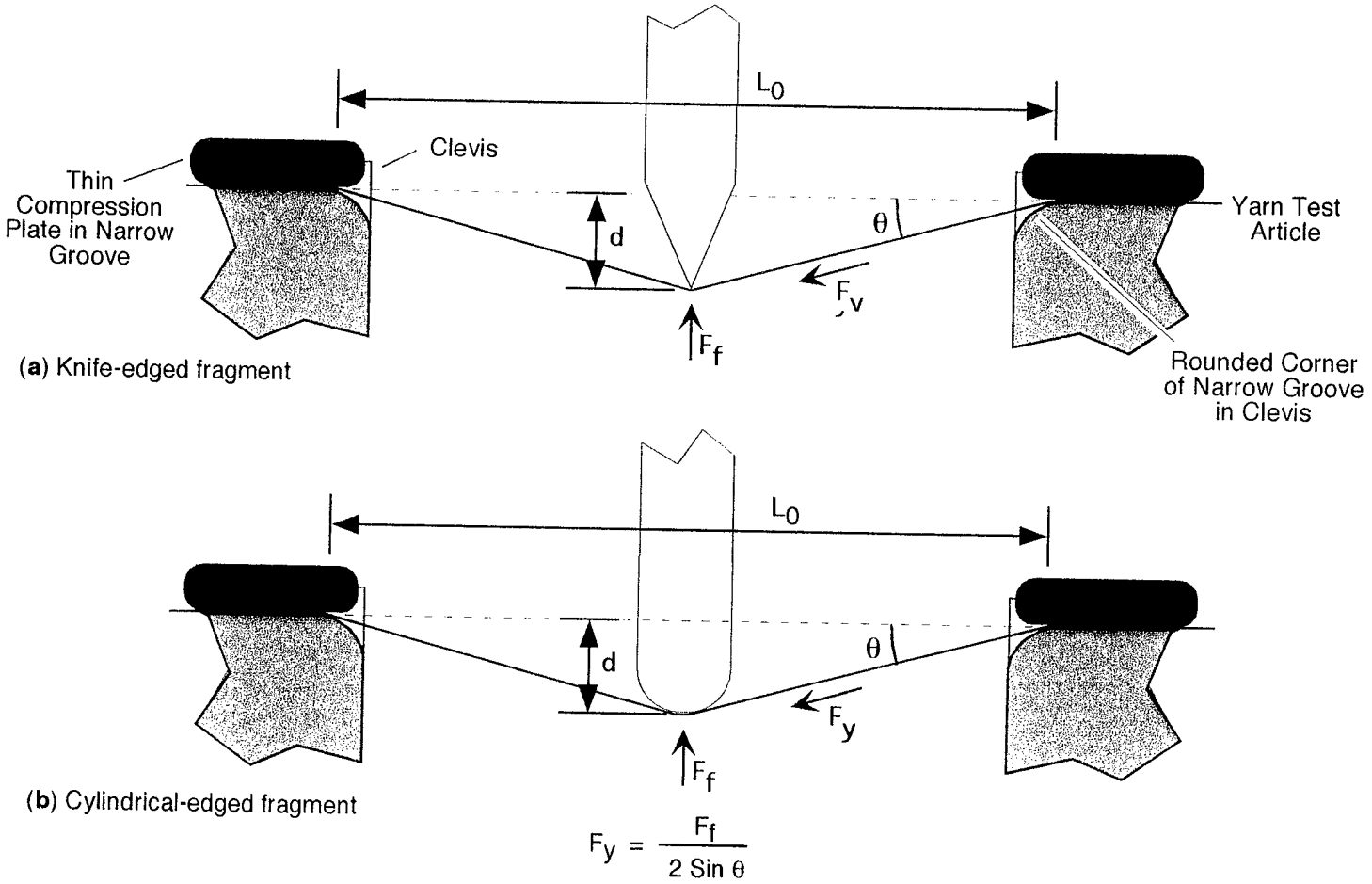

[F_y = Axial Force along Yarn, F_f = Vertical Force on Fragment

θ = Arctan ($2d/L_0$), d = ram deflection, and L_0 = distance between grips]

FIGURE 41. GEOMETRY FOR ANALYSIS OF TRANSVERSE LOAD TESTS

sectional area, and by dividing the yarn elongation by the gauge length, the stress–strain curve was obtained. Although the stroke rate is constant, the strain rate is not. Figure 42 shows the variation of the stroke, strain, and strain rate in a typical transverse load test.

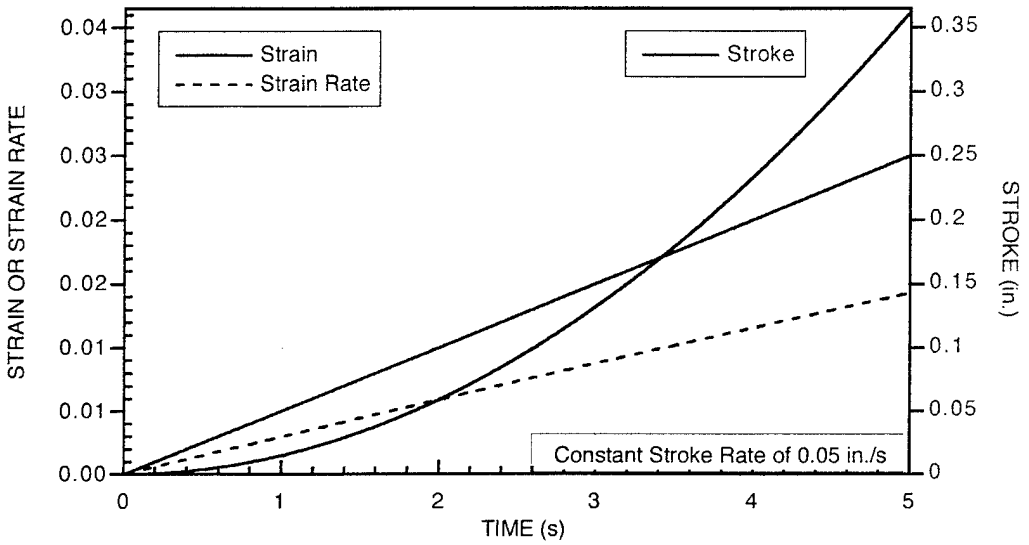

FIGURE 42. STRAIN, STRAIN RATE, AND STROKE VARIATION IN A TYPICAL TRANSVERSE LOAD TEST

The test was recorded by a video camera positioned close enough to observe individual fiber failure as well as the overall yarn deformation. The video pictures can be correlated with the recorded histories and resultant stress-strain curve (to obtain the stress and strain values at first fiber break, for example).

Test Results. Figure 43 shows selected video stills from a transverse load test for the knife-edge fragment loading a Zylon yarn. Although a few fibers fail remotely at locations distant from the knife edge, most of the fibers in the yarn fail by local rupture directly at the point of contact. At the end of the test, when the load reaches zero, the yarn looks as if it has been cut, with only a few fibers still appearing to be continuous.

This result is in sharp contrast to what was observed for transverse tests with the cylindrical loader and in the standard tensile tests reported above (see figure 36(b)), where the individual fibers fail at various points along the length of the yarn. Although the ends of some failed fibers in these tests have emerged from the yarn envelope, giving the yarn a frizzy appearance, most of the failed fiber ends remain trapped within the envelope, and even after the load drops to zero, the yarn appears largely intact.

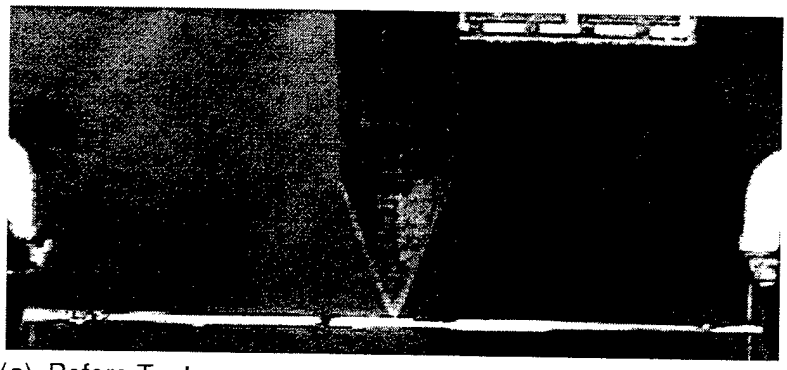

(a) Before Test

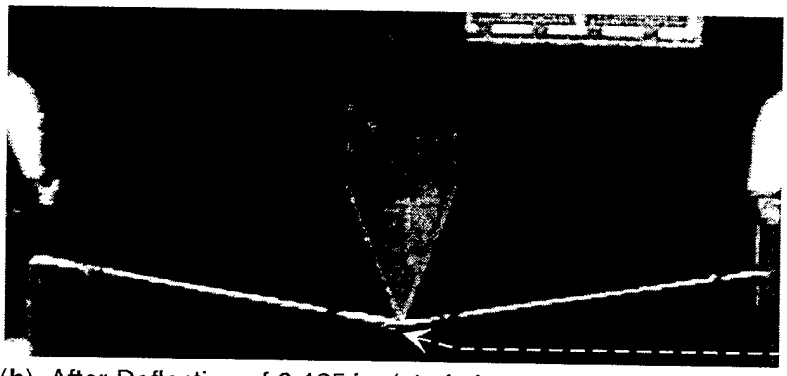

(b) After Deflection of 0.125 in. (strain in yarn = 0.92%)

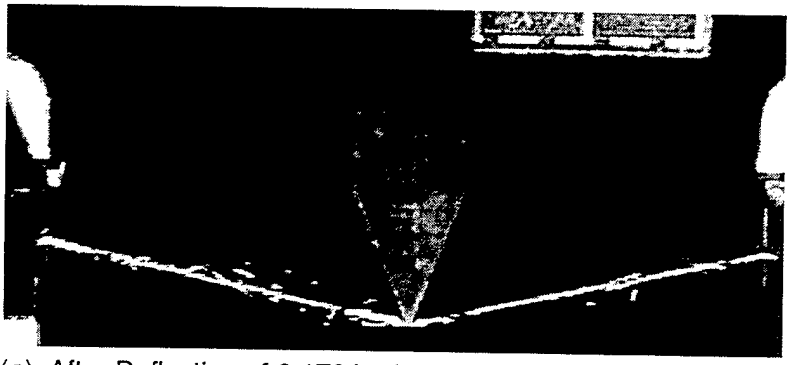

(c) After Deflection of 0.172 in. (strain in yarn = 1.73%)

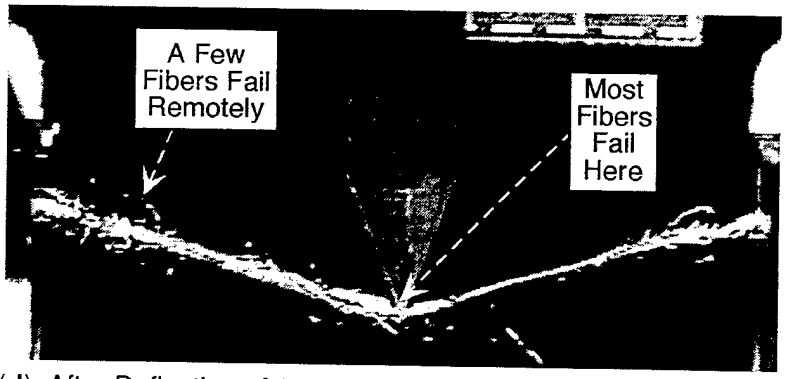

(d) After Deflection of 0.214 in. (strain in yarn = 2.67%)

FIGURE 43. VIDEO STILLS FROM ZYLON TRANSVERSE LOAD TEST

SEM photos of individual failed (or damaged) fibers reveal the difference in deformation and failure behavior between those loaded in tensile tests and in transverse load tests with knife-edge loaders. For both Zylon (figures 44(a) and 44(b)) and Kevlar (figure 45(a)), tensile failure occurs over a diffuse area, resulting in frayed ends with many separated microfibrils or bundles of microfibrils. In contrast, knife-edge transverse load failure (figures 44(c) and 44(d) for Zylon, figure 45(b) for Kevlar) is more localized and is characterized by bending of the fiber, transverse slicing at the point of contact, plastic deformation as the sliced material is forced out of the wedge-shaped groove, and finally complete separation at an angle with respect to the original load direction. Because failure appears to begin on the loaded side (rather than on the opposite side, which, because of the bending, is under more tension), it is likely that there is a shear component as well as a tensile component in the failure mode.

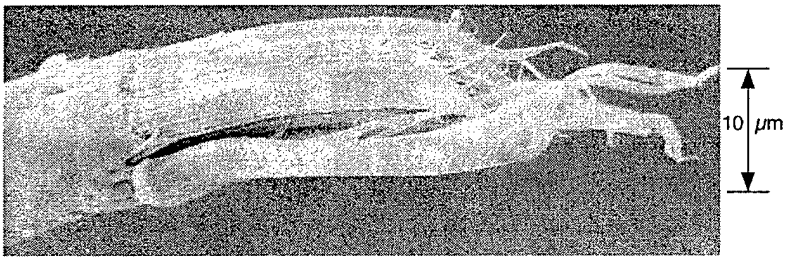

(a) One end of fiber failed in standard tensile test

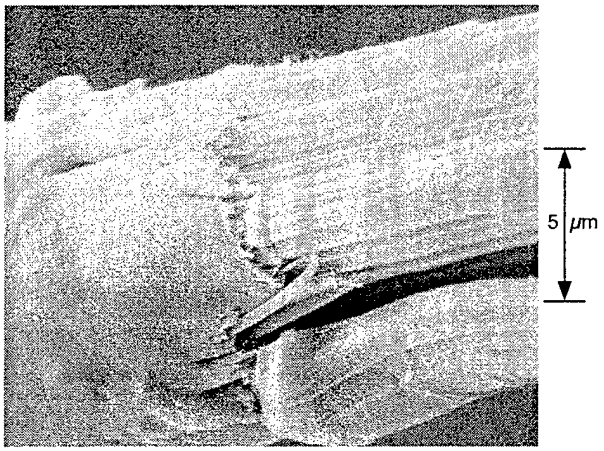

(b) Higher magnification view of (a), showing microfibril failure

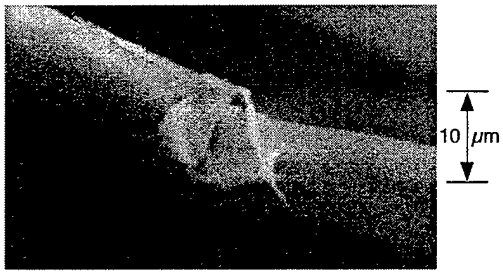

(c) Damaged fiber from transverse load test with knife-edge loader

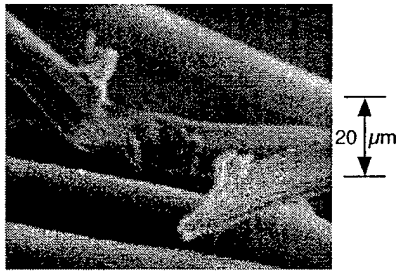

(d) Completely failed fiber from same test as (c)

FIGURE 44. SCANNING ELECTRON MICROSCOPE VIEWS OF FIBERS FROM UNWOVEN ZYLON YARNS RECOVERED FROM VARIOUS TENSILE AND TRANSVERSE LOAD TESTS

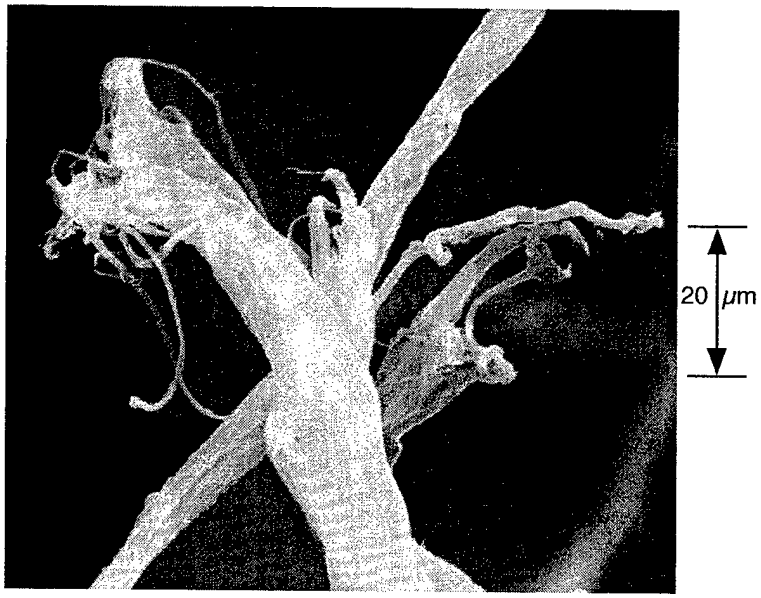

(a) Fibers failed in standard tensile test

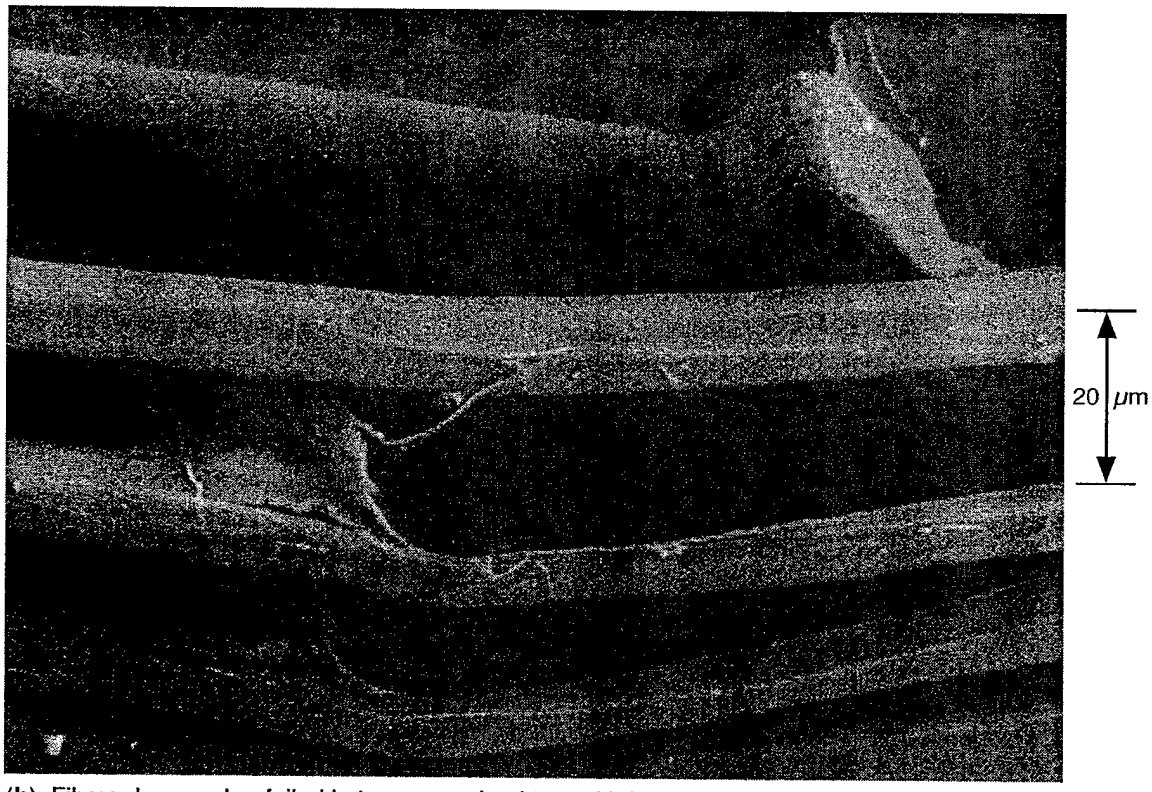

(b) Fibers damaged or failed in transverse load test with knife-edge loader

FIGURE 45. SCANNING ELECTRON MICROSCOPE VIEWS OF FIBERS FROM WOVEN KEVLAR YARNS RECOVERED FROM VARIOUS TENSILE AND TRANSVERSE LOAD TESTS

Table 9 gives the results from transverse load tests on high-strength fabric yarns. The stress-strain curves for unwoven Zylon, transversely loaded by both knife-edge and cylindrical loaders, are shown in figure 46, along with the curve for the standard tensile test. The most obvious result is that the transverse load test with the cylindrical loader followed almost exactly the same stress-strain path as the standard tensile test. Given the similarity in both yarn failure mode (namely, remote failure) and stress-strain path, these two tests can be considered identical as far as the yarn behavior is concerned.

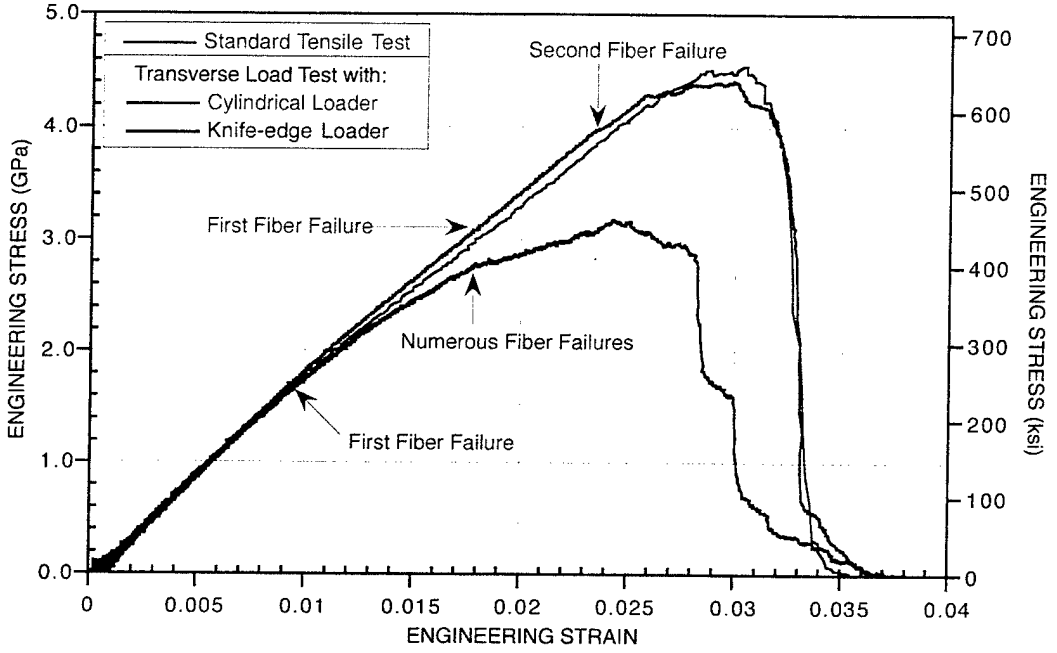

FIGURE 46. TRANSVERSE LOAD AND TENSILE TESTS RESULTS FROM UNWOVEN ZYLON YARN

The transverse test with the knife-edge loader followed a very different stress-strain path from that of the other two types of tests. The UTS and the SYE were both about 30% lower. From a correlation of the curve and the videotape records, it was determined that the first fiber failure occurred at a strain of only about 0.9%, and numerous fiber failures had occurred by 1.8% strain. In contrast, the first fiber failure in the cylindrical loader test did not occur until 1.8% strain, and the second not until 2.35% strain.

The differences between the knife-edge transverse load test and the standard tensile test are shown in figure 47 for Kevlar yarns. The UTS for the knife-edge test is 25% lower, while the SYE is 45% lower.

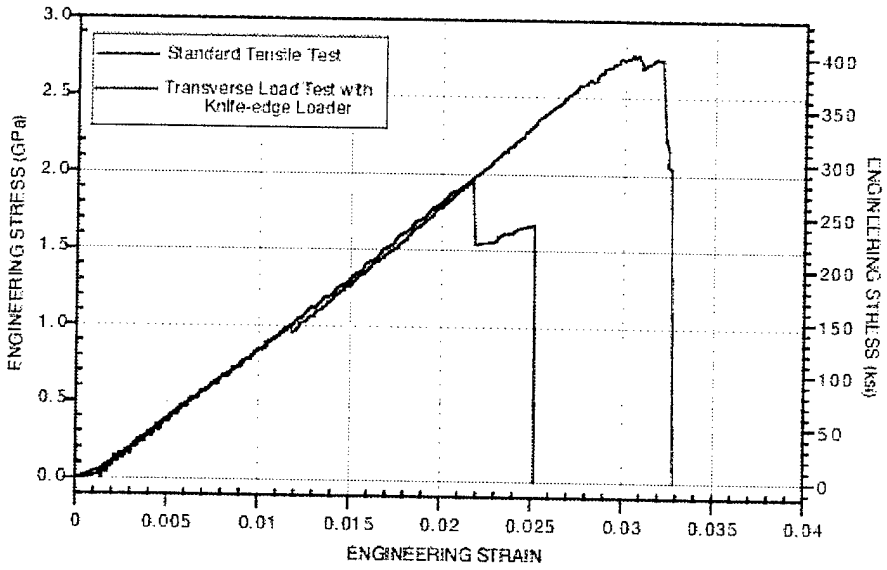

FIGURE 47. TENSILE AND KNIFE-EDGE TRANSVERSE LOAD TESTS FOR KEVLAR FILL YARN

SUMMARY AND CONCLUSIONS. A variety of tests were performed to subject various high-strength yarns to loads that would cause either local rupture or remote failure and then to characterize their deformation and failure. When loaded transversely by a fragment with a blunt contact edge (radius of curvature much greater than the yarn thickness), the yarns respond in the same manner as if they were simply loaded in tension—by remote (purely tensile) failure of the fibers all along the length of the yarn. When loaded by a fragment with a sharp contact edge (radius of curvature on the same order as the fiber diameter), the yarn responds by local rupture (combination of tensile and shear failure) at the point of contact.

SRI's fabric penetration computational simulations currently use a yarn failure model based on the results of the tensile tests. Inclusion of a shear component to the failure model, based on results of the transverse load tests, will now be attempted.

YARN PULLOUT TESTS.

Frictional forces between intersecting fill and warp fibers play a significant role in the deformation of high-strength woven fabrics subjected to fragment impact. Impacted yarns can slide along the intersecting transverse yarns during the fabric deformation. If the impact zone is near an ungripped edge of the fabric, yarns can be pulled through the surrounding fabric by the motion of the impactor. As discussed in the section on the push tests, frictional forces are involved in the load transfer from impacted to adjacent, unimpacted yarns during remote failure.

A new test was designed to characterize the frictional forces between intersecting orthogonal yarns, so that realistic frictional coefficients could be used in the computational fabric model. The test, called the pullout test, records the force on a single yarn as it is pulled out of a rectangular piece of fabric preloaded in tension in the direction transverse to that of the yarn being pulled.

EXPERIMENTAL TECHNIQUE. The experimental setup is shown in figure 48. A mounting frame, similar to that used in SRI gas gun impact tests, but modified to include one sliding grip, is attached to the ram of the MTS mechanical testing machine. The fabric is clamped on two edges into the fixed and sliding grips of the mounting frame (the gripping technique is similar to that previously shown for the gas gun tests in figure 13(b)). The distance between the clamped edges is roughly 7.25 in. (18.4 cm). The fabric is cut so that, on one of the unclamped edges, a number of unclamped yarns extend beyond the clamped region (the intersecting yarns in this region are removed). One of these yarns is attached through a high-sensitivity load cell to the testing machine's crosshead.

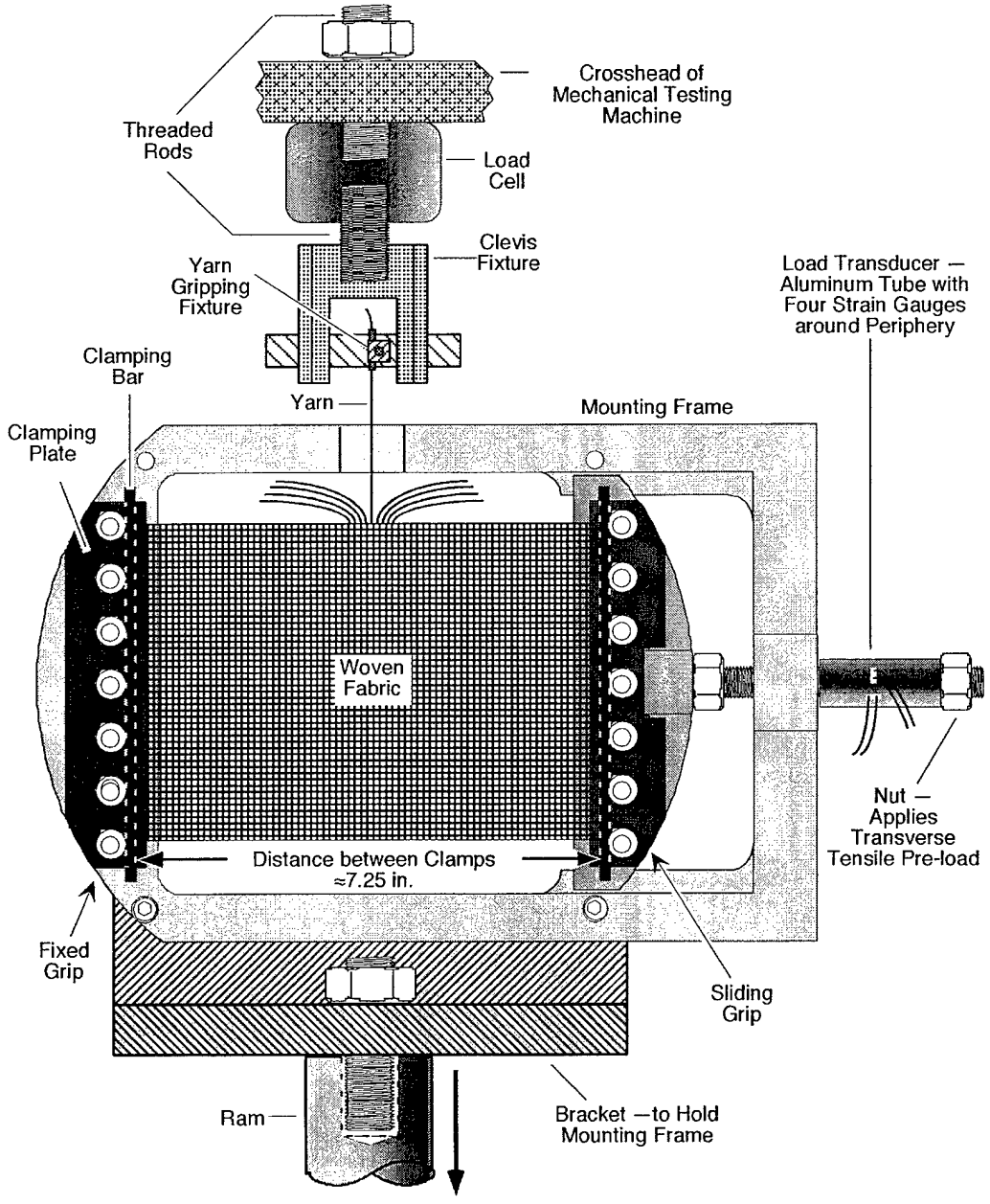

FIGURE 48. EXPERIMENTAL SETUP FOR YARN PULLOUT TESTS

A tensile preload is applied to the fabric by tightening a nut on the threaded rod attached to the sliding grip. This transverse force on the fabric is measured by a custom load transducer, a metal tube with four strain gauges (two axial and two circumferential glued at 90° intervals around the periphery, and wired in a Wheatstone bridge circuit).

The ram moves downward at a constant rate, first loading the individual gripped yarn in tension, and then gradually pulling it out from the fabric. During the test, the displacement of the ram, the force on the pulled yarn (by means of the load cell), and the transverse load on the fabric (by means of the load transducer) are recorded. A video camera aimed perpendicular to the plane of the fabric records the pullout of the yarn (i.e., the number of intersecting yarns that the distal end of the fiber passes).

The coefficient of static friction can be determined from the peak axial load and the geometry of the interfaces between the pulled yarn and the intersecting yarns. However, this interface geometry can be quite complex, as was shown in figures 9 and 10. The fill yarns are relatively straight (only 0.6% increase in length when removed from fabric and straightened), while the warp yarns are quite kinked (5.2% increase in length when removed and straightened). Although both are lenticular in cross-sectional shape, the fill yarns are more compact (slightly thicker, but significantly less wide) than the warp yarns. Whereas the fill yarns do not touch their adjacent fill yarn neighbors, the warp yarns do touch their adjacent warp neighbors at the cross-over point between fill yarns. Because of the complexity of the geometry and the fact that this geometry can change under transverse pretension, determining the frictional coefficient requires simulation of the test with the computational fiber model.

Figure 49 shows two videotape images of a typical Zylon 30 x 30 fabric pullout test. Figure 50 graphs the results of the test in terms of the axial tensile force on the pulled yarn and the transverse tensile load on the fabric specimen, plotted against the stroke (or ram deflection). The graph and the pictures reveal two distinct phases of the pullout test.

During the first phase of yarn deflection, the axial force rises, but no yarn pullout occurs. The yarn straightens itself out somewhat (reducing its crimp), while stretching and deforming the intersecting gripped yarns (therefore increasing the transverse load—significantly when the initial transverse load is small, negligibly when it is large). If the axial force exceeds the force necessary to break the yarn before it exceeds the static frictional forces on the yarn, the yarn breaks, effectively ending the test. Otherwise, the load on the yarn will rise to a peak, at which point pullout begins to occur. It should be noted that the force necessary to break a kinked yarn within a fabric is less than that necessary to break a yarn removed from the fabric (as in a tensile test). Because of the geometry, the tensile force along a kinked section of the yarn is higher than the axial force at the end of the yarn.

During the second phase of yarn deflection, the yarn is pulled out of the fabric at a constant rate, resulting in a gradual decrease in the axial force to zero and a return of the transverse force to near its initial value. The axial force does not decrease at a constant rate in proportion to the number of remaining yarns intersection, as might be expected, but instead drops more rapidly at first. This behavior could be caused by the relaxation of the tension on the yarns adjacent and parallel to the pulled yarn as the yarn pullout proceeds, which can reduce the frictional forces on

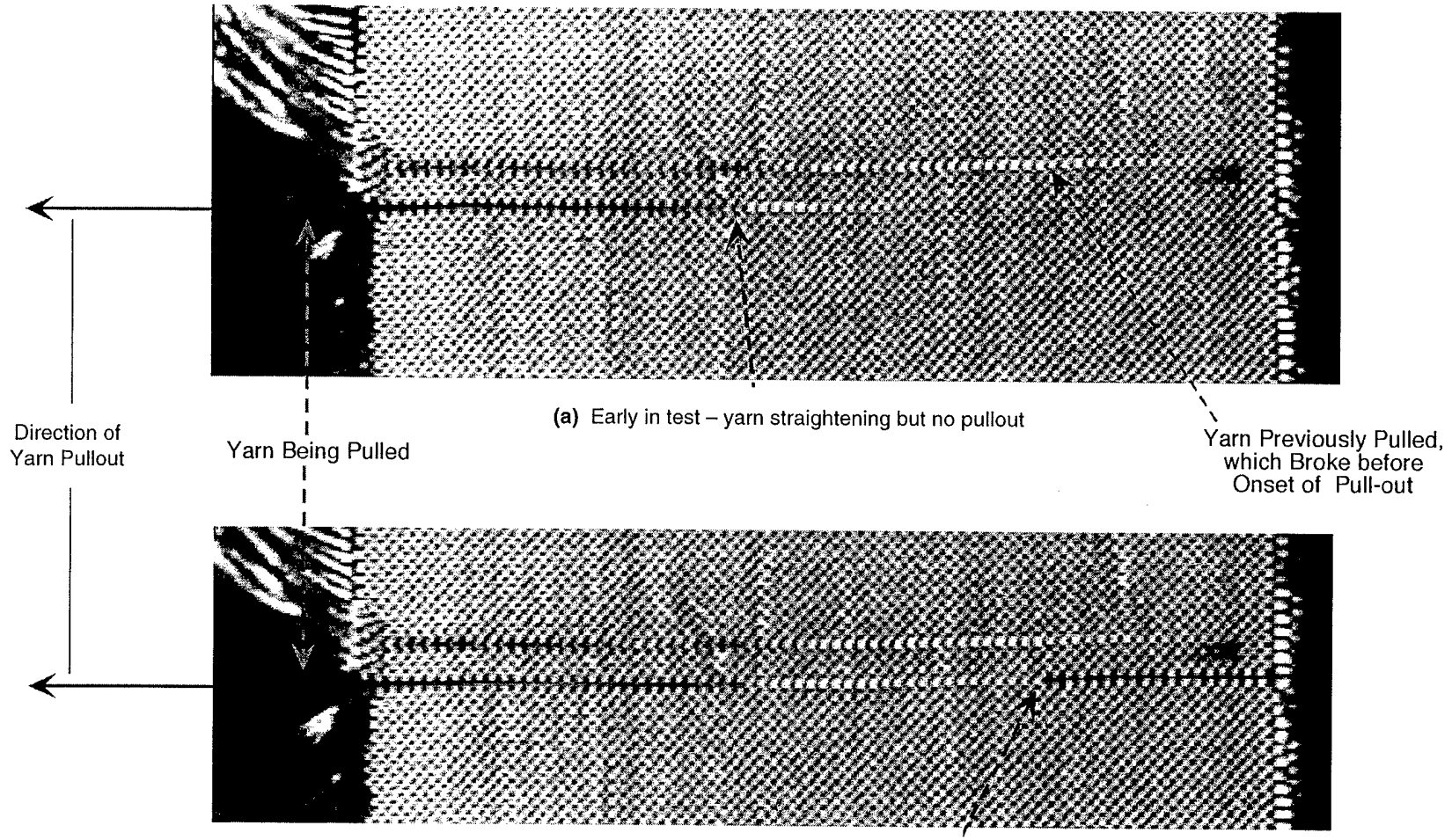

FIGURE 49. VIDEOTAPE IMAGES FROM ZYLON PULLOUT TEST

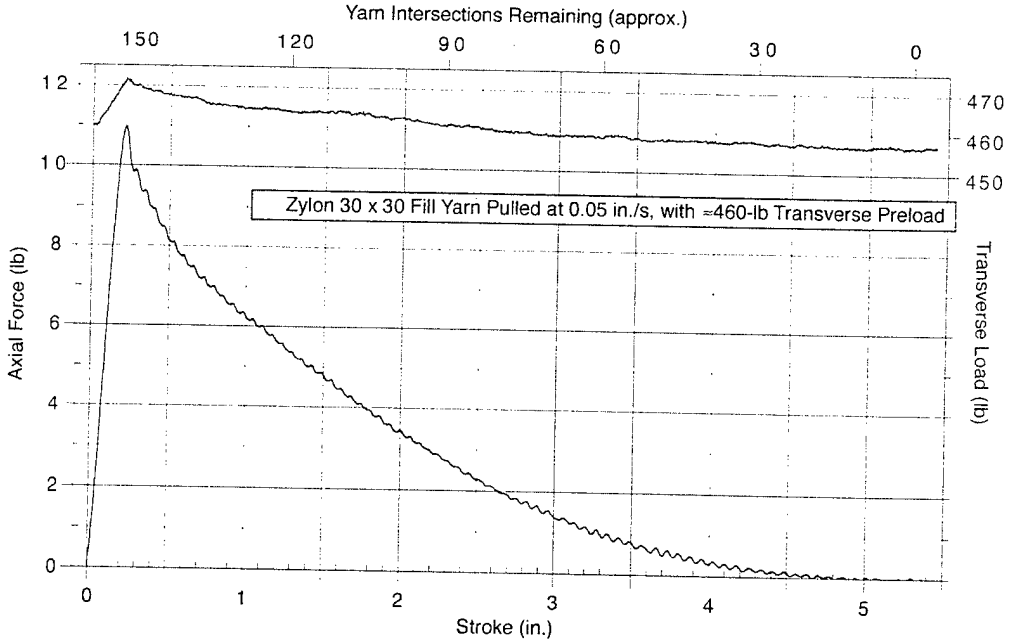

FIGURE 50. REPRESENTATIVE PULLOUT TEST RESULTS

the pulled yarn ahead of the pulled-out zone. It could also be affected by the dynamic coefficient of friction being lower than the static coefficient. The precipitous axial load drop following the peak in the composite plot for the Spectra 32 x 32 pullout tests (as shown in figure 51), followed by the relatively constant-slope decline, are more indicative of the latter explanation. Confirmation of these explanations must await computational simulation of the tests.

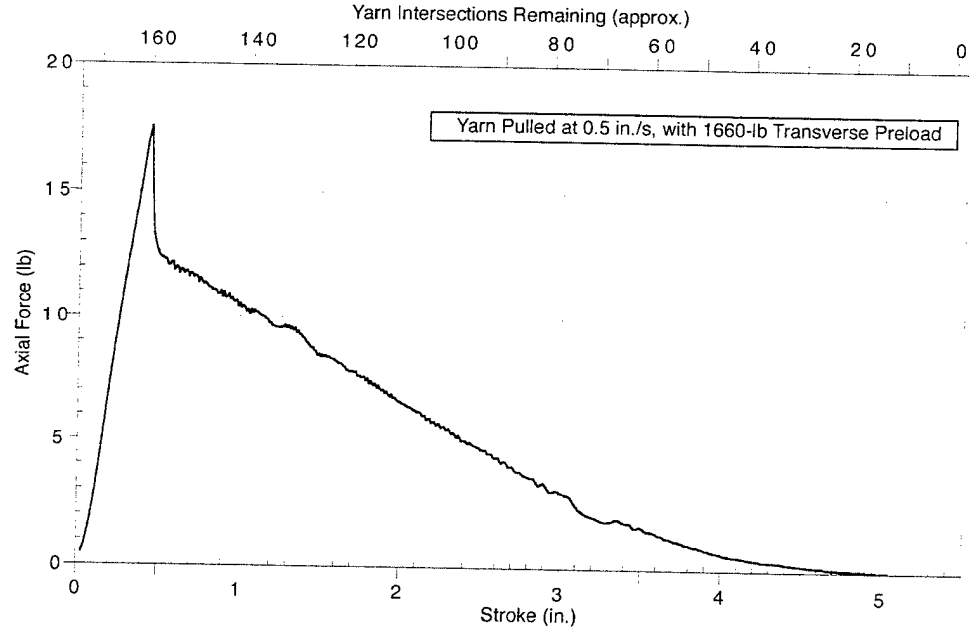

FIGURE 51. PULLOUT TEST RESULTS FOR A SPECTRA 32 x 32 WARP YARN

TEST MATRIX AND RESULTS. Eighty-three pullout tests were performed successfully on the high-strength fabrics. The tests included a variety of the high-strength fabrics and spanned a wide range of conditions that might be encountered during fragment impacts scenarios. Test parameters and the results of these tests are shown in table 10, grouped by fabric specimen. The setup allowed each fabric specimen to be used for a number of tests (usually 10 to 15 per specimen, each with a different pulled yarn), simply by changing the location of the yarn grip within the clevis fixture. A study was performed (Tests 22 through 27 in table 10) to determine how close a test yarn could be to a previously pulled-out yarn without altering the test results. Results showed that, if one or both adjacent parallel yarns were missing, the pullout force was significantly reduced, but negligible changes occurred if one or more yarns were present between the test yarn and previously pulled yarns. In all other tests, there were always two or more yarns between the test yarn and any missing yarns. The following parameters were varied during the tests:

- Material and weave density: Zylon 30 x 30 and 40 x 40, Kevlar 32 x 32, and Spectra 32 x 32.

- Yarn orientation: For most tests, the pulled yarns were the warp yarns and the gripped yarns were the fill yarns; however, for one series with Zylon 40 x 40, the reverse was true.

- Transverse tensile preload: From <10 to ≈2250 lb (<2.5 to ≈1000 N) for the test specimen or from <0.07 to 20 lb (<0.03 to 9 N) per transverse yarn.

- Yarn pullout rate (ram velocity): From 0.05 to 7.5 in./s (0.13 to 17.8 cm/s) the maximum rate attainable in the SRI testing machine.

- Specimen width (equals length of gripped edge): 1.2 and 5.0 in. (3.0 and 12.7 cm) or about ≈50 and ≈200 yarn intersections.

Pullout test results, in terms of the peak axial force plotted against the peak transverse load per transverse yarn, are shown in the next series of figures. The results for warp yarn pullout from 5-in.-wide specimens of Zylon 30 x 30, Spectra 32 x 32, and Kevlar 32 x 32 materials are shown in figures 52, 53, and 54, respectively, for various pullout rates. The results show a significant effect of pullout rate for the Zylon, a smaller effect for the Spectra, and a negligible effect for the Kevlar. The results for similar tests on two different specimens of the Zylon (see figure 52) show fairly good repeatability.

Figure 55 shows the expected large differences in results for Zylon 40 x 40 warp yarn pulled out from two specimens of different widths. Figure 56 shows a comparison of results from Zylon 40 x 40 fill and warp yarns. At relatively low transverse loads (such as 2 lb/yarn), there is negligible difference between the pullout forces for fill and warp yarns, but at much higher transverse loads (such as 20 lb/yarn), the fill yarns require more force to pull out than the warp yarns. This result is somewhat unexpected, because the fill yarns are straighter (less kinked) than the warp yarns. Again an explanation of this effect must await computational simulation.

TABLE 10. YARN PULLOUT MATRIX AND RESULTS

Test No.	Transverse Load Initial	Transverse Load Maxi-mum	Transverse Load Final	Average Transverse Load/Yarn	Pull-out (Stroke) Rate	Peak Pull-out Force	Stroke at Peak Force	Energy per Unit Length Needed to Pull Yarn Out*		Comments
	(lb)	(lb)	(lb)	(lb)	(in./s)	(lb)	(in.)	(J/m)	(ft-lb/ft)	
Warp Yarns from Zylon 30x30 fabric 5.0 in. wide (152 intersecting transverse yarns)										
11	46	54	43	0.32	0.05	3.2	0.18	4.24	0.95	
12	235	238	234	1.55	0.05	7.4	0.20	9.49	2.13	
13	348	356	350	2.31	0.05	10.2	0.23	11.97	2.69	
14	347	353	348	2.30	0.05	9.8	0.22	11.64	2.62	
15	460	472	457	3.05	0.05	11.0	0.21	12.69	2.85	
16	692	698	690	4.56	0.05	14.0	0.24	15.74	3.54	
17	929	931	921	6.10	0.05	16.2	0.23	17.24	3.88	
18	1158	1158	1153	7.61	0.05	19.7	0.23	19.29	4.34	
19	1612	1612	1606	10.59	0.05	21.0	0.24	20.95	4.71	
20	2211	2211	—	14.55	0.05	22.1	0.22	—	—	Yarn Broke
21	2267	2267	2259	14.90	0.05	23.1	0.26	21.10	4.74	
Warp Yarns from Zylon 30x30 fabric 5.0 in. wide (153 intersecting transverse yarns)										
22	918	928	925	6.04	0.05	14.3	0.23	14.93	3.36	Yarn 0
23	928	933	915	6.05	0.05	14.5	0.24	14.83	3.34	Yarn 8
24	930	934	931	6.09	0.05	14.6	0.24	14.77	3.32	Yarn 4
25	937	938	934	6.12	0.05	14.8	0.24	14.77	3.32	Yarn 6
26	939	941	941	6.15	0.05	3.3	0.19	4.68	1.05	Yarn 5 (no adj. yarns)
27	937	939	941	6.14	0.05	7.5	0.19	7.78	1.75	Yarn 1 (adj. yarn: 1 side)
28	468	481	475	3.10	0.05	11.2	0.22	12.57	2.83	
29	<10	—	—	<0.07	0.05	1.3	0.24	1.52	0.34	Transv. Load Not Recorded
30	201	212	201	1.34	0.05	5.2	0.13	6.23	1.40	
31	1960	1963	1956	12.81	0.05	20.4	0.22	18.74	4.21	
32	1950	1955	—	12.76	0.5	26.0	0.28	—	—	Yarn broke
33	915	917	910	5.97	0.5	19.2	0.27	18.56	4.17	
34	927	931	928	6.07	5	23.4	0.26	18.88	4.25	
35	922	929	924	6.05	7.5	25.1	0.30	19.01	4.28	
36	1479	1480	—	9.67	7.5	26.0	0.30	—	—	Yarn Broke
37	460	486	468	3.08	7.5	16.2	0.30	14.44	3.25	
38	465	480	465	3.07	0.5	12.5	0.26	13.41	3.02	
39	192	237	199	1.37	7.5	11.0	0.30	11.66	2.62	
Warp Yarns from Zylon 40x40 fabric 5.0 in. wide (204 intersecting transverse yarns)										
40	95	146	81	0.53	0.05	12.9	0.50	15.82	3.56	
41	100	179	107	0.63	0.5	15.7	0.59	19.93	4.48	
42	102	204	106	0.67	7.5	21.5	0.67	22.74	5.11	
43	474	501	—	2.39	0.05	20.0	0.55	—	—	Yarn Broke
44	302	368	319	1.62	0.05	22.7	0.61	30.44	6.85	
45	314	365	—	1.66	0.5	23.1	0.60	—	—	Yarn Broke
46	196	222	—	1.02	0.05	13.1	0.53	—	—	Yarn Broke
47	50	104	42	0.32	0.05	11.6	0.63	12.73	2.86	
48	46	111	44	0.33	0.5	11.3	0.60	13.03	2.93	
49	48	126	46	0.36	7.5	16.2	0.68	15.94	3.58	

*Not included is the energy required to stretch the yarn before pullout begins. The length used here is the length of the yarn within the fabric, which equals the fabric width (the minor correction for yarn crimp was ignored).

TABLE 10. YARN PULLOUT MATRIX AND RESULTS (Continued)

Test No.	Transverse Load Initial (lb)	Transverse Load Maximum (lb)	Transverse Load Final (lb)	Average Transverse Load/Yarn (lb)	Pull-out (Stroke) Rate (in./s)	Peak Pull-out Force (lb)	Stroke at Peak Force (in.)	Energy per Unit Length Needed to Pull Yarn Out* (J/m)	Energy per Unit Length Needed to Pull Yarn Out* (ft-lb/ft)	Comments
Warp Yarns from Kevlar 32x32 fabric 5.0 in. wide (162 intersecting transverse yarns)										
50	51	63	50	0.34	0.05	3.8	0.31	4.88	1.10	
51	49	61	49	0.33	0.5	3.6	0.29	4.46	1.00	
52	47	59	47	0.31	7.5	3.9	0.30	4.22	0.95	
53	495	503	484	3.05	0.05	15.8	0.38	21.06	4.74	
54	499	509	497	3.10	0.5	15.9	0.42	19.87	4.47	
55	479	487	—	2.98	7.5	15.0	0.40	—	—	Yarn Broke
56	983	987	—	6.08	0.05	16.8	0.29	—	—	Yarn Broke
57	757	768	—	4.71	0.05	17.7	0.36	—	—	Yarn Broke
58	201	222	216	1.31	0.05	8.0	0.40	10.66	2.40	
59	200	216	202	1.27	0.5	7.8	0.38	10.06	2.26	
60	204	212	203	1.27	7.5	6.9	0.38	9.11	2.05	
Warp Yarns from Spectra 32x32 fabric 5.0 in. wide (160 intersecting transverse yarns)										
61	49	57	41	0.31	0.05	2.5	0.45	3.05	0.69	
62	48	61	46	0.32	0.5	2.4	0.42	2.76	0.62	
63	50	68	48	0.35	7.5	3.5	0.43	3.68	0.83	
64	494	494	462	3.02	0.05	9.9	0.44	12.64	2.84	
65	495	497	491	3.09	0.5	10.6	0.46	12.58	2.83	
66	494	495	491	3.08	7.5	12.7	0.51	14.26	3.21	
67	195	199	176	1.19	0.05	6.1	0.48	8.04	1.81	
68	198	209	197	1.26	0.5	5.3	0.44	6.52	1.47	
69	200	219	201	1.29	7.5	7.7	0.53	9.05	2.04	
70	992	992	955	6.12	0.05	14.5	0.46	16.69	3.75	
71	982	985	977	6.13	0.5	15.0	0.44	15.55	3.50	
72	981	981	977	6.12	7.5	16.3	0.47	16.93	3.81	
73	1682	1683	1637	10.42	0.05	17.7	0.51	22.40	5.04	
74	1663	1663	1660	10.39	0.5	17.5	0.44	19.27	4.33	
75	1692	1694	1691	10.58	7.5	19.9	0.47	21.31	4.79	
Warp Yarns from Zylon 40x40 fabric 1.2 in. wide (49 intersecting transverse yarns)										
76	71	79	70	1.50	0.05	3.3	0.19	3.21	0.72	
77	75	90	76	1.64	7.5	5.7	0.28	4.13	0.93	
78	75	88	78	1.64	0.5	3.4	0.19	2.35	0.53	
79	500	500	500	10.20	0.05	6.5	0.20	5.24	1.18	
80	505	507	506	10.33	0.5	8.1	0.20	6.28	1.41	
81	501	502	501	10.23	7.5	9.1	0.17	7.05	1.59	
82	990	991	989	20.20	0.05	7.0	0.16	5.46	1.23	
83	992	993	992	20.25	0.5	8.4	0.22	5.97	1.34	
84	990	990	990	20.20	7.5	9.9	0.19	6.95	1.56	
Fill Yarns from Zylon 40x40 fabric 1.2 in. wide (49 intersecting transverse yarns)										
85	72	77	72	1.50	0.05	3.2	0.17	3.89	0.88	
86	70	76	70	1.47	0.5	3.9	0.20	5.06	1.14	
87	59	68	59	1.27	7.5	5.8	0.23	5.58	1.26	
88	493	494	492	10.06	0.05	7.5	0.14	6.98	1.57	
89	497	498	497	10.15	0.5	8.9	0.16	8.68	1.95	
90	497	497	497	10.14	7.5	9.7	0.16	8.74	1.96	
91	992	993	986	20.21	0.05	8.3	0.13	7.47	1.68	
92	1003	1005	1003	20.48	0.5	10.7	0.14	9.82	2.21	
93	956	956	954	19.50	7.5	11.6	0.16	9.39	2.11	No Video

*Not included is the energy required to stretch the yarn before pullout begins. The length used here is the length of the yarn within the fabric, which equals the fabric width (the minor correction for yarn crimp was ignored).

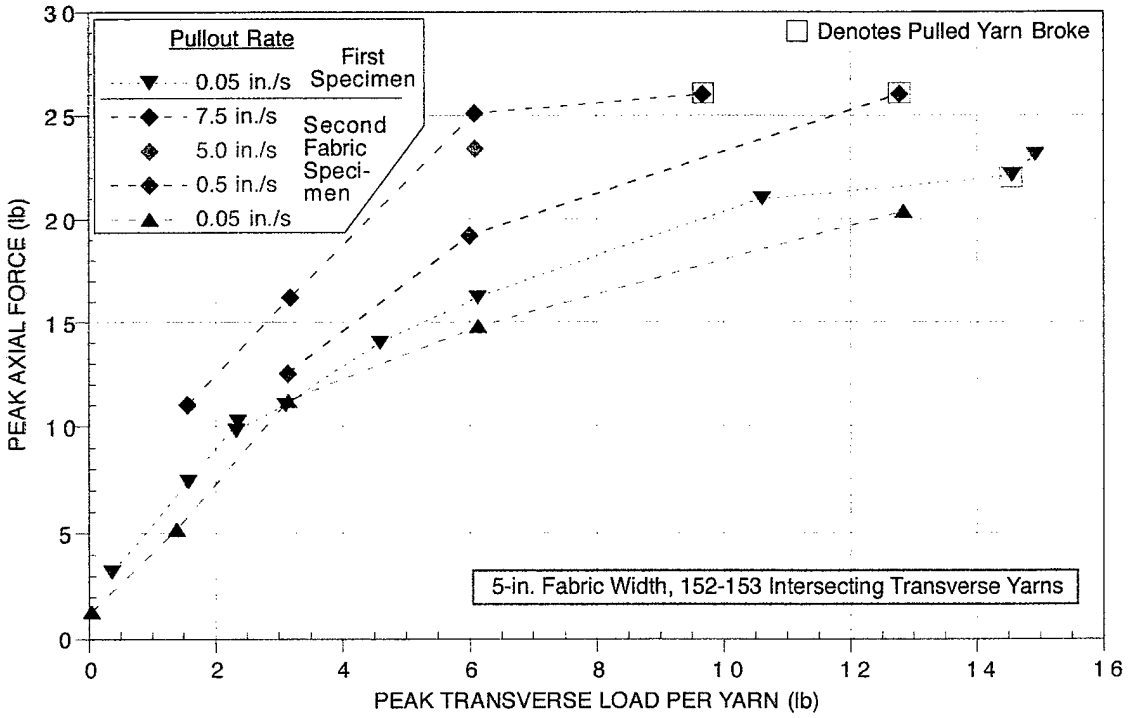

FIGURE 52. PULLOUT TEST RESULTS FOR ZYLON 30 x 30 WARP YARNS

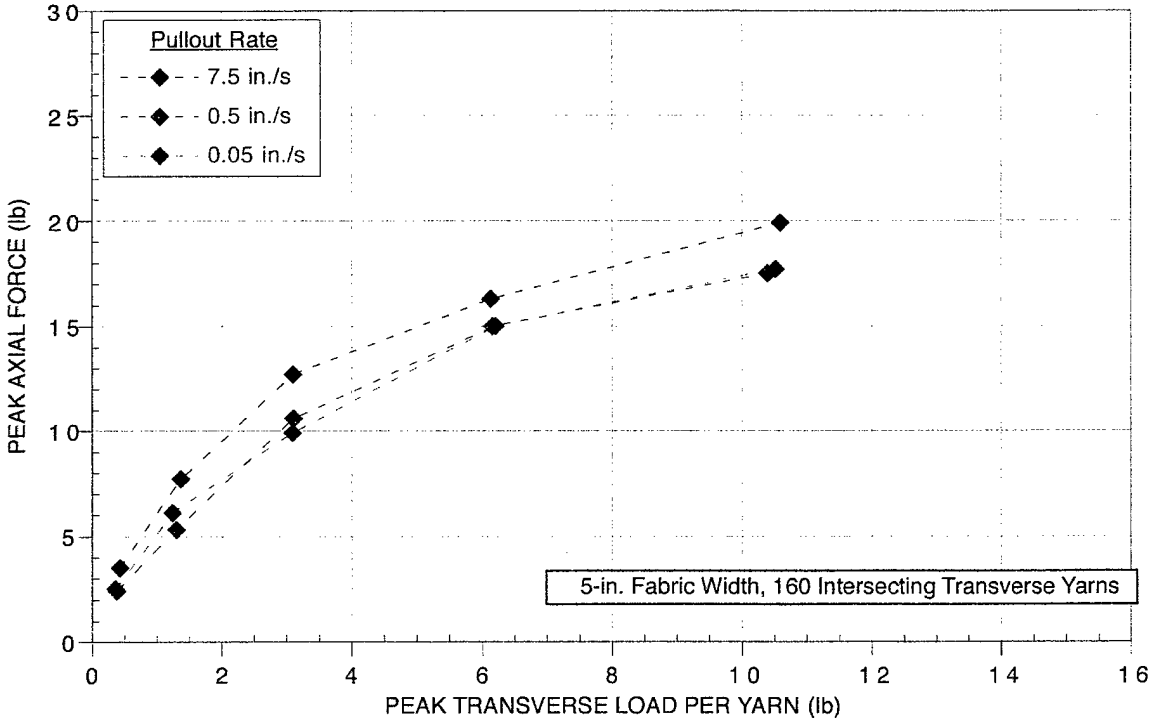

FIGURE 53. PULLOUT TEST RESULTS FOR SPECTRA 32 x 32 WARP YARNS

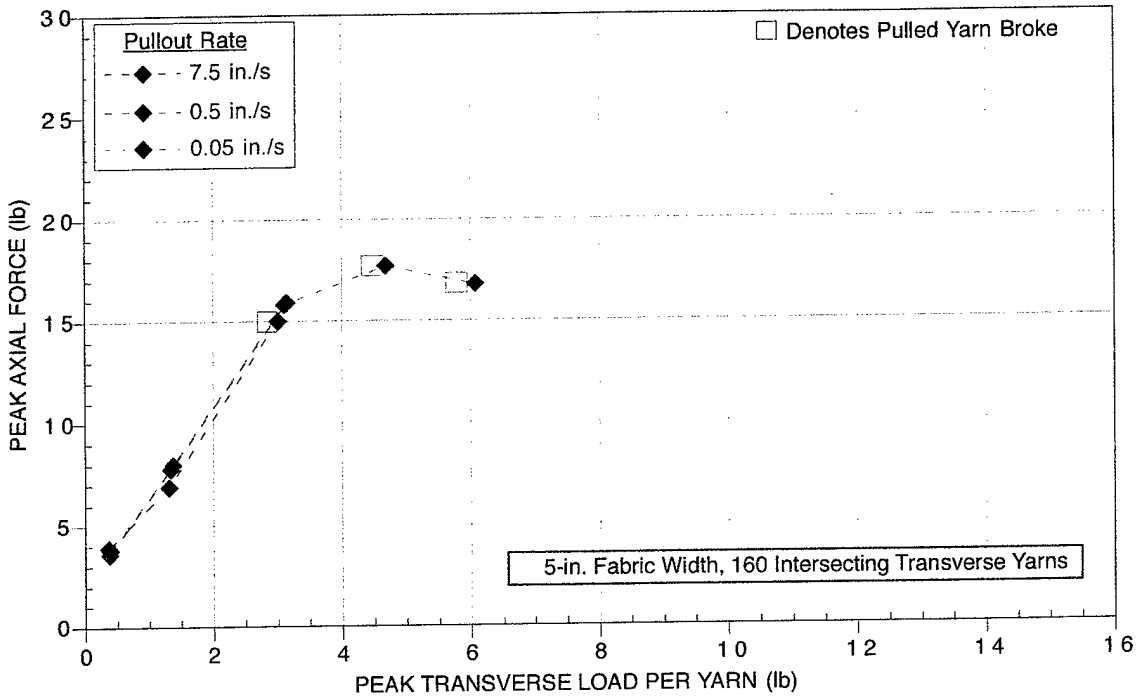

FIGURE 54. PULLOUT TEST RESULTS FOR KEVLAR 32 x 32 WARP YARNS

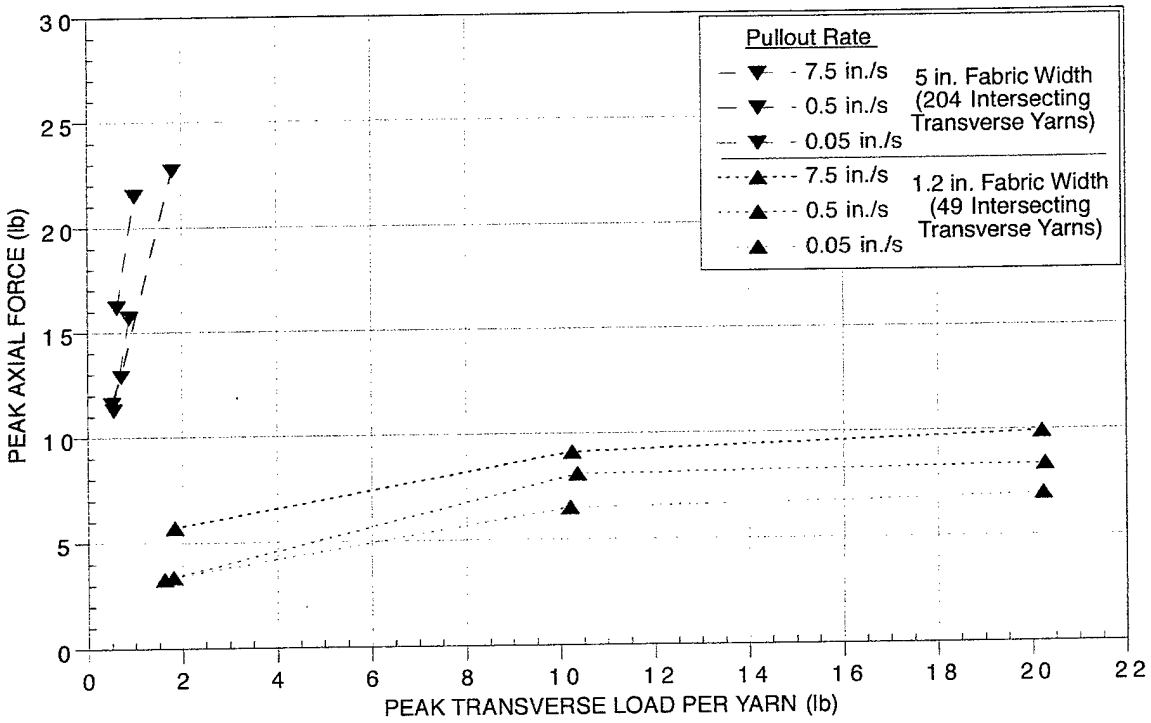

FIGURE 55. PULLOUT TEST RESULTS FOR ZYLON 40 x 40 WARP YARNS

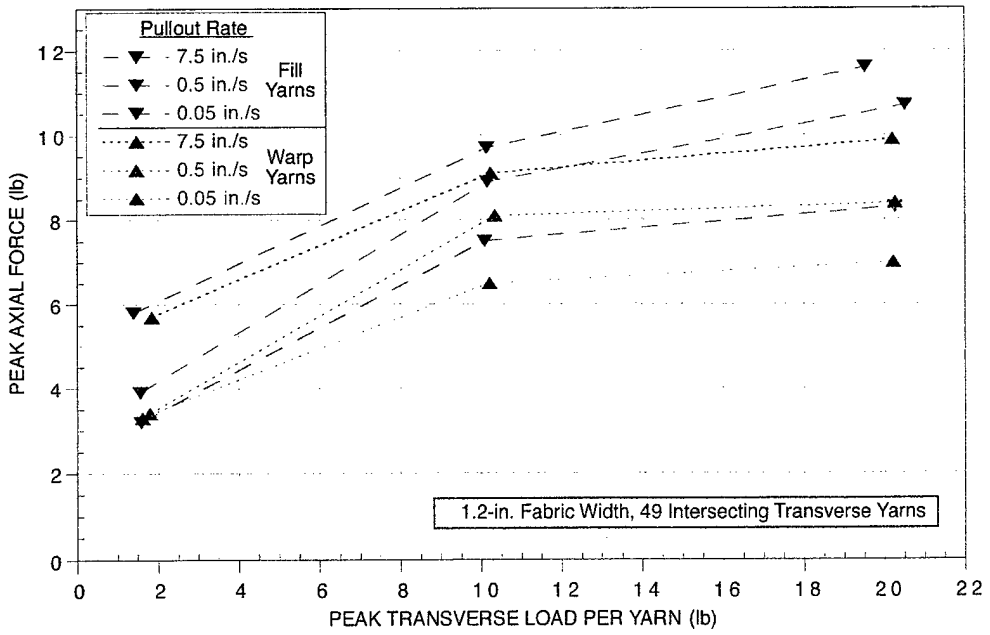

FIGURE 56. PULLOUT TEST RESULTS FOR ZYLON 40 x 40 FILL AND WARP YARNS

Comparisons of the results from 5-in.-wide specimens of all four of the materials tested are shown in figures 57, 58, and 59 for three pullout rates. At low pullout rates, Kevlar 32 x 32 requires more force than either Spectra 32 x 32 or Zylon 30 x 30, but at higher pullout rates, Zylon 32 x 30 exceeds the other two.

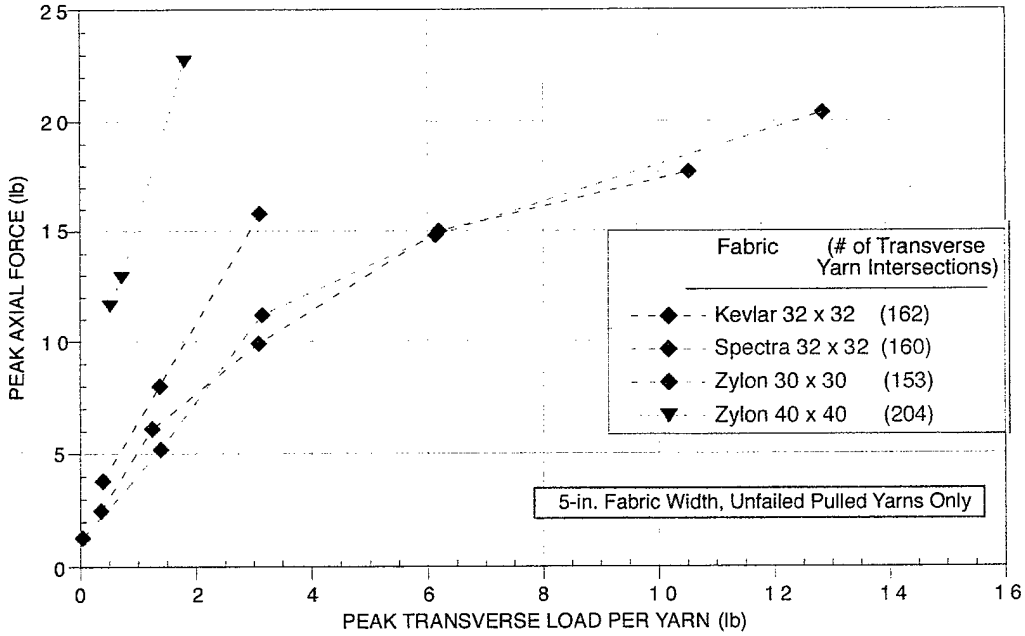

FIGURE 57. PULLOUT TEST RESULTS FOR SEVERAL FABRICS AT 0.05 in./s PULLOUT RATE

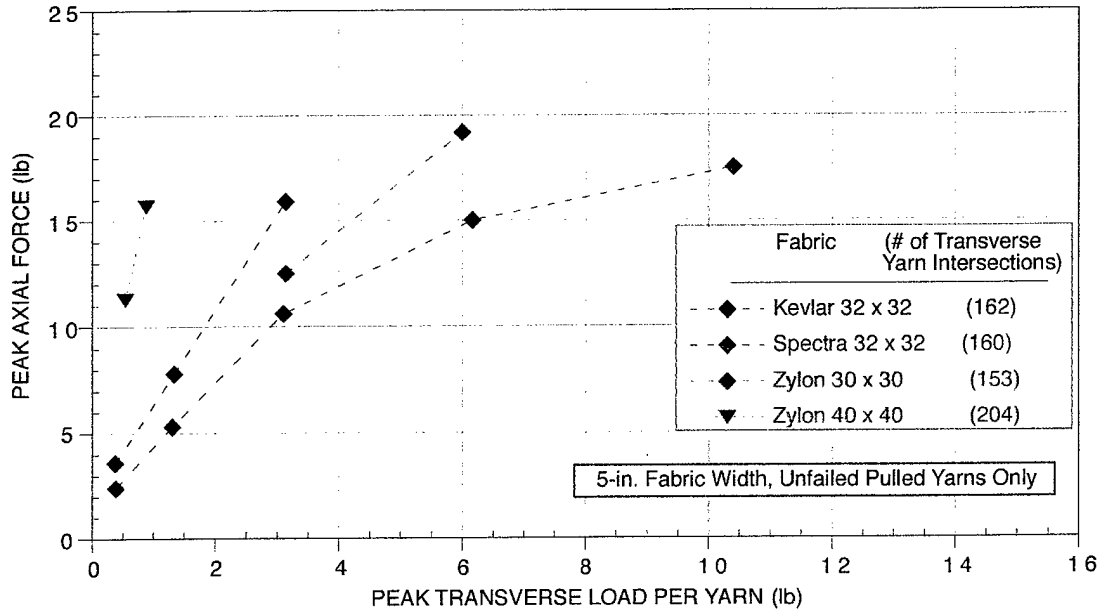

FIGURE 58. PULLOUT TEST RESULTS FOR SEVERAL FABRICS AT 0.5 in./s PULLOUT RATE

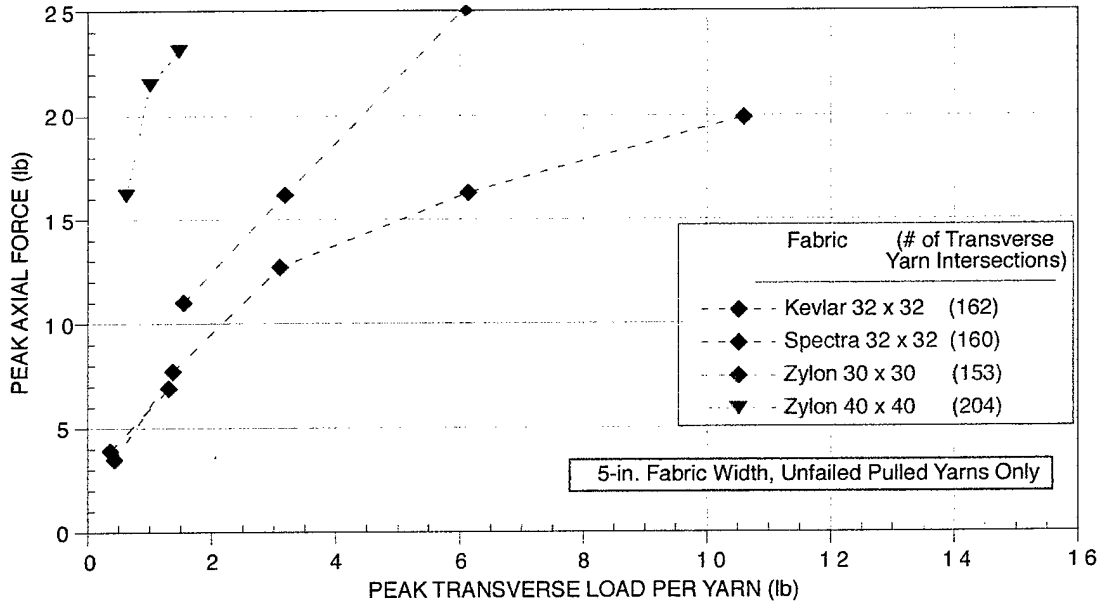

FIGURE 59. PULLOUT TEST RESULTS FOR SEVERAL FABRICS AT 7.5 in./s PULLOUT RATE

DISCUSSION AND SUMMARY. The energy needed to pull a yarn out of a fabric is equal to the area under the load-deflection curve after the peak axial force is reached (see table 10). A comparison can be made of the energy per unit length required to pull out a yarn in these tests and the energy per unit length required to stretch and break the yarn in the tensile tests (as shown in table 9). For the Zylon 30 x 30 warp yarns, for example, the pullout energy varies from only

1.5 J/m (0.34 ft-lb/ft) for a negligible transverse tensile load (<0.07 lb/yarn) to as high as 21 J/m (4.7 ft-lb/ft) for a significant transverse load (10 to 15 lb/yarn). The same yarns required 3.0 J/m (0.67 ft-lb/ft) to fail in the tensile tests. So if fiber pullout occurs in a fragment impact scenario (as was observed in some tests, including all those involving remote yarn failure), it will likely be a significant energy absorption mechanism.

In summary, many yarn pullout tests were performed using various high-strength fabrics under a wide range of transverse loads and pulling rates. A computational fabric model will be used to simulate these tests to obtain the coefficients of friction for the fabrics. These coefficients will then be used in future fabric penetration simulations to more realistically model the fabric behavior.

COMPUTATIONAL MODEL FOR BALLISTIC FABRICS

The objective of this task was to develop two distinct modeling capabilities for analyzing the response of woven fabrics. The first capability is a detailed computational model in which the individual yarns are modeled explicitly. Woven fabric is modeled by interweaving models of individual yarns. The goals of the detailed model are to understand the mechanisms of response for woven fabrics, including interactions between yarns and between yarns and fragments, and to explicitly model the failure mechanism of yarns and fabrics to study how to better design fragment barriers. The second capability is a simple computational design model that can be used to scope fragment barrier designs, for example, to determine how many layers of woven fabric are needed to stop a given fragment threat.

Both models are implemented into the three-dimensional finite element code LS-DYNA3D as user-defined materials. The detailed model is implemented for brick elements and the simplified model is implemented for shell elements. LS-DYNA3D allows simulation of a wide range of impact scenarios, including variations in the fabric size, shape, and design and variations in the fragment size, weight, shape, velocity, and trajectory.

DETAILED MODEL.

GEOMETRY. The geometry for the detailed model was determined using micrographs taken of woven fabrics, such as the one shown in figure 60 for a 30 x 30 Zylon fabric. The shape and dimensions of yarn cross-section were estimated from micrographs. As shown in figure 60, the yarns are lenticular, with a height-to-width ratio between 4 and 5. The amount of crimp in the fill and warp yarns can be deduced from the offset between adjacent yarns.

Figure 61 shows a representative finite element mesh for a section of crimped fill yarn from a 35 x 35 woven fabric. For this case, the width of the yarn is 0.82 mm and the height is 0.16 mm. The cross-sectional area of the modeled yarn is 0.10 mm^2. From the measured yarn denier of 500, the overall density of the yarn modeled as a continuum is 0.55 g/cm^3. This compares to a fiber area of 0.037 mm^2 and a fiber density of about 1.6 g/cm^3, which indicates that the yarns contain significant void volume.

(a) Fill Yarns

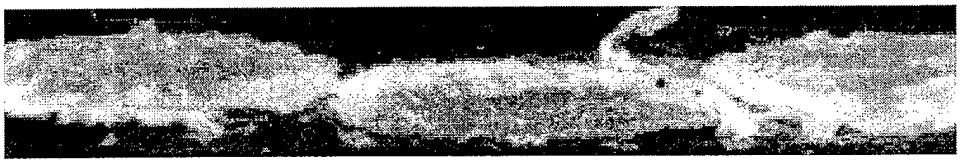

(b) Warp Yarns

0.020 in.
(0.51 mm)

FIGURE 60. GEOMETRY OF YARNS FOR 30 x 30 MESH FABRIC

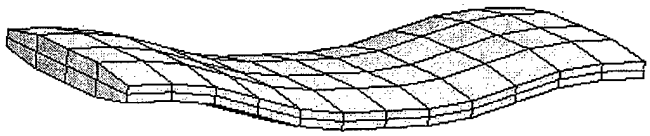

FIGURE 61. FINITE ELEMENT MESH FOR A SECTION OF CRIMPED YARN

A mesh with 8 brick elements in the cross section of the yarn and 12 elements along a crimp wavelength was used for the detailed yarn model. This rather low level of resolution was chosen to allow modeling of large enough patches of woven fabric to include yarn interactions. The chosen number of elements is about the minimum number that gives a realistic description of the geometry without introducing severe numerical instabilities that would result from too few elements. Four elements across the width is about the minimum number to define the surface in enough detail for the contact algorithms to function properly. Because the yarn material is strongly orthotropic, it is important to have enough resolution along the length to avoid any significant changes in fiber direction for adjacent elements.

Figure 62 shows the finite element model configuration for a woven fabric. Fill yarns, shown in figure 62(a), and warp yarns, shown in figure 62(b), are modeled individually and combined to form a fabric mesh as shown in figure 62(c). The weave is not symmetric; the warp yarns typically have more crimp than fill yarns. The amount of crimp was taken from micrographs similar to the one shown in figure 60. The example shown is representative of 35 x 35 fabric; the offset for the crimp (center to center) is about 0.12 mm for the fill yarns and 0.40 mm for the warp yarns.

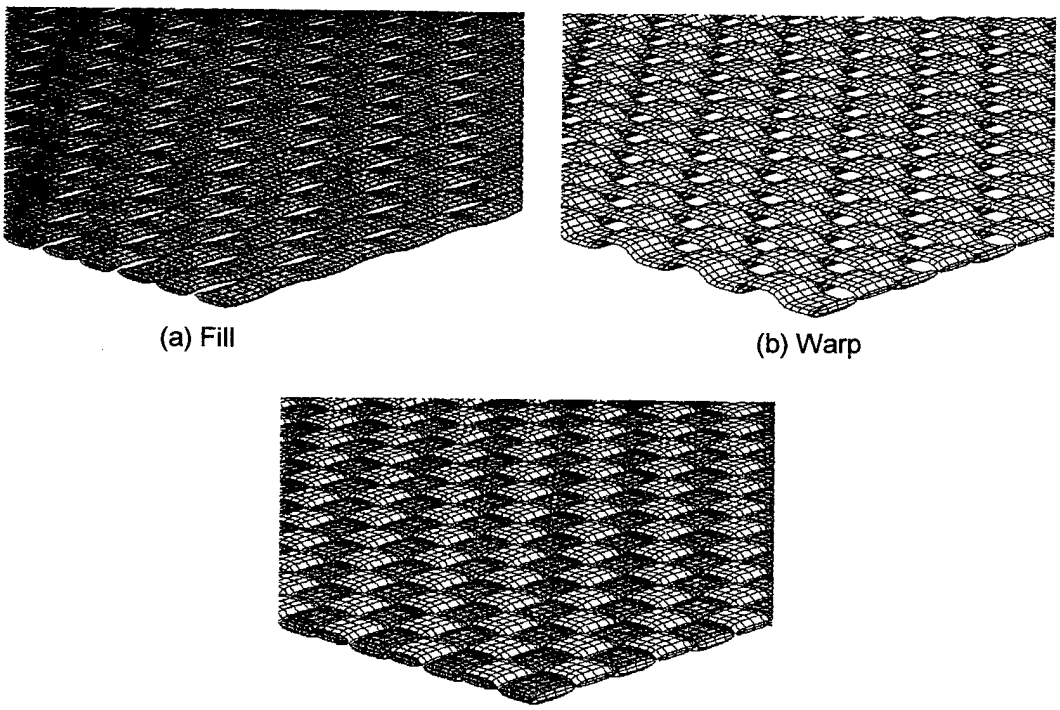

FIGURE 62. FINITE ELEMENT CONFIGURATION FOR WOVEN FABRICS

CONSTITUTIVE MODEL. The yarns that make up the woven fabrics have properties that are strongly directional. An important characteristic of the yarn response is that a crimped yarn does not have appreciable stiffness until it straightens out. This is not orthotropic behavior but bilinear or nonlinear behavior. This is because each yarn is made up of many (200-250) fibers that easily bend independently when a crimped yarn is straightened. To obtain a continuum treatment of this feature, an orthotropic constitutive model was used, which allows definition of independent Young's modulus, Poisson's ratio, and shear modulus in each of three orientations. The yarns are less stiff in orientations other than the fiber direction, and the yarns do not support compression loading. Table 11 lists the constants chosen for the orthotropic model. In the detailed model, the fiber direction for each element is defined by the alignment of specified nodes.

TABLE 11. MATERIAL CONSTANTS FOR DETAILED MODEL

E_f	Young's Modulus (fiber direction)	164 GPa
E_o	Young's Modulus (nonfiber directions	3.28 GPa
G	Shear Modulus (all directions)	3.28 GPa
ν	Poisson's ratio (all directions)	0
ρ	Density	0.50 g/cm^3

FAILURE MODEL. To develop a failure model for the Zylon yarn, the mechanism of tensile failure of the fibers in the yarn was considered. Each yarn is made up of 200 to 250 fibers. The fibers are assumed to be elastic until they break in tension. For the continuum model the axial stress in the yarn, σ_a, was assumed to be the elastic stress from the strain in the unbroken yarns,

$$\sigma_a = E(1-d)\varepsilon_a \tag{3}$$

where, E is the fiber modulus, d is the fraction of broken yarns which varies from zero to one, and ε_a is the strain,. For a dynamic analysis, the rate of stress is given by

$$\dot{\sigma}_a = E(1-d)\dot{\varepsilon}_a - E\dot{d}\varepsilon_a \tag{4}$$

The rate of fiber breakage is assumed to be a simple function of strain as shown in figure 63, namely, that at some minimum value of strain, ε_{min}, fibers start to break and the fraction of fiber breakage increases linearly with strain up to a maximum strain, ε_{max}, at which all fibers are broken. In incremental form, equation 4 is given by

$$\Delta\sigma_a = E(1-d)\dot{\varepsilon}_a\Delta t - E\Delta d\varepsilon_a \tag{5}$$

For numerical stability, the increase in damage Δd at any computational step is limited to a small number, e.g., 0.002. When all the fibers are broken (i.e., the damage equals one), the element is removed from the calculation (eroded).

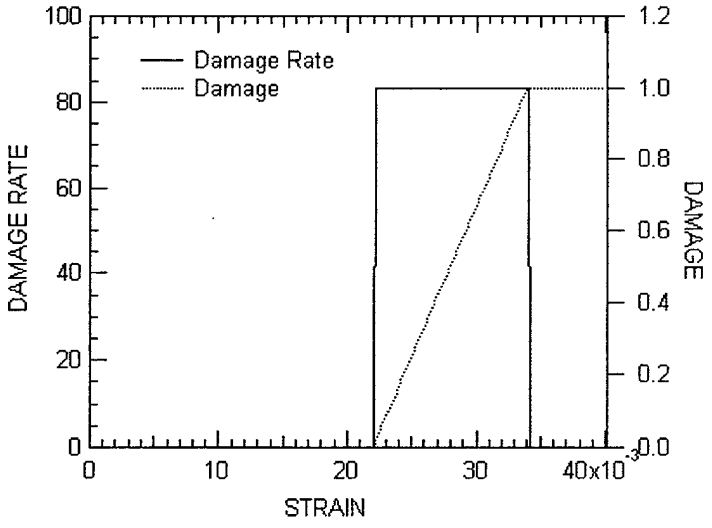

FIGURE 63. FIBER DAMAGE AS A FUNCTION OF STRAIN

Figure 64 shows the calculated stress-strain response for an uncrimped yarn. The calculated response shows very good agreement with the measured stress-strain curve over the range of response including the peak and the softening portion of the curve.

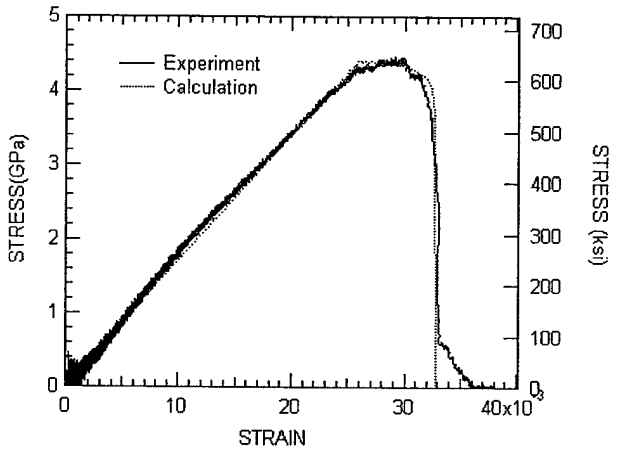

FIGURE 64. STRESS-STRAIN CURVES FOR TENSILE TEST OF UNCRIMPED YARN

SINGLE YARN EXAMPLES. The calculational reliability of the detailed model was examined by performing several simulations of tests on single yarns: a single crimped yarn pulled axially, a single crimped yarn loaded transversely, and a single crimped yarn hit by a projectile.

Single Crimped Yarn Pulled in the Axial Direction. The first simulation was a single crimped yarn pulled in the axial direction. The finite element mesh for a short section of a crimped yarn is shown in figure 61. The amount of crimp is representative of the fill yarns in 35 x 35 Zylon fabric weave and is equivalent to about 2% strain.

The left end of the yarn was pulled at 20 m/s and the right end was held. Figure 65 shows a nominal stress-strain curve for the yarn as it is pulled, and figure 66 shows the shape of the yarn as it straightens out. As shown in figure 65, the stress in the yarn is small initially and increases as the yarn is straightened. For this example the initial strain in the yarn was assumed to be -2.5% to adjust for the crimp. The stress reaches a peak of about 4.5 GPa at a strain of about 3%, and then the yarn breaks.

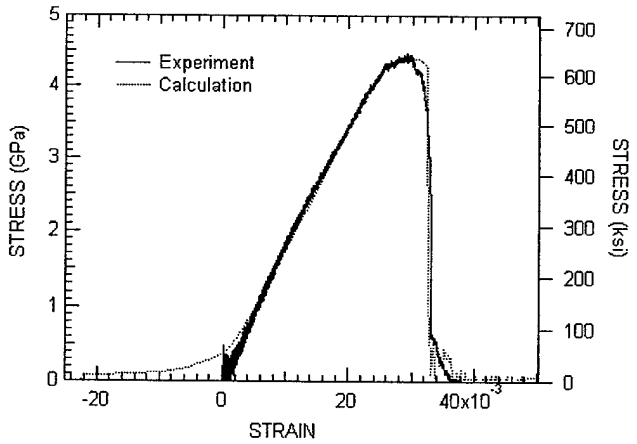

FIGURE 65. STRESS DEVELOPED IN CRIMPED YARN FOR AXIAL TENSION TEST

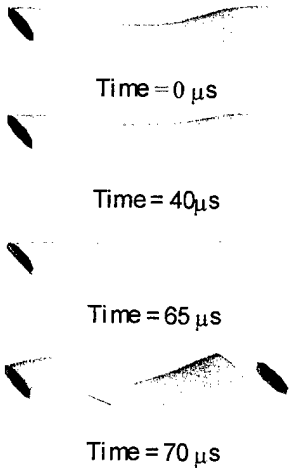

FIGURE 66. CALCULATED SHAPE OF A SINGLE YARN PULLED TO FAILURE IN AXIAL TENSION

Single Crimped Yarn Loaded Transversely. For the second simulation, the left end of a crimped yarn was displaced transversely at 20 m/s while holding the right end fixed. This example requires that the model undergo large displacements and rotations as well as stretching without developing any appreciable resisting load.

Figure 67 shows the calculated resisting stress developed in the yarn. The peak stress reached is just under 3 GPa. The shape of the yarn as it deforms is shown in figure 68, along with fringes of effective stress in the yarn.

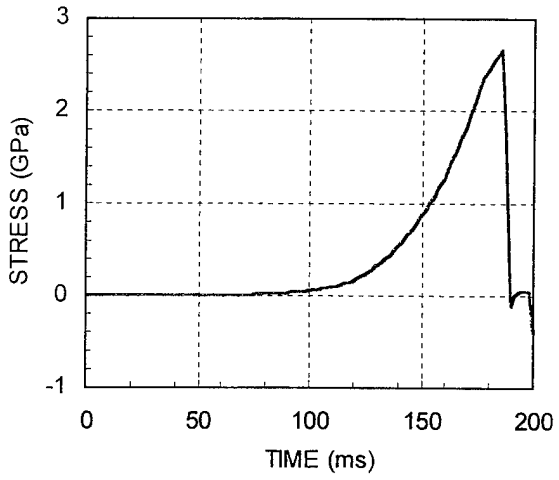

FIGURE 67. TIME HISTORY OF EFFECTIVE STRESS

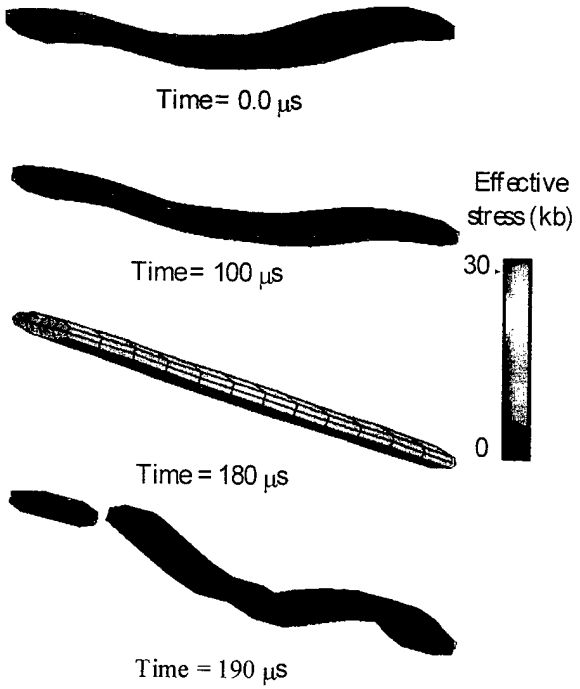

FIGURE 68. EFFECTIVE STRESS FOR A SINGLE TRANSVERSELY LOADED CRIMPED YARN

Transverse Impact of a Crimped Yarn by a Projectile. The third example was to test the capabilities of modeling the interaction between a projectile and a Zylon yarn. This example simulates a 5-cm (2-inch) length of crimped yarn being impacted by a small round-nosed titanium projectile at 80 m/s. The finite element model is shown in figure 69 at time t = 0.0. Also shown are the response of the impacted yarn and the calculated effective stress in the yarn at various times after impact.

Figure 70 shows the time history of the resisting force of the yarn on the projectile. The force is small up to about 25 μs. As the yarn straightens, the force increases. The force reaches a peak of about 1.4×10^7 dyne (30 lb).

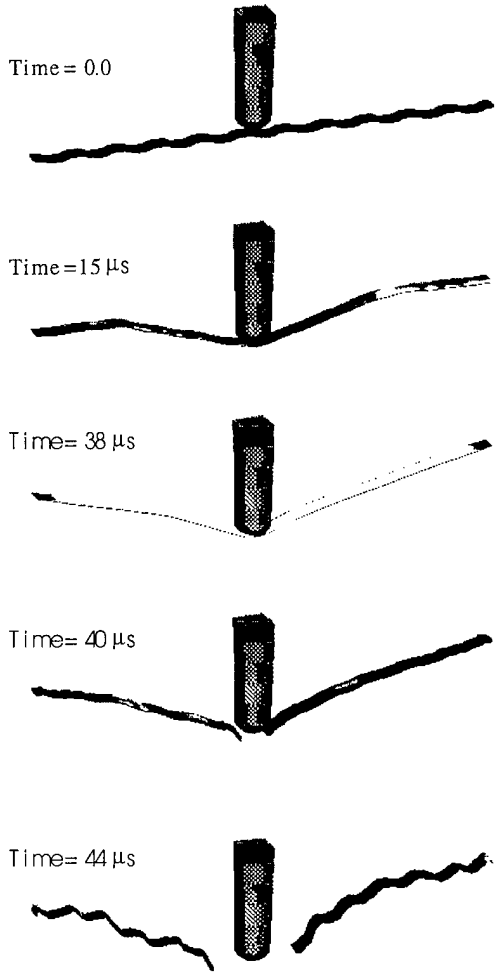

FIGURE 69. SINGLE YARN IMPACTED BY A PROJECTILE AT 80 m/s

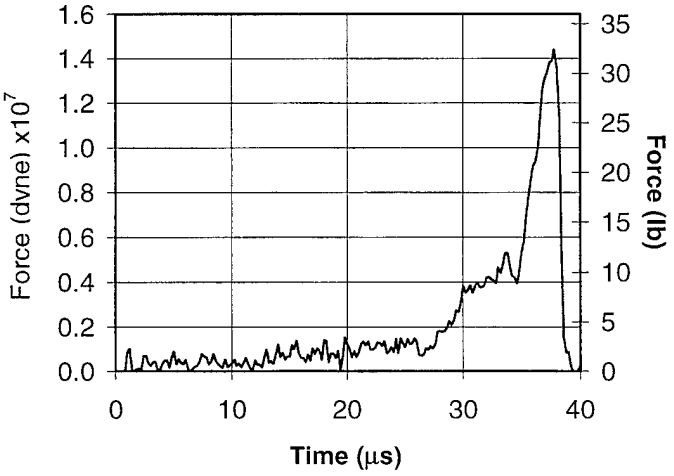

FIGURE 70. RESISTING FORCE OF YARN HIT BY PROJECTILE AT 80 m/s

From the displaced shape of the yarn, the speed of the transverse displacement wave in the fabric is estimated to be only about 320 m/s. This velocity is much less than the sound speed in a taut yarn of about 14,000 m/s.

EFFECT OF DENSITY. The resistance of the yarn is due to both the strength of the yarn and its inertia. To determine the relative importance of these two factors, a small titanium fragment striking a single yarn at 200 m/s was simulated for yarn density values of 0.5 g/cm^3 and 1.0 g/cm^3. The resisting force on the fragment is shown in figure 71(a) and the fragment velocity is shown in figure 71(b). Increasing the density of the yarn from 0.5 g/cm^3 to 1.0 g/cm^3 yarn significantly increases the resisting force. Thus, for this range of velocity, much of the fabric's effectiveness is due to inertia.

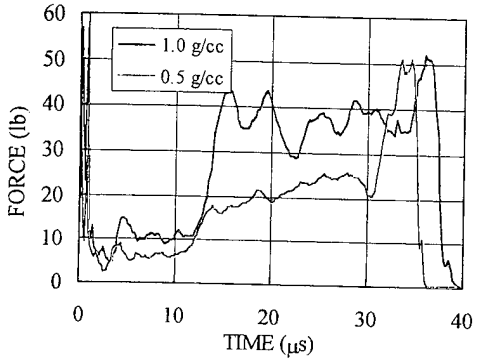

(a) Force on Projectile

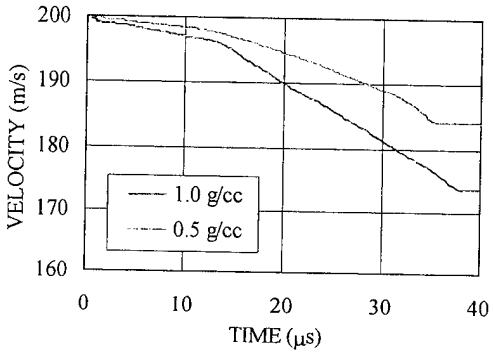

(b) Projectile Velocity

FIGURE 71. EFFECT OF YARN DENSITY ON BALLISTIC PERFORMANCE

EFFECT OF CRIMP. To quantify the effect of crimp, two simulations of a fragment impacting a single yarn were performed, one with crimp and one without crimp. The results of the simulations are shown in figure 72. The main effect of crimp is that it delays the resisting force. The crimped yarn does impart a slightly larger peak resisting force, but the overall effect on velocity change, as shown in figure 72(b), is small. The difference in change of velocity (i.e., impulse) is roughly equivalent to the difference in weight between the crimped and uncrimped yarn.

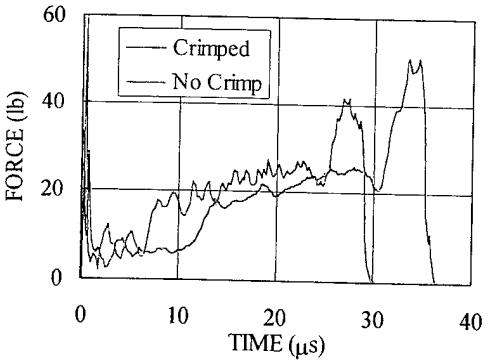

(a) Force on Projectile

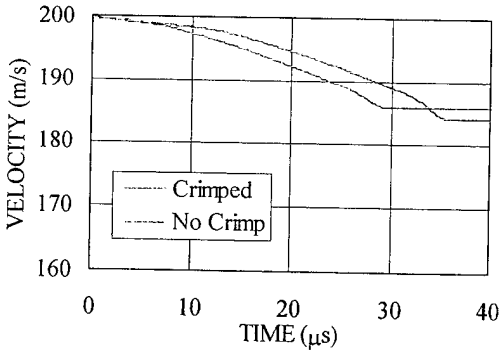

(b) Projectile Velocity

FIGURE 72. EFFECT OF CRIMP ON BALLISTIC RESISTANCE

WOVEN FABRIC. A model of a woven fabric was developed by interweaving single yarns. The mesh for a section of woven fabric is shown in figure 62(c). The interfaces between the yarns were typically modeled as frictionless. The effects of friction will be included after the results of the friction pull tests are analyzed.

EFFECTS OF BOUNDARY CONDITION. Three cases of boundary conditions were simulated for the geometric configuration shown in figure 73(b): (1) four sides held, (2) two sides held, and (3) no sides held. Figure 73(a) shows the force on the impactor for the three cases. The peak force for four sides held is the greatest, but at 50 ms the yarns break in both directions and the impactor is free to penetrate. For the case held on two sides, the initial peak is less than for four sides held, but as held yarns break, the unheld yarns transfer the load to adjacent held yarns, resulting in a longer duration resisting force on the impactor. For the case with no sides held, the fabric still provides some resistance due to inertia, and that is significant for the engine fragment barrier situation.

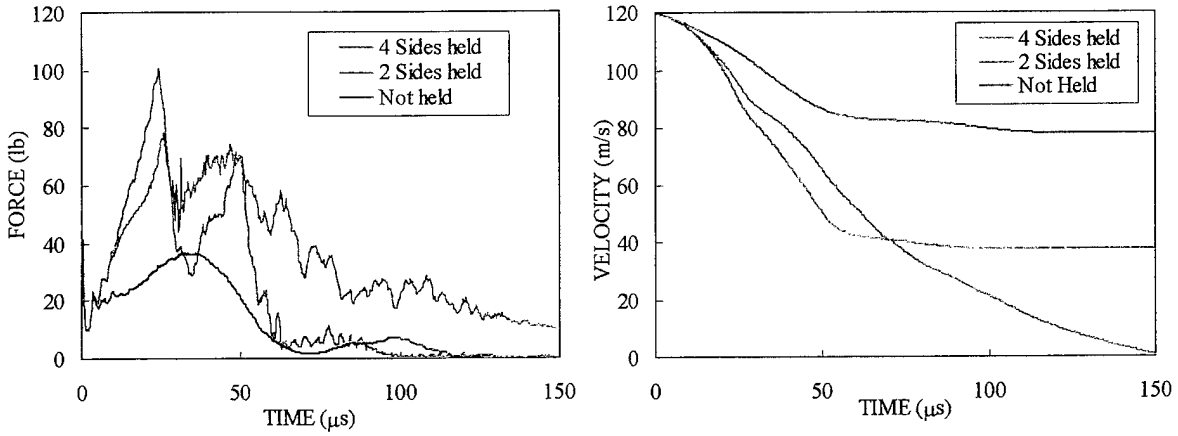

(a) Force on Projectile

(b) Projectile Velocity

FIGURE 73. RESULTS FOR PARAMETRIC STUDY ON BOUNDARY CONDITIONS

Figure 73(b) shows the calculated velocity of the impactor. For the case with no sides held, the impactor slows from 120 to about 80 m/s. This result is consistent with conservation of momentum for a simple inelastic collision. For four sides held, the velocity is reduced from 120 to about 38 m/s, and for two sides held, the velocity of the impactor is reduced to zero. The result that holding on two sides is more effective than holding on four sides agrees with the experimental results described above and helps explain that result. The result for no sides held shows that, if the impactor is prevented from cutting through the fabric, significant energy can be absorbed by inertial effects.

For the case held on two sides, the held yarns break locally, but the unheld yarns do not break and are able to shed some load to adjacent held yarns, as shown in figure 74.

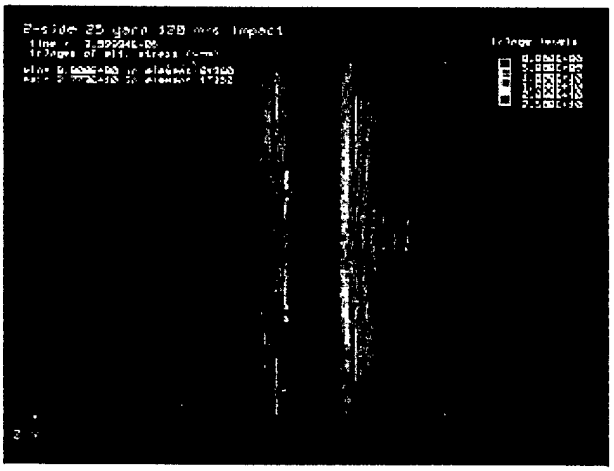

FIGURE 74. LOAD SHEDDING FOR FABRIC HELD ON TWO SIDES

EFFECT OF FABRIC SIZE. To investigate the effect of the size of the fabric, three cases of square fabric patches were simulated: 15 yarns, 25 yarns, 35 yarns, as shown in figure 75. In all cases the fabric was held on two sides. The fragment was a small steel impactor at 120 m/s.

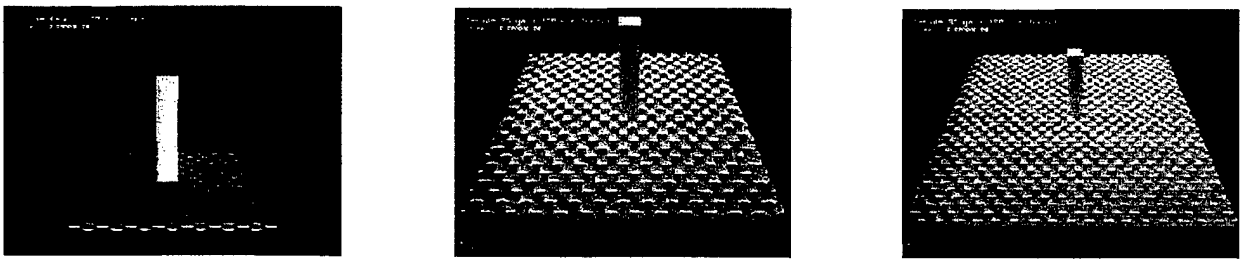

(a) 15 Yarns (b) 25 Yarns (c) 35 Yarns

FIGURE 75. MODEL MESHES FOR SIZE EFFECT INVESTIGATION

Figure 76 shows the results of the simulations for the three sizes of fabrics. As seen in figure 76(a), the timing of the oscillations for the three cases is quite different. As expected, the larger the fabric, the slower the oscillations. However, the overall resistance, as shown in figure 76(b), is virtually the same for the three cases, up until the 15-yarn case breaks.

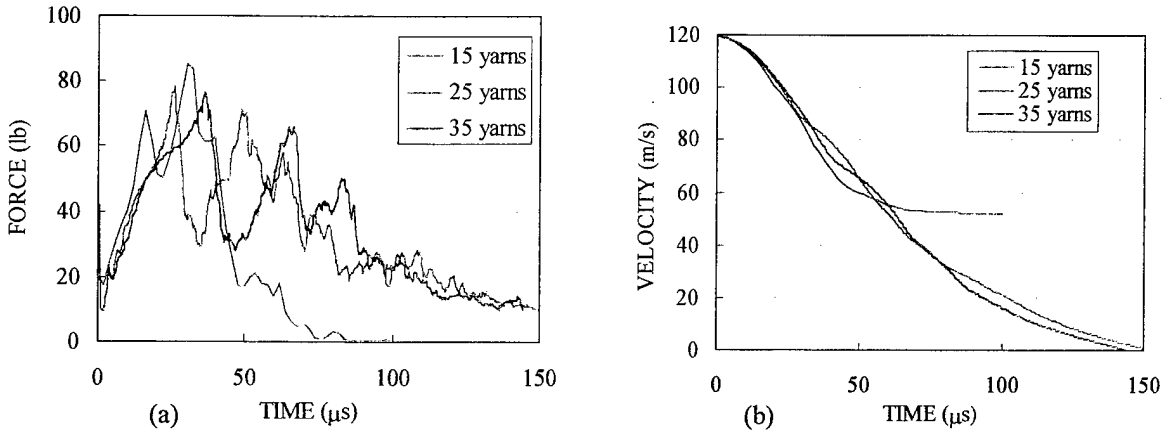

FIGURE 76. EFFECT OF SIZE ON RESISTANCE

COMPUTATIONAL CONSIDERATIONS. The computational requirements for these detailed calculations are considerable, both for CPU and for disk space. For example, the 25-yarn mesh has about 200,000 nodes and 100,000 elements and takes 24 hrs to run on a Silicon Graphics Incorporated (SGI) Octane workstation with a single R10000 CPU.

SUMMARY. The detailed model is at the stage where it can be used to study methods to improve the efficiency of the fabric for barriers. The effects of density, crimp, boundary conditions, and fabric size on ballistic resistance were investigated.

The effect of varying parameters such as stiffness and strength of yarns and interyarn friction, on barrier efficiency will be investigated. The possibility of investigating different weave geometries, including three-dimensional weaves, will be considered.

SIMPLIFIED MODEL.

A simplified model is being developed that can be used as a design tool for choosing or evaluating parameters for fragment barriers. The design tool uses a simplified description of the fabric so that the calculations run very quickly (about 2 minutes on an SGI Origin 200) to quickly evaluate changes in size of fabric, number of layers, or yarn pitch. The simplified model uses shell elements with an orthotropic continuum formulation to model the fabric.

MODEL PARAMETERS. To calculate parameters for the shell material model (see table 12), measured values for thickness and areal density were used. From the measured value of strength for a single yarn (1.61×10^7 dyne [36 lb]), a linear fabric strength (e.g., in dyne/cm) was calculated by multiplying the pitch (number of yarns/cm) by the strength of a yarn. The Young's moduli in the two orthogonal directions along the yarns were calculated by taking the measured yarn load at 1% strain, multiplying by the pitch, and distributing the load over the fabric thickness. The shear modulus in all directions is assumed to be 10% of the Young's modulus, and the Poisson's ratio is assumed to be 0 in all directions. The fabric density is calculated by dividing the measured areal density by the measured fabric thickness. For multiple plies, the fabric thickness is simply the number of layers times the single layer thickness; the modulus and

density values remain the same. The model assumes that, for a multi-ply target, the fabric yarns are all aligned in the same directions (e.g., 0 and 90 degrees).

TABLE 12. SIMPLIFIED MODEL PARAMETERS

No. of Plies	Pitch (ypi)	Thickness (mm)	Areal density (g/cm^2)	Force @ 0.01 (dyne)	Modulus ($dyne/cm^2$)	Density (g/cm^3)
1	30	0.15	0.0130	2.00×10^8	5.25×10^{11}	0.867
1	35	0.19	0.0158	2.34×10^8	4.84×10^{11}	0.832
1	40	0.23	0.0185	2.67×10^8	4.57×10^{11}	0.804
1	45	0.27	0.0219	3.00×10^8	4.38×10^{11}	0.811

FAILURE MODEL. The material model is assumed to be elastic-plastic with linear hardening to failure in the two orthogonal directions. The yield stress is set to 12.0×10^9 $dyne/cm^2$ with 20% strain hardening. The failure criterion is based on accumulated plastic strains in the two directions both exceeding a specified limit. The limit values for strain, which depend on the number of layers, are listed in table 13.

TABLE 13. LIMIT VALUES OF STRAIN

No. of Layers	Limit Value of Strain
1	0.035
2	0.060
3	0.085
4	0.110
5	0.135
6	0.150

EXAMPLE SIMULATIONS. Simulations were performed using the simplified model for 15 of the gas gun tests performed at SRI. Table 14 lists the results of these calculations. The tests included Zylon targets from 30 to 45 ypi, from 1 to 6 plies, held on 2 sides and 4 sides, and with a range of pitch and roll angles. For each calculation the residual velocity of the fragment and the energy dissipated by the target are listed. For calculations in which the fragment did not penetrate the target, the residual velocity was set to zero.

Figure 77 shows the calculated response for gas gun test 58. Test 58 was a single layer of 40 x 40 Zylon held on two sides. The 25-g fragment simulator had an impact velocity of 80 m/s, a roll angle of 16 degrees, and a pitch of 1 degree. Figure 77 shows snapshots of the response at 0.1-ms intervals. As seen in figure 77(c), the deformation wave reaches the target edges at about 0.2 ms. In the simulation, the left and right edges are held and the upper and lower edges are not held. As shown in figure 77(e) the fragment begins to penetrate at about 0.4 ms and is nearly through the target at 0.5 ms, as seen in figure 77(f). The calculated residual velocity of 38 ms is about 10% less than the measured velocity of 42 ms, indicating that the model target was stronger than the actual target.

TABLE 14. SIMPLIFIED MODEL CALCULATIONS

Test No.	Sides Held	Plies	Pitch (ypi)	Mass (g)	Velocity (m/s)	Vo Test (m/s)	Vo Model (m/s)	KE total (J)	Dissipated Energy (J)		Error (% of total)
									Test	Model	
49	2	1	35	25	52.0	0	5	33.8	33.8	33.5	-0.9
39	2	1	30	25	79.5	45	48	79.0	53.2	50.2	-3.8
47	2	1	35	25	80.0	49	52	80.0	49.7	46.2	-4.4
58	2	1	40	25	80.0	42	38	80.0	58.2	62.0	4.7
71	2	2	30	25	95.0	20	0	112.8	107.8	112.8	4.4
61	2	3	30	96	79.5	0	0	303.4	303.4	303.4	0.0
66	2	1	30	96	83.0	75	72	330.7	60.7	81.8	6.4
67	2	2	30	96	83.0	53	56	330.7	198.4	180.1	-5.5
25	4	1	35	25	77.5	59	45	75.1	31.6	49.8	24.2
13	4	1	45	25	78.0	29	35	76.1	65.5	60.7	-6.3
20	4	1	30	25	79.0	62	54	78.0	30.7	41.6	13.9
24	4	1	40	25	79.0	50	40	78.0	47.4	58.0	13.6
26	4	1	30	25	82.5	63	59	85.1	35.5	41.6	7.2
29	4	4	40	96	79.0	28	0	299.6	263.3	299.6	12.1
32	4	6	40	96	79.0	0	0	299.6	299.6	299.6	0.0

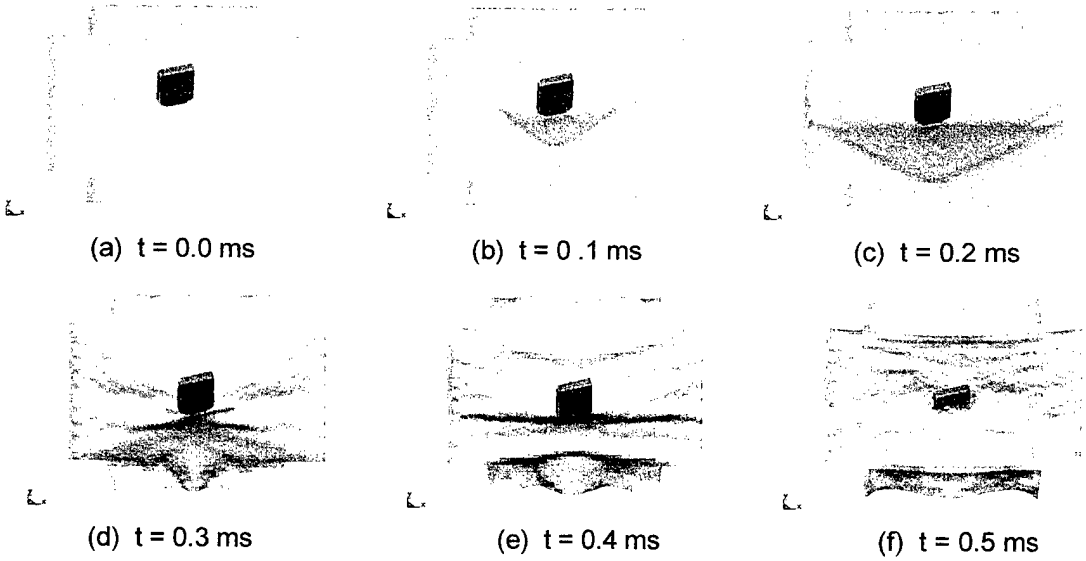

FIGURE 77. SIMPLE MODEL SIMULATION FOR GAS GUN TEST 58

The last column in table 14 is the error, calculated by normalizing the difference in the calculated and measured dissipated energy by the total kinetic energy of the fragment. The average of these errors is +4.4% with a standard deviation of 8.7%. Although the design model does a good job overall, it tends to overpredict the dissipated energy for the tests with four sides held. Figure 78 shows a plot for all the tests of the calculated dissipated energy as a function of the measured

energy dissipated. A linear fit through the data passing through the origin gives a slope of 1.03 and an R^2 value of 0.98.

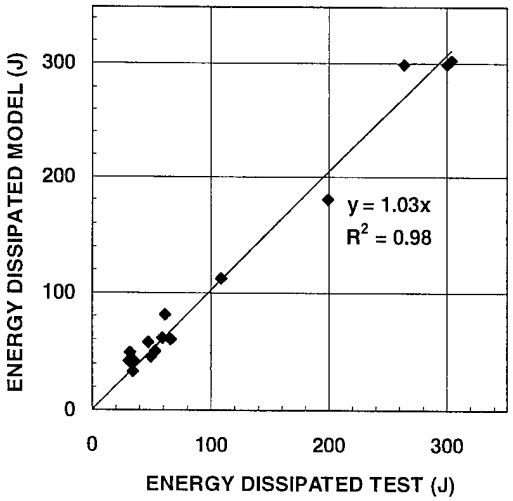

FIGURE 78. SIMPLIFIED MODEL SIMULATIONS OF GAS GUN TESTS

FURTHER WORK FOR DETAILED MODEL.

- Model the friction between yarns. The current detailed model allows for definition of a friction coefficient between yarns, but a friction coefficient has not yet been included. It is expected that a reasonable value for a friction coefficient between yarns will be determined by simulating the yarn pullout experiments. Then parameter studies could be run to determine how friction affects the ballistic response of the fabric.

- Improve computer power. Currently the scale of our calculations are limited by lack of computer resources. Assembling a multiprocessor machine is planned by connecting several PCs together to make a multiprocessor parallel platform.

- Develop shear failure criterion. The current model has a criterion for tensile failure of the yarns. Experiments with yarns loaded by sharp versus rounded fragments suggest that local tearing or shearing of the yarn may be an important mechanism to model. Implementation of a shear criterion for yarn failure is planned in addition to the tensile failure criterion.

- Investigate changes in weave design. So far only simple basket weaves have been analyzed. Investigation of other weave designs is needed as well. The objective would be to design the weave to involve as many yarns as possible. Weave design parameters as well as weave pattern can be varied to determine which parameters in the weave design have significant effects on ballistic performance.

- Further investigate the effects of boundary conditions on the ballistic performance. Full-scale tests so far have shown that unheld fabrics provide very high ballistic resistance.

The ultimate resistance, however, is limited by the strength of the IWP, which is small. Practical barrier designs will be investigated that use the strength of supports to develop the strength of the fibers. For implementation in an aircraft, the existing structural members may be used as a reaction frame.

- Conduct Verification. Although the yarn models have been verified with experiments, fabric response has not, because the size of the available computers is limited. There are plans to increase computer capabilities by assembling a multiprocessor parallel machine by combining Pentium-based PCs.

FURTHER WORK FOR SIMPLIFIED MODEL.

- Investigate other formulations. The shell model has done a fairly good job in simulating the gas gun tests, but it has some obvious limitations in terms of modeling failure mechanisms such as yarn pullout. Investigations of other formulations are needed, such as one-dimensional elements (beams or springs).

PLANS

EXPANDED AND USER-FRIENDLY DESIGN CODE.

The computational capability that was developed treats very reliably the tensile failure of high-strength fabric under ballistic impact. To be more useful in barrier design, the model needs to be expanded by adding treatments of other penetration and fragment-slowing mechanisms not currently considered in the existing model. Specifically, these are the cutting mechanism and the fragment cloaking and dragging mechanism. The experiments performed this year and last show that both mechanisms can operate and can very substantially affect whether the fragment is arrested or not. Thus, the model should be expanded to include the effects of insulation and other fuselage wall materials that contribute to fragment energy absorption.

The code consists of constitutive and damage models that are implemented in LS-DYNA3D, but because designers are not typically experienced users of DYNA, tutorial information should be developed that barrier designers can understand. This will require interaction with designers to learn their methods and needs.

VALIDATED BARRIER DESIGN FOR GENERALIZED IMPACT SCENARIOS.

To develop a code that can evaluate realistic uncontainment scenarios, the barrier structures need to be evaluated in barrier impact tests performed under conditions other than fragments hitting edge-on (zero degree yaw) and at zero degree obliquity. The effect of parameters such as fragment yaw-pitch-roll, angle of attack, edge sharpness, fragment mass and cross-sectional area, and multiple fragments should be ascertained in small-scale tests and verified in full-scale tests. The following barrier design parameters should also be examined: fabric material, number of plies, location of fabric within the fuselage wall, and boundary conditions (how the fabric is attached). The data and observations from such tests are needed to design barriers that will perform as intended.

REFERENCES

1. Aircraft Catastrophic Failure Prevention Research Program, Program Plan, January 1994, U.S. Department of Transportation, Federal Aviation Administration, William J. Hughes Technical Center, Atlantic City International Airport, NJ, 1994.

2. D.A. Shockey, J.H. Giovanola, J.W. simons, D.C. Erlich, R.W. Klopp, and S.R. Skaggs, "Advanced Armor Technology: Application Potential for Engine Fragment Barriers for Commercial Aircraft," DOT/FAA/AR-97/53, July 1997.

3. D.C. Erlich, D.A. Shockey, and J.W. Simons, "Full-Scale Tests of Lightweight Fragment Barriers on Commercial Aircraft," DOT/FAA/AR-99-71, July 1999.

4. C.E. Franeknberger, III, "Large Engine Uncontained Debris Analysis," DOT/FAA/AR-99/11, May 1999.

5. D.A. Shockey, J.W. Simons, and D.C. Erlich, "Improved Barriers to Engine Fragments: Report I," DOT/FAA/AR-99/8,I, May 1998.

6. D.A. Shockey, J.W. Simons, and D.C. Erlich, "Improved Barriers to Engine Fragments: Report II," DOT/FAA/AR-99/8,II, January 1999.